THE RESPONSE OF PILES DURING EARTHQUAKES: DYNAMIC SOIL-PILE-SUPERSTRUCTURE INTERACTION

by

Ross W. Boulanger, Bruce L. Kutter, and Daniel W. Wilson
Department of Civil & Environmental Engineering, University of California, Davis, CA

Research supported by the California Department of Transportation (Caltrans) under Contract Number 65V495. The contents of this report reflect the views of the authors who are responsible for the facts and the accuracy of the data presented herein. The contents do not necessarily reflect the official views or policies of the STATE OF CALIFORNIA or the FEDERAL HIGHWAY ADMINISTRATION. This report does not constitute a standard, specification, or regulation.

Report No. UCD/CGM-98/01

Center for Geotechnical Modeling
Department of Civil & Environmental Engineering
University of California
Davis, California

February 1998

Technical Report Documentation Page

1. Report No.	2. Government Accession No.	3. Recipient's Catalogue No.
FHWA/CA/ESC-98-09		Report No. UCD/CGM-98/01

4. Title and Subtitle	5. Report Date
The Response of Piles During Earthquakes: Dynamic Soil-Pile-Superstructure Interactions	February 1998
	6. Performing Organization Code n.a.
7. Authors	8. Performing Organization Report No.
Ross W. Boulanger, Bruce L. Kutter, and Daniel W. Wilson	n.a.
9. Performing Organization Name and Address University of California Department of Civil and Environmental Engineering Davis, California 95616	PB99122780 11. Contract or Grant No. 65V495
12. Sponsoring Agency Name and Address State of California Department of Transportation Sacramento, California	13. Type of Report and Period Covered Final report 14. Sponsoring Agency Code
15. Supplementary Notes	

16. Abstract

The dynamic response of pile foundations in soft clay and liquefiable sand during strong earthquake shaking was evaluated. The research consisted of two major components: (1) a series of dynamic centrifuge tests of pile-supported structures in soft clay and liquefiable sand; and (2) an evaluation of dynamic "beam on a nonlinear Winkler foundation" (BNWF) analysis methods against the centrifuge model results.

The dynamic centrifuge modeling techniques were critically evaluated in detail because these tests were among the first performed using the new shaking table on the 9-m radius centrifuge. The results of this evaluation will benefit other current and future projects utilizing the large centrifuge.

Several BNWF computer programs were shown to give consistent results for similar idealizations of a physical problem. Two new p-y elements were implemented into the program GeoFEAP. The representation of radiation damping was shown to be important in certain cases, with series radiation damping being technically preferred over parallel radiation damping in such cases. Calculated responses for a single pile in soft clay were in good agreement with the centrifuge data when using series radiation damping and a p-y element with gapping ability.

The p-y resistance of liquefied sand was shown to be strongly dependent on relative density and displacement level. Time histories of p-y resistance were obtained by back-calculation techniques for the soft clay and liquefied sand tests. The p-y resistance of liquefied sand shows characteristics that are consistent with the expected stress-strain behavior of liquefied sand, including the effects of relative density, dilation, cyclic degradation, and prior displacement history. If a scaling factor approach is used to approximate the effects of liquefaction on p-y resistance, then pseudo-static p-y analyses suggest a scaling factor of about 0.1-0.2 would be appropriate for Dr≈35-40% sand and a scaling factor of about 0.25-0.35 would be appropriate for Dr≈55-60% sand. It is emphasized that the use of an apparent p-y-scaling factor for liquefied sand was shown to be a simplistic approximation to a complex phenomenon, and therefore its use in design requires considerable judgment.

17. Keywords	18. Distribution Statement
Piles, earthquakes, dynamic response, liquefaction, soft clay, centrifuge modeling, p-y analyses.	No restrictions.

19. Security Classif (of this report)	20. Security Classif. (of this page)	21. No. of Pages	22. Price
Unclassified	Unclassified	125	n.a.

Form DOT F 1700.7 (2-86)

ABSTRACT

The dynamic response of pile foundations in soft clay and liquefiable sand during strong earthquake shaking was evaluated. The research consisted of two major components: (1) a series of dynamic centrifuge tests of pile-supported structures in soft clay and liquefiable sand; and (2) an evaluation of dynamic "beam on a nonlinear Winkler foundation" (BNWF) analysis methods by comparison with the centrifuge model results.

The dynamic centrifuge modeling techniques were critically evaluated in detail because these tests were among the first performed using the new shaking table on the 9-m radius centrifuge. The results of this evaluation will benefit other current and future Caltrans projects utilizing the large centrifuge.

Several BNWF computer programs were shown to give consistent results for similar idealizations of a physical problem. Two new p-y elements were implemented into the program GeoFEAP. The representation of radiation damping was shown to be important in certain cases, with series hysteretic/viscous damping being technically preferred over parallel hysteretic/viscous damping in such cases. Calculated responses for a single pile in soft clay were in good agreement with the centrifuge data when using series hysteretic/viscous damping and a p-y element with gapping ability.

The p-y resistance of liquefied sand was shown to be strongly dependent on relative density and displacement level. Time histories of p-y resistance were obtained by back-calculation techniques for the soft clay and liquefied sand tests. The p-y resistance of liquefied sand shows characteristics that are consistent with the expected stress-strain behavior of liquefied sand, including the effects of relative density, dilation, cyclic degradation, and prior displacement history. If a scaling factor approach is used to approximate the effects of liquefaction on p-y resistance, then pseudo-static p-y analyses suggest a scaling factor of about 0.1-0.2 would be appropriate for Dr≈35-40% sand and a scaling factor of about 0.25-0.35 would be appropriate for Dr≈55-60% sand. It is emphasized that the use of an apparent p-y-scaling factor for liquefied sand is a simplistic approximation to a complex phenomenon, and therefore its use in design requires considerable judgment.

ACKNOWLEDGEMENTS

The California Department of Transportation (CALTRANS) supported this research under research contract number 65V495. The contents of this report reflect the views of the authors who are responsible for the facts and the accuracy of the data presented herein. The contents do not necessarily reflect the official views or policies of the STATE OF CALIFORNIA or the FEDERAL HIGHWAY ADMINISTRATION. This report does not constitute a standard, specification, or regulation.

The National Science Foundation, Caltrans, the Obayashi Corporation, and the University of California funded the design and construction of the earthquake simulator on the large centrifuge at U.C. Davis.

Abbas Abghari was the contract monitor for Caltrans, and provided valuable collaboration throughout this project. The work presented in this report includes contributions from the MS theses of S. Wang and M. J. Chacko. The authors would also like to acknowledge the suggestions and assistance of I. M Idriss, D. P. Stewart, T. Kohnke, P. Robins, C. Curras, G. Fiegel, and W. Sluis. A joint presentation by R. W. Boulanger and K. Tokimatsu at an U.S.-Japan Workshop was the basis for the review of lessons from the Kobe earthquake. J. D. Bray graciously provided the program GeoFEAP, and T. Lok provided valuable assistance with its use. T. Kagawa provided the computer codes for NONSPS and SRANG. PMB Engineering, Inc. provided the program PAR at a reduced cost. All of the above assistance is greatly appreciated.

TABLE OF CONTENTS

1 INTRODUCTION

Damage to piles and pile foundations during earthquake loading with soft clay or liquefiable sand foundation soils poses a hazard to the public and threatens the post-earthquake functionality of many new and existing bridges. The potential significance of the liquefaction-related damage to piles during earthquakes was clearly demonstrated during the 1964 Alaskan earthquake (e.g., Youd and Bartlett 1989) and re-demonstrated most recently during the 1995 Kobe earthquake. Nonetheless, only a limited number of well-documented case histories exist that can be used to evaluate design methodologies or interpret the physical phenomena of soil-pile-superstructure interaction. Thus, the reliability of design procedures remains uncertain, and the fundamental mechanisms of soil-pile-structure interaction in soft or liquefiable soils under strong shaking continue to be poorly understood.

This report describes the results of study of the dynamic response of pile foundations in soft clay and liquefiable sand during strong shaking. The research consisted of two major components. Firstly, a series of dynamic centrifuge tests of pile supported structures in soft and liquefiable soils were performed using the recently completed shaking table on the large centrifuge at U.C. Davis. Secondly, dynamic "beam on a nonlinear Winkler foundation" (BNWF) analysis methods were evaluated by comparison with the results of dynamic centrifuge model tests.

The dynamic centrifuge tests performed in this study were among the first performed using the recently completed shaking table on the large centrifuge, and thus it was necessary to evaluate the centrifuge modeling system before analyzing the recorded physical data. The importance of characterizing the centrifuge modeling system was demonstrated by the recent VELACS cooperative study (e.g., Arulanandan et al. 1994) and further discussed by Scott (1994). Quantifying modeling limitations was considered essential before using the data to evaluate seismic design methodologies for pile-supported structures.

Dynamic centrifuge experiments were performed using several different structural models, different earthquake input motions (varying level of shaking, frequency content, and waveform), and different soil profiles. Experiments were performed with the upper soil layer being either liquefiable sand or soft, normally consolidated clay. The results of these experiments have been documented in detail with individual hard-copy data reports and diskettes with raw time histories (Wilson et al. 1997 b-f).

Several computer programs for analyzing pile response as a BNWF problem were evaluated. The programs evaluated were NONSPS (Kagawa 1983), DRAIN-2D (Prakash and Powell 1993), PAR (PMB Engineering 1988), and GeoFEAP (Bray et al. 1997). Two new p-y element subroutines, describing the relationship between lateral soil resistance (p) and the relative pile-to-free-field-soil displacement (y), were developed for GeoFEAP (Wang 1997). The computer programs used to analyze the free-field site response were SHAKE (Schnabel et al. 1972), SRANG (Kagawa 1980), and SUMDES (Li et al. 1992). These different analysis methods were compared to results obtained from a set of dynamic centrifuge experiments involving soft clay foundation soils (Chacko 1995, Wang et al. 1997). Results of these experiments and their comparisons are summarized herein.

The dynamic centrifuge experiments with liquefiable sand were analyzed using simplified pseudo-static nonlinear BNWF methods, and using back-calculation procedures to obtain time histories of p-y resistance at different depths. The pseudo-static BNWF analyses

proved valuable for evaluating the p-y resistance of liquefied soils. The use of back-calculation procedures to better define the p-y resistance of the liquefied sand and soft clay is a departure from the original proposal, but was adopted as a promising means of providing a more rational interpretation of the p-y resistance of liquefied soil and soft clay. The results of the back-calculation procedures are expected to provide a better basis for developing p-y elements for use in dynamic BNWF analysis methods.

Continuing research efforts that are based on the experimental findings of this project, and recommendations for future research, are also described. It is hoped that the results of this research will contribute to the ongoing efforts to mitigate future earthquake hazards..

2 PERFORMANCE OF PILES IN PAST EARTHQUAKES

2.1 CURRENT ISSUES

The behavior of pile foundations under earthquake loading is an important factor affecting the performance of many essential structures. Evaluating pile foundation behavior requires consideration of the loads imposed on the piles and their pile-cap connections, transient or permanent deformations of the foundation, and the influence of the pile foundation on the dynamic response of the superstructure. Observations of modern pile foundations during past earthquakes have shown that piles in firm soils generally perform well, while the performance of piles in soft or liquefied ground can range from excellent to poor (i.e., structural damage or excessive deformations). Analysis and design procedures have been developed for evaluating pile behavior under earthquake loading, but their application to cases involving soft or liquefied ground is uncertain due to a lack of physical data against which they can be evaluated. Addressing this uncertainty has been identified as an urgent need of earthquake hazard remediation programs currently in progress.

The review of pile performance in recent large earthquakes presented in this section can only address observations of pile damage (or lack thereof) because the field data does not allow a direct evaluation of the effect of soil-pile interaction on dynamic response. Observations of pile damage have been largely associated with liquefaction, and these observations are described in detail because they relate to the second part of this study.

Physical data on the performance/behavior of pile foundations in soft or liquefied ground under earthquake loading would ideally be available from the detailed documentation of case histories that include cases of good and poor performance. Physical modeling, such as dynamic centrifuge or shaking table tests, with detailed instrumentation can also be used to obtain physical data, gain insight into the mechanisms involved, and perform parametric studies. In this way, physical modeling and case history studies are complementary tools.

An associated need is a systematic evaluation of the ability of available analysis or design procedures to predict the performance (good or poor) of pile foundations in soft or liquefied ground during earthquakes. Systematic evaluations against case history or physical model data can lead to improvements, or increased confidence, in analysis or design procedures.

Another important issue is the question of what constitutes satisfactory performance of a pile foundation. The most common design approach in the U. S. is to avoid inelastic behavior of piles and their connections below the ground surface where damage would be difficult to detect or repair. This criterion of maintaining elastic behavior in the structural components of a pile foundation often governs the design. Thus, the possibility of allowing for inelastic behavior of the piles and their connections may provide significant economy in certain cases, but will require broader discussions of what constitutes satisfactory performance (e.g., life safety versus level of functionality, how readily pile damage should be detectable or repairable, and other related issues). In fact, the possibility of inelastic behavior in the structural components of pile foundations during past earthquakes has generally not been fully investigated; direct inspections below the ground surface have generally not been performed when there is no visible damage to a pile foundation. Experiences at Kobe support the need to distinguish between the absence of structural yielding in the pile foundation and the absence of damage to the superstructure.

2.2 LESSONS LEARNED FROM THE LOMA PRIETA EARTHQUAKE

Damage to pile foundations from the Loma Prieta earthquake appears to have been very limited. Known cases involving damage to pile foundations include the highway bridges at Struve Slough and the Seventh Street Terminal at the Port of Oakland. The parallel bridges on Highway 1 at Struve Slough near Watsonville were heavily damaged, with the bridge carrying southbound traffic collapsing. Each bent was supported by a row of single pile columns passing through soft organic soils into stiffer soils. The limited lateral support provided by the upper soft organic strata likely contributed to the observed damage. At the Seventh Street Terminal at the Port of Oakland, considerable damage occurred to most of the battered piles supporting the concrete wharf. The battered piles were on the inboard side of the wharf, and passed through a rockfill and sand dike separating the filled land from the bay. Extensive liquefaction of the hydraulic fills on the inboard side of this dike contributed to the observed pile damage. Significantly lower damage rates occurred for the battered piles supporting the concrete wharf at the nearby Matson Terminal. At this wharf, the battered piles were located further outboard and thus had a greater free length above the mud-line. The lower damage rates are likely a result of this more flexible arrangement.

On the other hand, apparently good performance of pile foundations was observed in many areas, some of which involved liquefied ground. At Treasure Island, several pile-supported buildings performed well despite liquefaction of the surrounding ground and subsequent ground surface settlements of up to 20 cm. At the Bay Bridge tollbooth plaza, pile-supported structures performed well despite liquefaction in the surrounding fills. At Moss Landing, a new reinforced concrete pile-supported pier for the Monterey Bay Aquarium Research Institute was undamaged despite 8-30 cm of lateral spreading of the adjacent shoreline. In the Marina District, the newer portions of the yacht club supported on reinforced concrete piles experienced lateral movements ranging from negligible to 10 cm, while liquefaction in the surrounding fills caused up to 60 cm of lateral spreading. Only minor spalling was observed at the tops of the piles. It should be noted, however, that the region of strongest shaking during the Loma Prieta earthquake was outside the developed urban areas, and thus most of the pile-supported structures in the San Francisco Bay area were not subjected to design-levels of shaking.

Due to the absence of visible damage to pile-supported structures, there have apparently been no direct inspections of the piles or their connections below the ground surface. It is therefore possible that damage to piles has gone undetected.

2.3 LESSONS LEARNED FROM THE NORTHRIDGE EARTHQUAKE

No notable cases of damage to pile foundations during the Northridge earthquake have been reported. However, liquefaction was not very extensive and most pile-supported structures were in areas experiencing small permanent ground movements. Due to the absence of visible damage to pile foundations, there have apparently been no direct inspections of the piles or their connections below the ground surface. Thus it is possible that some pile damage below the ground surface has gone undetected. Overall, the apparently good performance of pile foundations in firm ground is consistent with past experience.

2.4 LESSONS LEARNED FROM THE KOBE EARTHQUAKE

There were numerous cases of damage to pile foundations in Kobe during the 1995 earthquake, largely because of the strong levels of shaking, the prevalence of liquefaction, and the high concentration of pile-supported structures in the area. Tokimatsu et al. (1996, 1997) and Matsui (1996) have presented excellent overviews of pile foundation performance. Additional cases of pile performance were presented by Oh-Oka et al. (1997), Akiyama and Morimoto (1997), Sasaki et al. (1997), and Fujii et al. (1997).

A consortium of Japanese researchers is currently compiling detailed and extensive information on pile foundation damage. The "Committee on Building Foundation Technology Against Liquefaction and Lateral Spreading" (BTL Committee) is supported by 26 member organizations, and has three sub-working groups for liquefaction, lateral spreading, and remedial measures. Each group has about 34 members. The BTL Committee is expected to continue its efforts for another one to two years, with the results being disseminated shortly after that.

2.4.1 Inspection Methods

Several methods for detecting pile damage below the ground surface have been used in Kobe (Oh-Oka et al. 1997; Sasaki et al. 1997; Tokimatsu et al. 1997). Sonic methods proved capable of identifying discontinuities in piles in many cases, but sometimes could not distinguish cracks from joints, and could not assess the severity of damage. Borehole cameras have proved reliable for identifying damage and assessing severity. Inclinometers have been used to estimate the deformed shapes of hollow piles, based on the assumption of verticality before the earthquake. The deformed shapes from the inclinometer data were then compared to measurements or estimates of surface displacements to check the reasonableness of the data. Sasaki et al. (1997) described two cases where post-earthquake excavations exposed damaged piles that had been inspected by sonic or borehole camera methods. The exposed patterns of damage were generally in agreement with the results of the sonic/borehole inspections, although some examples of mistaken interpretations were given (e.g., cracks versus joints). Examples of pile inspection data from Kobe are shown in Figure 2-1 (Matsui and Oda 1996) and Figure 2-2 (Tokimatsu et al. 1996).

X-ray inspections were a technique used to evaluate potential damage to the steel pipe pile foundations for elevated approach spans on the West Jetty of the Maya Wharf, which was an area of large lateral spreading deformations (Matsui 1996). The X-ray inspections of the upper portions (about 2 m) of the 1-m-diameter piles identified no damage.

Inspection tests showed that damage to piles was often concentrated near the ground surface or near interfaces between soils of different stiffness (i.e., the interface between the liquefied soils and the underlying nonliquefied soils or overlying nonliquefied crust).

In general, pile damage could not be discerned on the basis of surface observations, and thus the use of sonic testing and borehole cameras was invaluable in assessing pile foundation performance.

2.4.2 Damage Patterns

Damage to pile foundations can be grouped by the pile foundation type, the ground conditions, and the failure mechanisms (excessive displacements versus structural damage). Many cases of damage repeated lessons of past earthquakes, as will be described below.

Reinforced concrete pile foundations for newer buildings performed better than for older buildings, probably due to revisions in the design codes made in the 1970s-80s (Tokimatsu et al. 1996). In fact, it is possible that the effects of soil liquefaction or lateral seismic forces were not even considered in the design of many older pile foundations. For large diameter piles that support large elevated structures/bridges, there were also cases of pile damage despite their recent designs (Matsui 1996). A few observations for small and large diameter piles suggest that steel pipe piles performed better than reinforced concrete piles because of their better ductility, although cases of damage to steel pipe piles have also been documented (Matsui 1996).

Soil liquefaction was the primary cause of foundation distress, with distress being most common in areas of laterally spreading ground. Damage to pile foundations was attributed to several mechanisms, as illustrated in Figures 2-3 and 2-4 (Tokimatsu et al. 1996):

(1) Pile heads were sometimes damaged by lateral forces and/or overturning moments imposed by the superstructure;

(2) Buildings supported on friction piles embedded within the zone of liquefaction often settled with the surrounding ground, and tilted by an amount that ranged from severe to negligible;

(3) Buildings supported on piles bearing on firm soils beneath the zone of liquefaction often had no apparent settlement while the surrounding ground had large settlements, and thus large vertical gaps occurred around the bases of many such buildings; and

(4) Pile foundations in areas of lateral spreading ground, particularly near distressed quay walls, were often damaged by the lateral forces of the spreading ground against the pile foundations, possibly with some contribution from inertial forces of the superstructure.

Pile damage by mechanisms (1) and (2) appeared to be more prominent in buildings with high aspect ratios (height to base dimension).

About 80% of the foundations for elevated highways in the Kobe, Ashiya, and Nishinomiya area are pile foundations (Figures 2-5 and 2-6; Matsui 1996). Most piles were cast-in-place reinforced concrete bored piles with diameters of more than 1 m, although some steel pipe piles of similarly large diameters were also used. Borehole TV (BHTV) cameras were used to inspect over a hundred piles for damage along their embedded length. Cracks were concentrated near the tops of the piles where the maximum moment occurs, but cracks were also observed in the middle to lower portions of piles (e.g., Figure 2-1). Cracks at lower depths possibly corresponded to the position of the second largest moment, a change in steel reinforcement density, or an interface between soft (liquefied) and stiff (nonliquefied) soils. Pile damage was divided into 4 categories: severe, heavy, light, and no damage (Figure 2-6). On the Hanshin Expressway, the Kobe Route has 92% no damage and 8% lightly damaged, while the Bay Route had 44% no damage, 48% lightly damaged, and 8% heavy damage. No cases of severe damage were identified. The degree of pile damage was found to not necessarily correspond to the degree of damage to the superstructure. Instances of damage depended mainly on the subsurface conditions; e.g., the Kobe Route is mostly on original land while the Bay Route is mostly on reclaimed land. Heavily damaged piles along the Bay Route were near sea walls that had spread from liquefaction.

The lateral capacity of damaged piles was discussed by Matsui (1996) by comparison to a 1993 full-scale field loading test on 3x3 pile group of 1-m-diameter cast in-place bored piles. This pile group was displaced as much as 45 cm under one-way loading-unloading-reloading cycles. The resulting damage to the piles corresponded to "heavily" damaged under the classification used to describe earthquake damage. The one-way lateral resistance of this pile group was apparently sufficient even after the piles became heavily damaged. The lateral

resistance of piles damaged by earthquake loading, however, must consider the effects of multidirectional versus one-way loading on the soil-pile systems behavior.

Good performance of pile foundations in liquefied ground was observed in areas with permanent lateral deformations ranging from relatively small to relatively large (which was strongly related to the proximity of a free face). For example, in the interior of Port Island, pile-supported structures were easily identified by the large surface settlements of the surrounding liquefied ground, and yet most of these structures appeared to be undamaged. Also on Port Island, large lateral and vertical movements of the liquefied ground exposed the pile foundation for the ferry terminal, and yet there appeared to be no damage to the structure or its foundation. In these and other cases, large diameter concrete piles often appeared to have resisted lateral spreading movements to some extent.

Large groups of piles appeared to perform better than small groups or isolated piles under similar loading conditions. Confirmation of this trend must await the documentation efforts of the BTL Committee.

Some caisson-type foundations for long-span bridges crossing water were displaced and inclined towards the water as a result of liquefaction and lateral spreading in the surrounding fills (Matsui and Oda 1996, Karube and Kimura 1996). For example, this type of caisson foundation damage occurred to the Kobe Bridge that connects Port Island to the mainland and to the Rocco-Liner bridge that connects Rocco Island to the mainland.

There were a few cases of pile foundations in areas of improved ground. In two cases described by Tokimatsu et al. (1996), pile foundations in an area treated by sand compaction piles and an area treated by deep cement mixing walls performed well despite large lateral spreading movements outside the treated areas.

2.4.3 Analyses of Pile Foundation Damage

Simplified design methods using p-y curves for pile foundations in liquefied soil were reviewed by Tokimatsu et al. (1997), and used in several studies of pile damage at Kobe. Three types of loading conditions were examined: (1) inertial force only; (2) inertial force and kinematic loading; and (3) kinematic loading only. Inertial forces are those expected from the superstructure alone, and depend on the ground motions (as affected by liquefaction). Kinematic loads were generally represented by assuming that the ground displacement profile varied linearly with depth across the liquefied layer. The assumed ground displacement profile was then applied to the free-field ends of the p-y springs. The procedure for defining the p-y curves for liquefied sand was not described in detail, but appears to have been based on scaling the static p-y curves. The three load cases illustrated the relative importance of kinematic versus inertial loading. Furthermore, the peak inertial loading would not be expected to occur at the same time as the peak kinematic loading.

Tokimatsu et al. (1997) then presented a case where piles located at different distances from a quay wall were connected by a rigid mat (Figure 2-7). Lateral spreading of the quay wall resulted in lateral ground displacements that decreased with distance from the wall (Figure 2-8), and thus the piles were subjected to different p-y support displacements (Figure 2-9). The resulting bending moment distributions were different between piles located nearest versus farthest from the quay wall, and were consistent with the observed pattern of damage during the Kobe earthquake (Figure 2-10 and 2-11). These results indicate that the interaction of piles across a foundation, as connected through a mat or grade beams, can influence the pattern of damage.

Two-dimensional finite element analyses of two pile-supported buildings on Port Island were described by Fujii et al. (1997). A fully coupled effective stress constitutive model was used for the soil. Pile nodes were connected to the soil nodes in these 2-D analyses. Calculations with and without the building mass showed that inertial forces were important in the upper few meters, but that kinematic loads dominated deeper in the profile. Predicted behavior was in reasonable agreement with field observations. The FE results were then compared to analyses using simple pseudo-static p-y analysis methods (see Section 3-3). The p-y analysis methods gave similarly reasonable results using static p-y curves scaled by factors of 0.01, 0.05, and 0.30. The p-y analyses were not sensitive to this range of scaling factors for the liquefied layer because it was the lateral loads from the thick nonliquefied crust that dominated the analysis.

2.5 Concluding Remarks

The Kobe earthquake has resulted in many valuable case histories of good to poor performance of pile foundations in liquefied ground. Lessons from these case histories will prove invaluable to the advancement of analysis and design procedures for pile foundations in liquefied ground. It also appears that the performance of pile foundations during the Loma Prieta and Northridge earthquakes needs to be investigated more closely since experience at Kobe shows that damage to pile foundations can occur without evidence of such damage being visible from the ground surface.

Predicting the behavior of pile foundations in soft clay or liquefied ground under earthquake loading is a very complex problem involving consideration of design motions, free-field site response, superstructure response, and soil-pile-superstructure interaction. There is a shortage of physical data for pile foundations in soft or liquefied ground under strong levels of shaking, and this translates into uncertainty in the predictive capability of current analysis or design procedures. Thus, the most pressing priority is the detailed documentation of case histories and physical model studies of pile foundations in soft or liquefied ground. In this regard, the continuing efforts of the BTL Committee in Japan are expected to lead to significant findings and invaluable data for U.S. and Japanese engineers.

Centrifuge or shaking table studies of the seismic behavior of pile foundations in soft clay or liquefied ground are needed as a means for understanding the fundamental mechanisms of soil-pile-superstructure interaction under these conditions, for evaluating the reliability of current design procedures, and for the development of improved design procedures. The obvious advantage of centrifuge or shaking table studies is the ability to obtain detailed measurements of response in a series of tests designed to physically evaluate the importance of varying the earthquake characteristics (level of shaking, frequency content, waveform), soil profile characteristics, and/or pile-superstructure characteristics. Used in conjunction with lessons from case histories and numerical analyses, results from centrifuge or shaking table studies are an essential tool for ongoing studies of this complex problem.

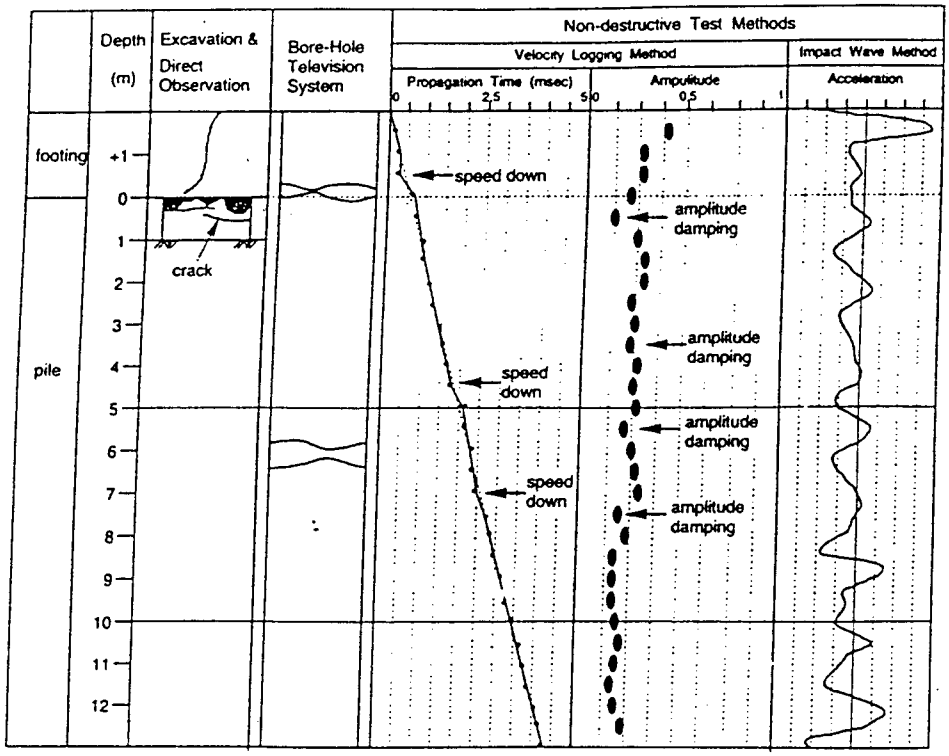

Fig. 2-1: Example of Inspection Data for Hanshin Expressway No. 3 Kobe Route (Matsui & Oda 1996)

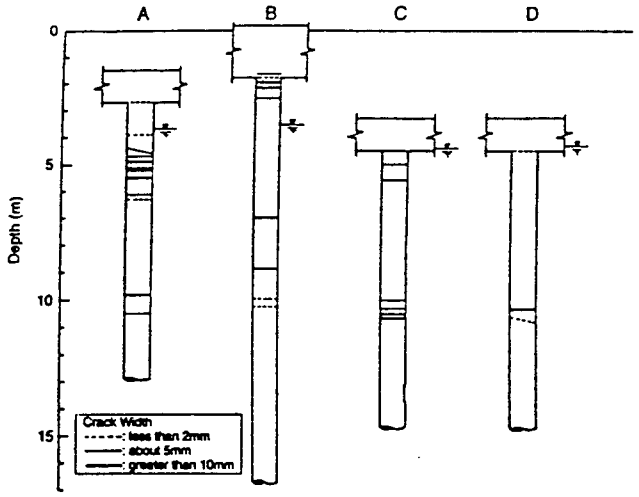

Fig. 2-2: Cracks in Piles Detected by Television Observation (Tokimatsu et al. 1996)

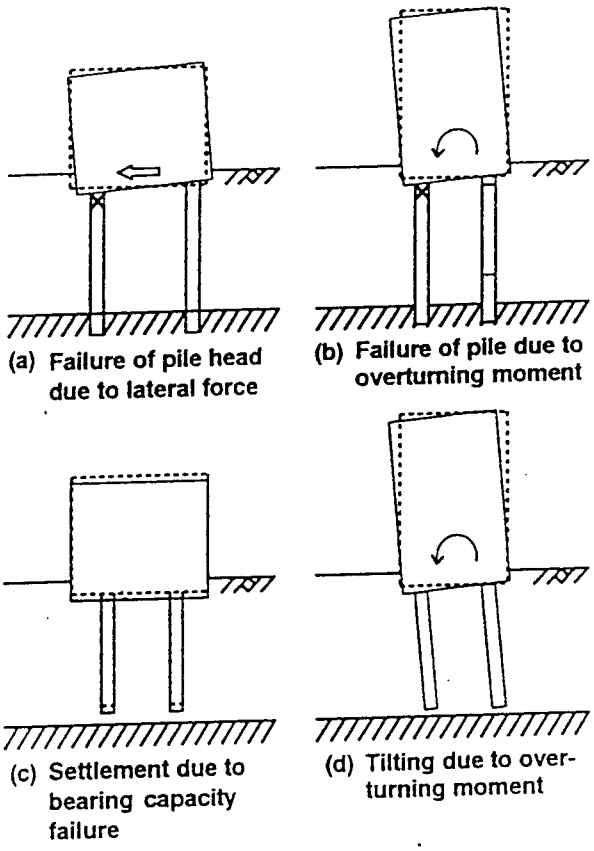

Fig. 2-3: Schematic of Pile Damage Mechanisms in Level Ground Areas (Tokimatsu et al. 1996)

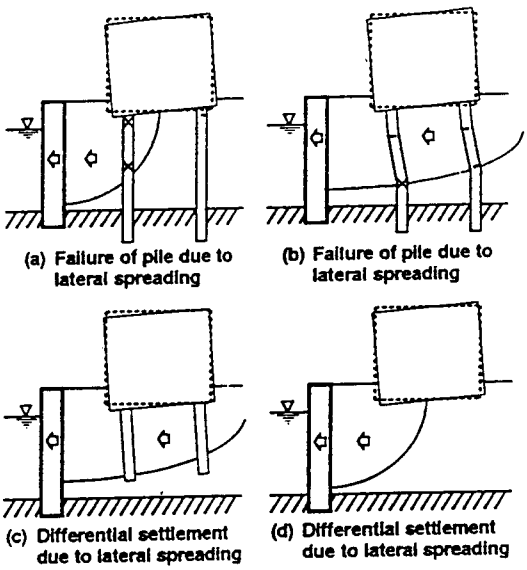

Fig. 2-4: Schematic of Pile Damage Mechanisms in Laterally Spreading Areas (Tokimatsu et al. 1996)

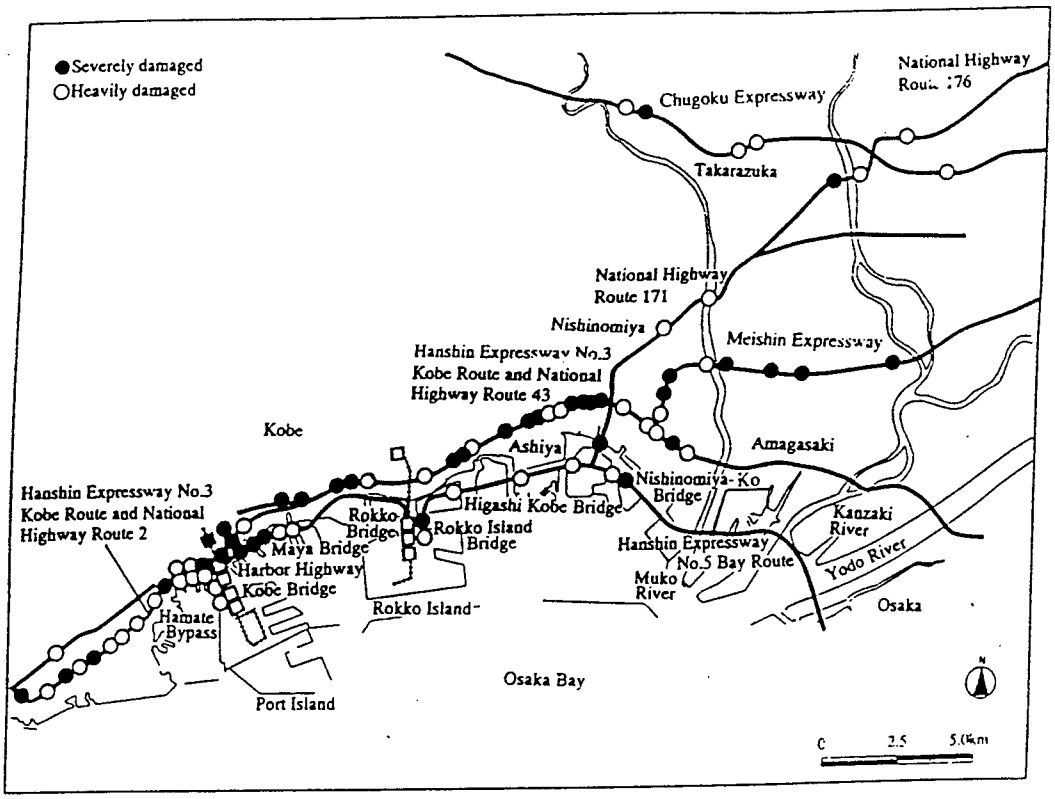

Fig. 2-5: Damage Location Map for Super- and Sub-structures of Elevated Highways (Matsui and Oda 1996)

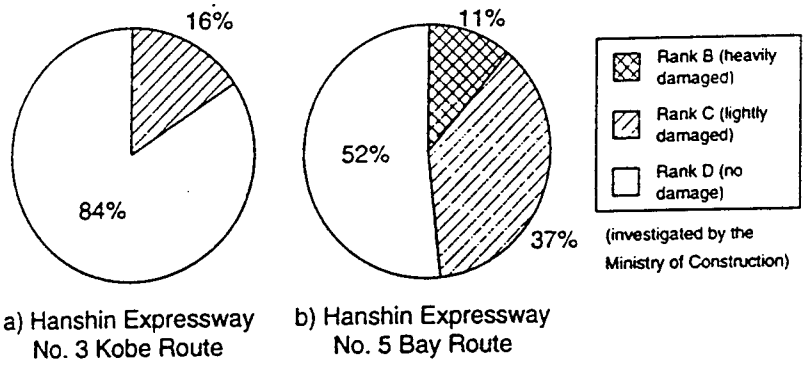

Rank Damage	A Severely damaged	B Heavily damaged	C Lightly damaged	D No damaged
Residual deformation and inclination of foundation	Large	Some	Little	No
Damage to pile	•many cracks and separation of concrete all over pile •buckling of some main reinforcing bars •discontinuity of pile shaft	•many cracks and separation of concrete at pile top •many cracks around middle to lower part of pile	•some cracks but no separation of concrete at pile top •some cracks around middle to lower part of pile in some cases	•almost no cracks
Capacity performance and restoration method	•anticipate inadequate capacity in vertical and horizontal directions •restoration by increasing piles or not possible to restore	•anticipate adequate vertical capacity and partial horizontal capacity •restoration by increasing piles for partial horizontal load	•anticipate sufficient capacity in vertical and horizontal directions •restoration of anticorrosion protection for reinforcing steel	•no restoration

Fig. 2-6: Pile Damage for Hanshin Expressway, and Pile Damage Classifications (Matsui & Oda 1996)

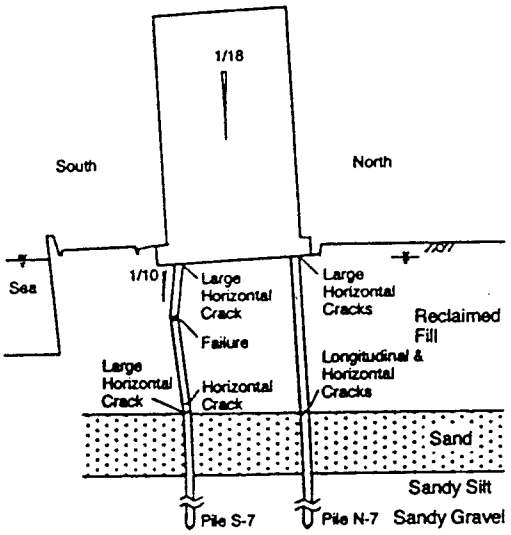

Fig. 2-7: Damage pattern of foundation (after Oh-oka et al., 1996)

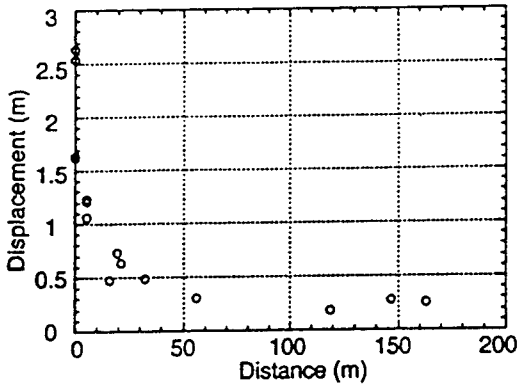

Fig. 2-8: Correation of ground movement with distance from the shoreline, Building A site

Tokimatsu et al. (1997)

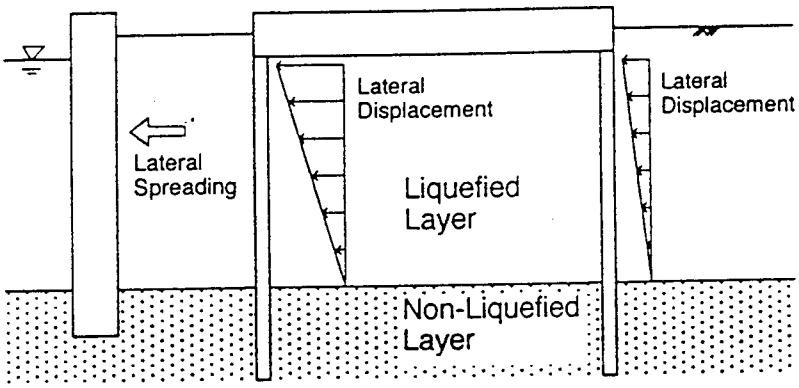

Fig. 2-9: Analytical mode of piles subjected to liquefaction-induced lateral spreading

Tokimatsu et al. (1997)

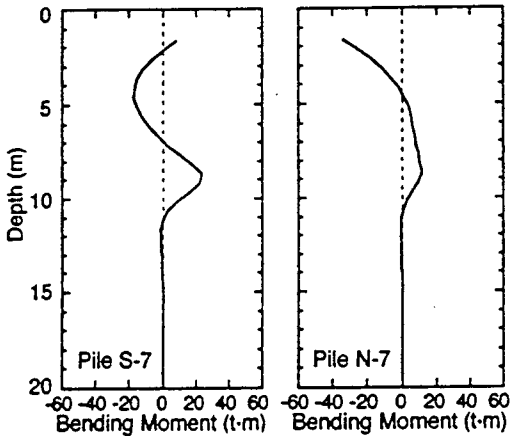

Fig. 2-10: Computed distribution of bending moment in piles at Building A site

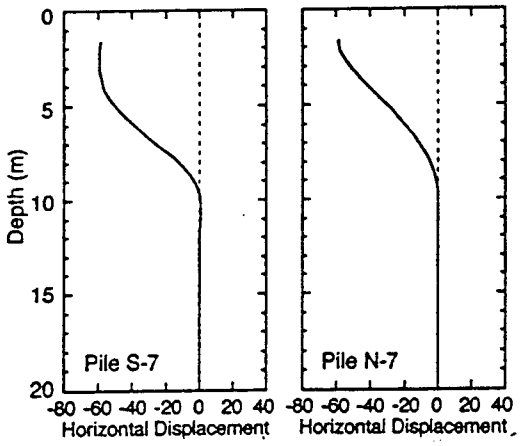

Fig. 2-11: Computed distribution of displacement of piles at Building A site

Tokimatsu et al. (1997)

3 RELATED STUDIES OF SOIL-PILE INTERACTION

3.1 PREVIOUS PHYSICAL MODELING STUDIES OF PILES UNDER SEISMIC LOADING

A review of the literature identified an abundance of research on soil-pile interaction, including behavior under axial, lateral, and uplift loading. Experimental data is available for monotonic, cyclic, free vibration, and dynamic testing. Experiments have been performed at full scale, at reduced scale, in shaking tables, and in centrifuges using a range of soil types. The review presented herein was therefore limited to research that: (1) revealed general features of behavior for lateral loading of piles; (2) specifically discussed large strain seismic loading of piles; or (c) discussed experimental procedures of direct relevance to the present study.

Many researchers perform cyclic load tests with the cyclic load applied at the pile head. They can then measure monotonic loading in addition to cyclic loading or simply consider the first load cycle to be monotonic. This was done by Brown et al. (1988), Crouse et al. (1993), Dunnavant and O'Niell (1989), and Ochaoa and O'Neill (1989). Degradation of the static p-y curves with increasing number of loading cycles can then be investigated. Procedures have been developed for coupling monotonic p-y curves with p-y degradation factors to derive an equivalent pile foundation stiffness for use in dynamic superstructure finite element models.

The extension of cyclic pile-head loading tests to seismic loading conditions has several limitations. With pile-head loading, the soil remains a passive resistor while in seismic events, the soil applies load to the pile. The kinematic loading from the soil can be particularly important at soft soil sites. Radiation damping effects are different for the two loading conditions. Excess pore pressures generated by pile-head loading can dissipate to the surrounding soil, while in seismic events the pore pressure increase will be more global. Some cyclic load tests have been done with cyclic base motion (Kobayashi et al. 1991b; Yan et al. 1991), which is a more appropriate model of seismic loading conditions. Free vibration tests in the field (e.g., Crouse et al. 1993; El Sharnouby and Novak 1984) have also been performed, but the small strain levels imposed on the soil make it difficult to extend the results to strong seismic shaking levels.

The only well-defined case history involving strong motion records of soil-pile interaction is the recorded response of the pile foundation for the Ohba-Ohashi Bridge (Gazetas et al. 1993).

A list of physical modeling studies involving seismic response of pile foundations is given in Table 3-1. The amount of detailed physical data (field or model) on the seismic performance of pile foundations in soft or liquefiable soil is very limited. Many of these physical modeling studies are very recent, and represent the increased awareness of the potential damage to pile foundations after recent large earthquakes. A brief review of each modeling study is given below.

Cafe (1991) modeled the Struve Slough bridge on the Schaevitz centrifuge at UC Davis. The prototype structure suffered major damage during the 1989 Loma Prieta earthquake. The centrifuge model was a bridge deck supported on piles through a layer of peat, representing a section of the prototype structure that collapsed during shaking. A scale model of the structure was constructed using peat from the site of the failure. The centrifuge-testing program included large (0.48 g) shaking events.

Table 3-1: Physical Modeling Studies Related to the Seismic Behavior of Pile Foundations

Reference	Soil type	Super-structure?	Base motion	Shaking level (prototype)	Method
Finn & Gohl (1987)	dry sand	simple mass	seismic	0.15 g	centrifuge
Chang & Kutter (1989)	dry sand	2-story structure	seismic	0.24 g	centrifuge
Cafe (1991)	peat	bridge deck	seismic	0.05-0.48 g	centrifuge
Kobayashi et al. (1991)	liquefied sand	2-story structure	uniform cyclic	variable	shaking table
Rashidi (1994)	clay	2-story bent	seismic	0.18-0.30 g	centrifuge
Honda et al. (1994)	dry sand		seismic	0.02-0.20 g	centrifuge
Tokida et al. (1992)	liquefied sand	None	none	single impact load to induce liquefaction	1-g tank
Liu & Dobry (1995)	liquefied sand	None	uniform cyclic	0.06-0.40 g; pile loaded monotonically after shaking ends.	centrifuge
Abdoun et al. (1997)	liquefied sand	None	uniform cyclic	0.25 g	centrifuge
Horikoshi et al. (1997)	liquefied sand	None	uniform cyclic	0.15 g	centrifuge

Kobayashi et al. (1991) performed their tests using a large-scale shear bin (4 by 2 by 2 m) on a shaking table. They modeled a two-story structure supported on four piles that extended through liquefiable sand. The model was shaken with a sinusoidal base motion of constant frequency but progressively increasing amplitude.

Rashidi (1994) modeled a bent from the Cyprus Viaduct that also suffered damage during the Loma Prieta earthquake. His tests on the Schaevitz centrifuge at UC Davis involved a two-story bent supported on pile groups founded in soft clay. The model was subjected to several simulated large earthquakes of varying magnitude.

Tokida et al. (1992) performed 1-g model tests in a tank of liquefied sand using different pile group arrangements. The results indicate that the lateral resistance of liquefied sand depends on the pile group arrangement, loading rate, and excess pore pressure ratio in the sand.

Liu and Dobry (1995) performed centrifuge tests involving quasi-static cyclic displacement loading of a pile embedded in sand that was liquefied by prior shaking (i.e., the pile head loading was applied after shaking had stopped). The appropriate scaling factor for p-y resistance decreased more or less linearly with excess pore pressure ratio ($r_u=\Delta u/\sigma_{vo}'$) and reached a minimum value of about 0.1 when r_u=100%.

Abdoun et al. (1997; presentation notes at U.S-Japan Workshop in 1997) performed centrifuge tests to evaluate the lateral pressures exerted by laterally spreading liquefied sand on piles (no superstructure). Analyses of the test data were performed using p-y curve methods and focussed on the kinematic loads from the spreading ground; inertial loads could be neglected since there were no superstructures involved. Their results showed that a nonliquefied crust could dominate the kinematic loads imposed on a pile. In such cases, results were not sensitive to the assumed p-y resistance of the liquefied soil as long as it was sufficiently soft relative to the

crust and underlying firm layer. Their results also showed that lateral pressures from the liquefied sand were dependent on group effects, installation methods, and ground displacement levels.

Centrifuge tests by Horikoshi et al. (1997) evaluated the lateral pressures exerted by laterally spreading liquefied sand on a single 0.325-m (prototype) diameter pile (no superstructure). The net lateral pressures against the pile over its embedded length during lateral spreading were up to about 20-40 kPa depending on the test configuration.

These physical modeling studies demonstrate that the lateral resistance of liquefied sand depends on several factors. Variables that have been shown to, or are expected to, significantly affect the lateral resistance of liquefied sand include the following,

- Soil type
- Soil density (this study, as described in later sections)
- Loading rate (Tokida et al. 1992)
- Excess pore pressure ratio (Liu and Dobry 1995, Tokida et al. 1992)
- Group and cap effects (Tokida et al. 1992, Abdoun et al. 1997; notes of Abdoun and Dobry)
- Installation method (Abdoun et al. 1997; presentation notes of Abdoun and Dobry)
- Displacement level (this study, as described in later sections)

The behavior of piles in soil deposits with liquefiable layers can also be strongly affected by factors that include:

- Presence of a non-liquefied crust overlying the liquefied layer (Abdoun et al. 1997), or other stratigraphic details
- Magnitude of lateral spreading displacements
- Ground motion characteristics

The results of these studies illustrate the complexity of soil-pile interaction phenomena in liquefied soils, and provide data for evaluating the analysis and design methods used to represent the soil-pile interaction phenomena. Most of the published studies, however, did not include superstructures and thus do not provide data on the effect of soil-pile interaction on the dynamic response characteristics of pile-supported structures in soft or liquefied soils.

Thus, there remains a strong need for physical modeling data on the effect of soil-pile interaction on the dynamic response characteristics of pile-supported structures in soft clay or liquefied soils. In such soft-ground conditions, the fundamental period of the structure may be significantly affected by the compliance of the pile foundation. In addition, the reliability of assuming that the pile-head motion is the same as the anticipated "free-field" ground surface motion may be questioned. These and other concerns regarding the design of pile foundations in soft clay or liquefied ground are not addressed by the data available in the open literature.

3.2 Dynamic Response Analysis Methods

Evaluating the interaction of soil-pile-structure systems to earthquake ground motions is an important step in the seismic design of both the structure and piles. In the case of relatively flexible piles in stiff soils it may be reasonable to model seismic excitation of a structure using only free field ground surface motion applied to a set of springs at the pile head representing the stiffness of the foundation. In the case of stiff piers that penetrate through soft surface deposits and into a deep stiff soil layer, the free-field ground motions of the stiff layer may be a more appropriate input excitation to the structure. For other cases, it is important to have a procedure to account for the dynamic interaction between the various layers of soil, the pile, and the superstructure.

Various approaches have been developed for the dynamic response analysis of single piles, including the finite element method (Kuhlemeyer 1979; Angelides and Roesset 1980; Randolph 1981; Faruque and Desai 1982) and the boundary element method (Sanchez 1982; Sen et al. 1985), which both treat the soil media as a continuum. The discretization of a three-dimensional continuum generates a multitude of degrees of freedom rendering the method impractical for the design of anything but extremely expensive structures (e.g., large toll bridges or major port facilities). The Beam on Nonlinear Winkler Foundation (BNWF) method is a simplified approach that can account for nonlinear soil-pile-structure interaction, and has proven useful in engineering practice (Abghari and Chai 1995). Trochanis et al. (1991) showed that the response of laterally loaded piles predicted using a BNWF formulation agreed well with static load test data and nonlinear 3-D finite element analyses. Trochanis et al. (1991) used a degrading constitutive model developed by Wen (1976) to represent the nonlinear soil-pile (p-y) springs.

The Winkler assumption is that the soil-pile interaction force at any depth is related to the pile shaft displacement at that depth only, independent of the interaction forces above and below. In the BNWF method, the pile itself is modeled as a series of beam-column elements, each with discrete springs connecting the pile to the soil. In addition to lateral support (p-y) springs, longitudinal support (t-z) springs may be included. In a program called SPASM ('Seismic Pile Analysis with Support Motion'), Matlock et al. (1978) extended the BNWF concept to seismic problems by calculating the ground motion time histories along the depth of the soil profile and then applying the ground motion time histories to the p-y springs as excitation to the system. Kagawa (1980a) further extended the BNWF analysis to seismic problems by including viscous dashpots in parallel with the nonlinear p-y springs to model the effects of radiation damping (Figure 3-1). This method of including radiation damping is termed "parallel radiation damping". The concept of "parallel radiation damping" has been used by Badoni and Makris (1996) and in practice (PMB 1988, Abghari and Chai, 1995).

Novak and Sheta (1980) and Nogami et al. (1992) studied the soil-pile-structure system for cases where the dynamic load is applied at the pile head or superstructure. They recognized that the soil around the pile shaft should be separated into different zones; i.e., the near field (plastic zone), where strong nonlinear soil-pile interaction occurs, and the far field, where the behavior is primarily linear elastic. This would be best modeled by "series radiation damping", a name coined herein to describe a nonlinear hysteretic element in series with a linear visco-elastic element (i.e., the hysteretic and viscous damping components are in series). Series radiation damping makes sense because stress waves radiating from a pile do not bypass the plastic zone; they must first be transmitted through the hysteretic element before being radiated into the far field. "Series radiation damping" is based on the model shown in Figure 3-2. The far field (approximately elastic) element includes radiation damping; the near field element incorporates the hysteretic damping through nonlinear p-y relationships. In the case of strong seismic loading, the situation is further complicated by nonlinearity in the far field site response. The polarity of the S waves in the free field (τ_{xz} and τ_{yz} shear stress waves) is different from the τ_{xy} stress waves and P waves that would be expected to emanate from a pile. Because of the difference in polarity, uncoupling the nonlinear free field response calculation from the nonlinear soil-pile interaction may be a reasonable approximation. It should be noted that Nogami and Konagai (1986) also suggested that the far field elements could consist of multiple linear spring dashpot pairs in order to more accurately model the frequency dependence of radiation damping. To permit simple comparisons between various calculations, the refinement of multiple spring-dashpot pairs was not included in the present report.

In the theory of plasticity, deformations are decomposed into elastic and plastic

components: $y = y^e + y^p$ (Figure 3-3). Gazetas and Dobry (1984a, 1984b) obtained radiation dashpot coefficients based on linear elastic models of a continuum. As they are based on elasticity concepts, these dashpots should act on the component of the deformation produced by the elastic spring, y^e. The load capacity of a plastic (hysteretic) spring in parallel with a linear viscous dashpot is rate dependent. While rate dependent load capacity is not unrealistic, it should be treated independently from the linear viscous dashpots used to simulate radiation damping. "Series radiation damping" provides a convenient means to independently treat hysteretic damping and viscous (radiation) damping.

Dashpot coefficients for representing radiation damping have been proposed by Berger et al. (1977) and Gazetas and Dobry (1984a; 1984b). Berger et al. (1977) assumed that the horizontally moving pile cross section only generates 1 dimensional P-waves traveling in the direction of shaking and 1 dimensional SH waves traveling perpendicular to the shaking as shown in Figure 3-4a. Consequently, the dashpot coefficient (c) is derived to be:

$$c = 2 B \rho (V_s + V_p)$$

where V_s is the shear wave velocity, V_p is the P-wave velocity, B is the pile width, and ρ is the soil density. For undrained analyses of clay, the soil is nearly incompressible, and the P-wave velocity can become large. In such cases, the above equation can lead to excessive damping. To avoid this, the Berger model has been modified to (PMB Engineering 1988):

$$c = 4 B \rho V_s$$

A more rigorous solution was given by Novak et al. (1978) for the dynamic stiffness for an infinitely long rigid massless cylinder embedded in an infinite elastic medium subject to harmonic motion (Figure 3-4b). A simpler explanation of radiation damping of a horizontal moving pile foundation was derived by Gazetas and Dobry (1984a, 1984b), by assuming that compression-extension waves propagate in the two quarter-planes along the direction of shaking and SH-waves propagate in the two quarter-planes perpendicular to the direction of shaking. By recognizing the fact that no perfect constraints in the two directions other than the direction of the compression-extension waves, Gazetas and Dobry recommended the use of Lysmer's analog "wave-velocity" instead of V_p for compression-extension waves. (Figure 3-4c).

Four different implementations of the BNWF approach were selected for evaluation in this study:

1. PAR — Pile Analysis Routine, PMB Engineering Inc. (1988).

2. NONSPS — NONlinear Soil-Pile-Structure, Kagawa (1983).

3. DRAIN-2D — Dynamic Response Analysis of INelastic 2D structures, Version 1.10, Prakash and Powell (1993).

4. GeoFEAP — Geotechnical Finite Element Analysis Program (Bray et al. 1997).

PAR is a commercial code with a user interface, options for automatic generation of p-y curves, a simple gap model, and cyclic degradation of p-y curves. NONSPS is a research code that can account for effective stresses, pore pressure generation, and cyclic degradation of p-y curves. Both PAR and NONSPS use "parallel radiation damping" as default, but can be made to use "series radiation damping" by experienced users. DRAIN-2D is a more general structural engineering code; it is well documented, has a rich element library, and the source code is available. GeoFEAP is a more flexible finite element platform that seems to offer the most flexibility for modifying new elements to account for the effects of liquefaction on soil-pile-

structure interaction, and has thus been adopted in our continuing efforts.

A major input to the BNWF calculation is the dynamic motions of the free field soil column. After all, the free field motions represent the input excitation to the BNWF analysis. In the BNWF approximation, the free field motions are uncoupled from the pile motions, hence free field motions may be calculated by any desired method (e.g., SHAKE, a nonlinear site response analysis, or even 2- or 3-D site response analyses). NONSPS, however, is presently linked to a specific site response program called SRANG (Kagawa, 1980b). SRANG assumes either hyperbolic or Ramberg-Osgood stress strain relations, and the shape of the p-y curves in NONSPS is related to the shape of the stress-strain curves in SRANG. In any case, the reliable calculation of dynamic site response remains a difficult task when dealing with soft or liquefiable soils under strong levels of shaking, and the resulting uncertainties will remain an important issue when predicting the dynamic response of pile-supported structures.

In summary, there are several existing computer programs that can be used for analyzing the dynamic response of pile-supported structures, but these programs all have serious limitations for the case of soft or liquefied ground conditions. The two main concerns are the ongoing difficulty in reliably estimating ground motions during strong shaking events (e.g., the free-field response problem) and the uncertainty in representing soil-pile interaction during strong shaking events. The consequence of these uncertainties can only be evaluated by comparing analysis results against physical data, and thus is further incentive for the physical modeling efforts undertaken by this study.

3.3 Simplified Pseudo-Static Analysis Methods for Piles in Liquefied Soil

Simplified pseudo-static analysis methods have been proposed for the design of pile foundations in liquefied soil, as reviewed by Tokimatsu et al. (1997). Three types of loading conditions were examined: (1) inertial force only; (2) inertial force and kinematic loading; and (3) kinematic loading only. Inertial forces are those expected from the superstructure alone, and depend on the ground motions (as affected by liquefaction), and thus must be estimated by some independent analysis method (as described in the previous section). Kinematic loads were generally represented by assuming that the ground displacement profile varied linearly with depth across the liquefied layer. The assumed ground displacement profile was then applied to the free-field ends of the p-y springs, with the p-y springs being reduced for the effects of liquefaction (as described below). The three load cases illustrated the relative importance of kinematic versus inertial loading. Furthermore, the peak inertial loading would not be expected to occur at the same time as the peak kinematic loading.

Current methods for representing the lateral resistance of liquefied soil are only crude approximations because the fundamental mechanisms of soil-pile interaction in liquefied soils are poorly understood. Three different approaches have been proposed. First, the lateral resistance of liquefied soil may be represented as a scalar multiple of its static drained lateral resistance. Scaling of static p-y curves has been used by the Architectural Institute of Japan (AIJ 1988) and the Japan Road Association (JRA 1980), as summarized in Tables 3-1 and 3-2. Liu and Dobry (1995) derived scaling factors from centrifuge model tests, and suggested that the scaling factor would vary linearly with excess pore pressure ratio (r_u) and have a minimum value of about 0.10 when r_u=100%.

A second approach for representing the lateral resistance of liquefied sand is to treat it as a material with an undrained residual shear strength (ϕ_u=0). This approach predicts that the ultimate lateral resistance of liquefied soil (with constant undrained shear strength) is roughly a

constant below a certain depth. This aspect seemed to be a reasonable representation of the physical model data presented for piles in laterally spreading ground by Abdoun and Dobry (Abdoun et al. 1997; presentation notes).

The third approach is to represent the effect of laterally spreading liquefied soil as a lateral pressure against the pile. This lateral pressure is commonly assumed to increase linearly with depth. Within the liquefied zone, the pile is no longer connected to any p-y spring supports. Thus, this approach is intended to represent the effects of lateral spreading on piles, and cannot be realistically used for modeling dynamic response.

The preceding three approaches for representing the lateral resistance of liquefied soil have been evaluated against several cases from Kobe, such as described in the presentations by Koseki, Fujii, and Tokimatsu at a recent U.S.-Japan Workshop. None of the three approaches had proven entirely satisfactory in distinguishing between cases of damage versus no damage for those sites that provided such a contrast in performance. However, these cases have many complicating factors, such as differences in superstructures, basements, and ground displacement levels. In addition, it was recognized that the reliability of these approaches for representing lateral resistance of liquefied soil may simply be limited by the fact that they are approximations of a rather complex phenomena that is poorly understood. For example, these three approaches were noted to give different distributions of lateral pressure versus depth, and hence predict different variations in bending moment versus depth. Additional studies are continuing to evaluate the reliability of these approaches by further comparisons with the growing database of documented cases from the Kobe earthquake.

Table 3-1. Scaling factor r_k on coefficient of lateral soil reaction for highway bridge foundations (Japan Road Association 1990; from Matsui 1993). Note: F_L is the factor of safety against liquefaction.

F_L-value	Depth of layer z(m)	Reduction factor r_k
$F_L \leq 0.6$	$0 \leq z \leq 10$	0
	$10 < z \leq 20$	1/3
$0.6 < F_L \leq 0.8$	$0 \leq z \leq 10$	1/3
	$10 < z \leq 20$	2/3
$0.8 < F_L \leq 1.0$	$0 \leq z \leq 10$	2/3
	$10 < z \leq 20$	1

Matsui (1993)

Table 3-2. Scaling factor r_k on coefficient of lateral soil reaction for building foundations (Architectural Institute of Japan 1988; from Matsui 1993).

F_L-value	Depth of layer z(m)	Reduction factor r_k			
		$N_a \leq 8$	$8 < N_a \leq 14$	$14 < N_a \leq 20$	$20 < N_a$
$F_L \leq 0.5$	$0 \leq z \leq 10$	0	0	0.05	0.1
	$10 < z \leq 20$	0	0.05	0.1	0.2
$0.5 < F_L \leq 0.75$	$0 \leq z \leq 10$	0	0.05	0.1	0.2
	$10 < z \leq 20$	0.05	0.1	0.2	0.5
$0.75 < F_L \leq 1.0$	$0 \leq z \leq 10$	0.05	0.1	0.2	0.5
	$10 < z \leq 20$	0.1	0.2	0.5	1

Note : N_a is the corrected N-value in SPT according to effective overburden pressure and fines content.

Matsui (1993)

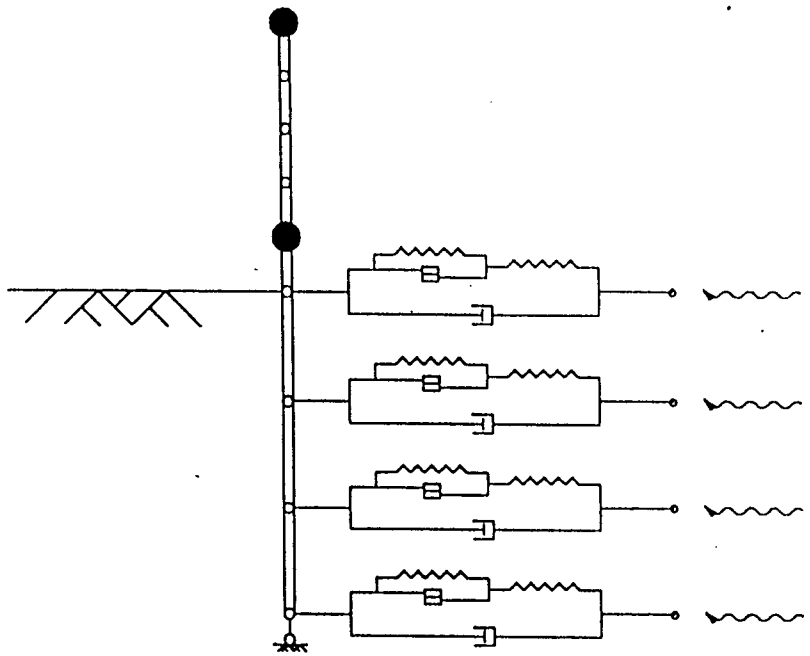

Fig. 3-1. Soil-Pile-Structure Model with Parallel Hysteretic/Viscous Damping

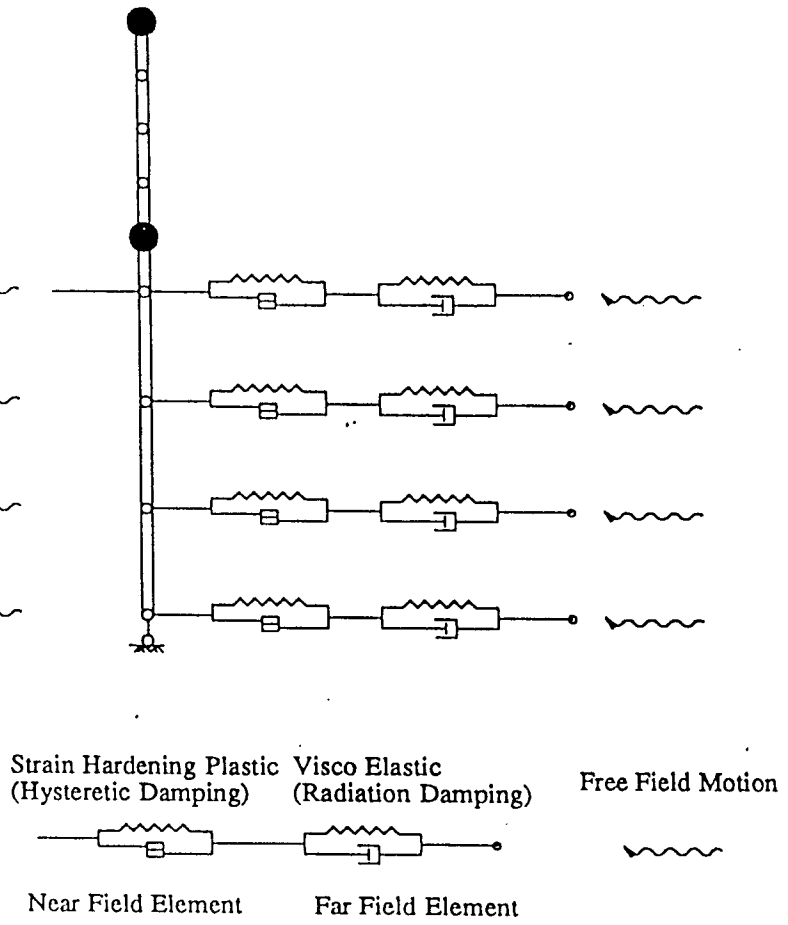

Fig. 3-2. Soil-Pile-Structure Model with Series Hysteretic/Viscous Damping

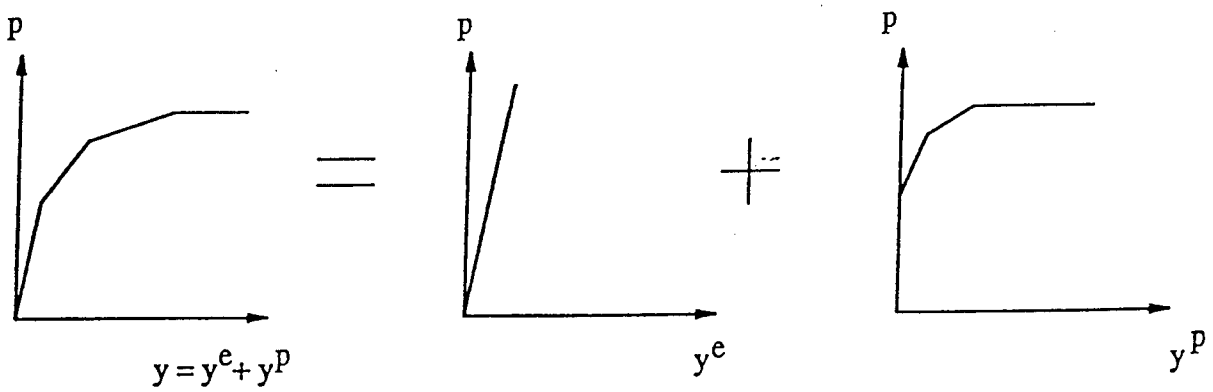

Fig. 3-3: Decomposition of p-y curve into elastic and plastic components

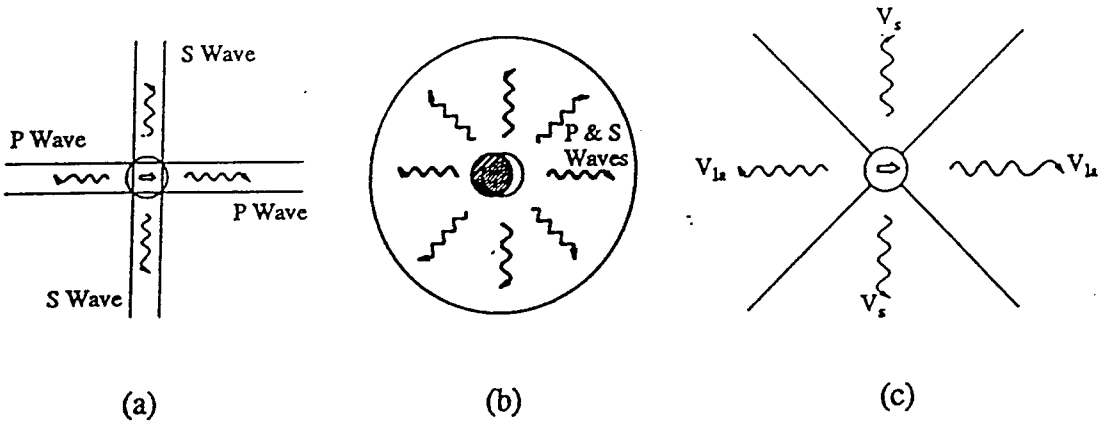

Fig. 3-4: Radiation damping of horizontally vibrating single pile
(a) Berger et al. (1977); (b) Novak et al. (1978)
(c) Gazetas and Dobry (1984);

4 CENTRIFUGE TESTING OF PILES UNDER SEISMIC LOADING

4.1 DYNAMIC CENTRIFUGE TESTS AT UCD

4.1.1 Description of the Small Schaevitz Centrifuge and Model Layouts

Two dynamic centrifuge model experiments were performed using the servo-hydraulic shaker (Chang 1990) on the small 1-m radius Schaevitz centrifuge at U.C. Davis. These tests modeled single-pile-column structures embedded in soft clay profiles. The data were used in evaluating different numerical analysis methods (Chacko 1995, Wang et al. 1997) while development of the large centrifuge shaker progressed.

The hinged plate container (Fiegel et al. 1994) was used to provide shear beam boundary conditions to the soil. Tests were performed on samples of normally consolidated San Francisco Bay Mud with a "crust" of dense sand on the surface of the clay. A single pile with an elevated superstructure was modeled using an aluminum tube and superstructure mass. The centrifuge tests were performed at a centrifugal acceleration of 50 g. Several earthquake events were then applied to the base of the centrifuge container with sufficient time between events for any induced excess pore pressures to dissipate.

The procedures used to perform these tests and typical experimental results are presented in the section, "Dynamic Analysis of Piles." The complete set of experimental data can be found in Chacko (1994).

4.1.2 Description of the Large NGC Centrifuge and Model Layouts

The National Geotechnical Centrifuge at UC Davis has a radius of 9 m and is equipped with a large shaking table driven by two servo-hydraulic actuators (Kutter et al. 1994). The earthquake simulator was recently completed with funding from the National Science Foundation, Obayashi Corporation, Caltrans and the University of California. The centrifuge has a maximum payload mass of 4500 kg, an available bucket area of 4.0 m^2, and a current maximum centrifugal acceleration of 53 g. The new earthquake simulator was designed to accommodate 1.75 m long models and provide 15 g shaking accelerations to 2700 kg payloads. Earthquake motions are produced by a pair of servo-hydraulic actuators acting in parallel, one mounted on either side of the model container. Details of the centrifuge and the new earthquake simulator are given by Kutter et al. (1991) and Kutter et al. (1994), respectively.

A new Flexible Shear Beam (FSB1) container was designed and constructed for this project. The new FSB1 container has inside dimensions of 1.72 m long, 0.685 m wide, by 0.70 m deep. FSB1 consists of six hollow aluminum rings separated by 20 durometer neoprene. The mass of each of the upper three rings is about one-half the mass of each of the lower three rings. The combined mass of the six rings is about 25% of the soil profile mass (assuming the container is full of soil). The amount of neoprene separating the rings is varied such that the shear stiffness of the container increases with depth. The shear stiffness of the neoprene also varies with strain level (Stewart et al. 1997), such that the fixed base natural frequency of the empty container is about 15-20 Hz for the larger shaking events presented herein. Complementary shear stresses are provided at the ends of the container by vertical shear rods in the soil near the container ends (Divis et al. 1997). A schematic of the rings, neoprene layers, and shear rods is shown in

Figure 4-1.

The experimental program progressively evolved as a result of our meetings, and reflected changes in response to new findings or needs within Caltrans. Comparing the final experimental layouts with the original proposal, the decision was made to go with fewer model structures, more shaking events covering a wider range of frequency content and intensity, and a far greater level of instrumentation detail within each experiment.

Five containers of soil-structure systems were tested on the large centrifuge. Full details for each centrifuge test can be found in Wilson et at. [1997 (a-e)]. Raw data from each test are available on diskette (100-Megabyte "zip" disk) to any interested party upon request; copies have been transmitted to Caltrans with this report. All tests were performed at a centrifugal acceleration of 30 g. Note that the centrifugal acceleration varies with radial position, and thus varied from 29.2 g at the soil surface to 31.5 g at the container base. All results are presented in prototype units unless otherwise noted. For details of the applicable scaling laws, see Kutter (1995).

The soil profiles used in the five containers are summarized in Table 4-1. In all cases, the soil profile consisted of two horizontal soil layers. The lower layer for all tests was dense Nevada sand, a fine, uniform sand (C_u=1.5, D_{50}=0.15mm). The upper layer was medium-dense Nevada sand in Csp1 and 3, loose Nevada sand in Csp2, and normally consolidated (NC) reconstituted Bay Mud (LL≈90, PI≈40) in Csp4 and 5. In all tests the sand was air pluviated, subjected to a vacuum (typically achieving about a 90 kPa vacuum), flushed with carbon dioxide, and then saturated under vacuum. Pore fluid was water or a hydroxy-propyl methyl-cellulose (HPMC)-water mixture having a viscosity ten times that of water alone. Note that the pore fluid's viscosity was increased to improve the simultaneous scaling of consolidation and dynamic processes. In these tests, the 10-fold increase in pore fluid viscosity and the 1/30th scale modeling can be viewed as having the net effect of causing the sand's prototype permeability (assuming pure water for the prototype's pore fluid) being 3 times greater than the sand's actual permeability (for pure water as the pore fluid). Saturation was confirmed by measuring p-wave velocities from top to bottom of the soil profile near the container center.

Table 4-1 - Summary of Soil Profiles

Container	Soil profile		Pore fluid
	Upper layer (9.1 m thick)[a]	Lower layer (11.4 m thick)	
Csp1	Sand (D_r≈55%)	Sand (D_r≈80%)	Water
Csp2	Sand (D_r≈35-40%)	Sand (D_r≈80%)	HPMC-water
Csp3	Sand (D_r≈55%)	Sand (D_r≈80%)	HPMC-water
Csp4 & 5	Reconstituted Bay Mud (NC)	Sand (D_r≈80%)	Water

[a]Upper layer was only 6.1 m thick (prototype) in Csp4 & 5.

The structural systems in each of the five containers are illustrated in Figures 4-2 to 4-6. Detailed drawings of each structure are given in Wilson et al. [1997 (b-f)]. Foundation models include single pile foundations, four-pile groups, and nine-pile groups. The superstructure mass was typically about 440 kN (prototype) per each supporting pile; i.e., 440 kN for a single-pile-supported structure, and 1760 kN for a four-pile-group supported structure. All piles approximated a prototype steel pipe pile 0.67 m in diameter, 16.8 m long, with a 19 mm wall

thickness. To represent typical bridge fundamental periods, column heights were selected to give fundamental periods for the structural systems ranging from 0.5 to 1.0 seconds. For all structural models, the pile tips were about 3.7 m above the container base (about 5.5 pile diameters); thus the end bearing of the piles should not have been significantly influenced by the container base.

Piles were driven into the sand at 1-g. Driving was done by dropping hammers from constant drop-heights onto the superstructure masses. A guide rod kept the hammer impact centered on the superstructure mass and a guide bar kept the piles aligned horizontally and vertically. Hammer blows per 2.54 cm (1 inch) of penetration were recorded.

Each container was subjected to a series of shaking events, beginning with very low-level shaking events to characterize the low-strain response the soil and soil-structure systems. Successive events progressed through very strong motions with peak base accelerations of up to 0.6 g. Earthquake events generally were sequenced in order of increasing amplitude, with periodic repeats of smaller events. Input base motions included step waves, and scalar multiples of motions recorded in the Kobe and Loma Prieta earthquakes. Each shaking event was separated by an amount of time that exceeded the time required for full dissipation of any excess pore pressures. All in all, the first three containers (all sand profiles) were subjected to 16 to 17 shaking events each, while the fourth and fifth containers (upper layer of clay) were subjected to five shaking events each.

4.2 Development of Signal Processing Procedures

Signal processing and integration methods were developed for calculating displacement time histories from acceleration time histories. The development of a reliable procedure for double-integration of accelerometers was necessary to: (1) evaluate the deformed shape of the free-field soil profile, which forms an essential input to several of the analysis methods; and (2) evaluate aspects of the modeling system such as container effects, container rocking, and coherency of motions.

There are many different ways to filter the acceleration records before integration, including causal and non-causal filters in both the time and frequency domains. Calculated displacements are very dependent on low frequency values of accelerations (displacement spectrum is acceleration spectrum divided by the frequency squared), and thus the procedure for high-pass filtering was of particular importance for calculating displacement time histories. The accelerometers used, like most accelerometers used in dynamic applications, are not capable of accurately recording very low frequencies. Below some frequency, high-pass analog filters are needed to prevent drift. These high-pass analog filters will corrupt the signals near their corner frequencies. Thus, digital high-pass filtering is required to eliminate the corrupted low-frequency information. Low-pass filtering of high frequency noise is accomplished with anti-aliasing analog filters on the large centrifuge, and thus digital low-pass filtering of the recorded time histories was not needed.

The determination of how much low frequency signal is noise and how much is real signal is at best an art. There are over 1400 acceleration time histories in this suite of tests, so looking at each individually was not deemed reasonable. Fortunately, the noise characteristics are generally similar in all acceleration time histories because they all (with few exceptions) come from the same accelerometer type and pass through the same electronic components before being recorded. Thus, a single high-pass corner frequency was selected for mass-processing of all the acceleration time histories. Selection of the optimum high-pass corner frequency was based on detailed analyses of representative recordings, and the following considerations.

1) The input base motions had been high-pass filtered at about 0.3 Hz to reduce the peak displacements to values that the shaker could physical accommodate. Consequently, there is little input motion below this frequency from the shaker.
2) Fourier spectra of acceleration time histories almost always had a sharp drop-off in spectral amplitude at about 0.1 Hz, and the spectral amplitude progressively increased below that frequency (a common characteristic of accelerometer noise; as illustrated in Figure 4-7). Integration of the acceleration time histories resulted in calculated displacements that were dominated by very large, low frequency drifts unless the spectral content below about 0.1 Hz was filtered out.
3) Several instrumentation "tests" were performed where pairs of accelerometers were placed on opposite ends of a linear potentiometer that was measuring the relative displacement between two objects on the centrifuge. Integration of the accelerometers gives absolute displacements, and thus the relative displacement could be obtained by subtracting the two integrated time histories. The relative displacement time histories recorded by the linear potentiometers could then be compared to those obtained by double-integrating the accelerometers. The best average agreement between the potentiometers and accelerometers was obtained using a corner frequency of about 0.15 Hz.
4) High-pass filtering with a 10^{th} order Butterworth filter applied only to the spectral magnitudes (acausal filter) was found to perform better than lower order Butterworth filters (e.g., a 4^{th} order filter is common). This evaluation is based on comparisons of calculated displacements with linear potentiometer recordings in the various instrument tests, as described above. This relatively "steep" filter appears to work best because of the acceleration spectra also have steep drop-offs with narrow windows of frequencies over which the spectral amplitudes are very small.

Several limitations on calculating displacements by integrating acceleration time histories should always be recognized.

1) Permanent displacements cannot be calculated using the acceleration recordings. The currently-used accelerometers are incapable of recording the very low frequencies required for calculating permanent displacements. Any real signal related to permanent displacement is obscured by noise, and thus removed by the high-pass filtering.
2) Each integrated displacement time history should be examined individually. The "default corner frequency" used to mass-process all acceleration time histories may not be the best choice for an individual recording (either passing too much noise or removing too much real signal).

Figures 4-8 and 4-9 show comparisons of displacement time histories obtained by integrating acceleration time histories versus recorded with linear potentiometers. Both figures show results for a range of corner frequencies. Figure 4-8 is for a case where no permanent deformations occurred, and illustrates the very good agreement obtained in such cases. Figure 4-9 is for a case with significant permanent deformations, and illustrates how the accelerometers captured the transient deformations but not the permanent deformations. Numerous comparisons such as shown in this figure provided an appreciation of this limitation on displacements obtained by integrating accelerometers.

4.3 Evaluation of the Centrifuge Modeling Techniques and Systems

4.3.1 Issues of Concern

The dynamic centrifuge tests of pile-supported structures in soft or liquefied soils performed in this study were among the first performed using the recently completed shaking table, and thus it was necessary to evaluate the centrifuge modeling system before analyzing the model structures. The importance of characterizing the centrifuge modeling system was demonstrated by the VELACS cooperative study (e.g., Arulanandan et al. 1994) and further discussed by Scott (1994). Difficulties or limitations with dynamic centrifuge modeling systems can include: (1) non-repeatability of model tests; (2) undesirable vertical motions; (3) inability to produce input motions with the broad frequency content of real earthquake motions; and (4) container effects. These and other aspects of the dynamic centrifuge modeling system on the large centrifuge at U.C. Davis are evaluated using the results of the soil-pile-superstructure interaction experiments. Quantifying these modeling limitations was considered essential before using the data to evaluate seismic design methodologies for pile-supported structures.

4.3.2 Uniformity of Sand Layers

The density, uniformity, and repeatability of sand layers were evaluated by measuring the force required to push a 6 mm diameter rod with a 60° conical tip at various locations while at 1 g (Divis et al. 1994). The force was divided by the tip area and presented as a penetration resistance (Q), although it is noted that Q reflects both tip and shaft resistances. Results of penetration tests on Csp3, after the pile groups were driven into the sand at 1 g, are shown in Figure 4-10. Tests in the free field showed nearly uniform profiles of Q, with Q being much higher in the lower dense layer than the upper loose layer. Three tests were located alongside the 2x2 and 3x3 pile groups, and these showed substantial increases in Q due to pile driving. Two tests were pushed between the piles of the 2x2 and 3x3 groups (through holes in the caps), and these showed even greater values of Q, particularly in the 3x3 group. Interpretation of these penetration tests is complicated by the low confining pressures (at 1 g), the mix of shaft and tip resistances, the relatively large zone of influence of the tip (e.g., 10-20 probe diameters is 9-18% of the total soil thickness), and the influence of the boundaries. Nonetheless, these data are a valuable indicator of specimen density and uniformity, and were useful for evaluating the pile installation effects.

4.3.3 Input Motions

Two important aspects of centrifuge input motions are: (1) the input motion should contain a reasonably full spectrum of earthquake frequencies for realistic dynamic modeling of pile-supported structures; and (2) the frequency content of the input motion should be reasonably unchanged when scaling the acceleration magnitude to minimize difficulties with evaluating nonlinear behavior between scaled shaking events. Note that gaps in the frequency content of input motions are a limitation of many dynamic centrifuge tests (Scott 1994).

The performance of the shaking table is shown in Figure 4-11. Each container was shaken with several simulated earthquake events, each being a scaled version of a record prepared by integrating and filtering strong motion records from Port Island (83 m depth) in the Kobe Earthquake or Santa Cruz in the Loma Prieta Earthquake. Acceleration response spectra (ARS,

5% damping) of the east and west base input motions recorded during three scaled Kobe events (a_{max}≈0.04, 0.23, and 0.6 g prototype) on each of three containers (total of nine events) are shown in Figure 4-11, with the ARS normalized to a zero period value of one on the east actuator. The ARS are very similar at each level of shaking, and show only small spectral variations across the full operational range of the shaker (i.e., a_{max}≈0.04 to 0.6 g prototype corresponds to a_{max}≈0.12 to 18 g model for a centrifugal acceleration of 30 g). East and west base motions are also seen to be closely in-phase and parallel, as shown at the bottom of Figure 4-11 by the nearly identical acceleration time histories during a typical Kobe event. The ARS of the original recording from Port Island is shown in Figure 4-11 for comparison. The base motions retain the full frequency spectrum of the original recording in the range of interest (0.5-5 Hz prototype in this study), with the differences at higher and lower frequencies partially due to low and high pass filtering performed in creating the centrifuge input motion.

4.3.4 Effect of Pore Fluid Viscosity

The effect of changing pore fluid viscosity was evaluated by comparing results from Csp1 and Csp3 for four comparable shaking events. Note that results from these tests are described in detail in later sections of this report, while select results are used here to address issues related to the centrifuge modeling techniques. These containers had identical soil profiles and an identical single-pile-supported structure [model details in Wilson et al. 1995, Boulanger et al. 1997, Wilson et al. 1997 (b) and (d)], but the viscosity of the pore fluid differed by a factor of 10 (Table 4-1). The responses of the soil profile and single-pile-supported structure were very similar for comparable shaking events except as follows. The rate of pore pressure dissipation was always faster in Csp1 than in Csp3, as illustrated in Figure 4-12 by pore pressure time histories at similar locations during a Kobe event with $a_{max,base}$≈0.23 g. During shaking, however, the pore pressures increased at similar rates and underwent similar rapid changes. ARS for various locations in the upper sand layer in Csp1 and Csp3 also had similar normalized shapes, although Csp1 consistently had slightly greater spectral accelerations near a period of one second and slightly lower spectral accelerations at shorter periods. It was noted that comparisons of individual measurements for one comparable shaking event often showed slight differences, but comparisons of several instruments for several events were required to evaluate whether such slight differences followed a consistent trend. The slight differences between the responses in Csp1 and Csp3 were likely due to a combination of factors, including slight variations in soil densities, model preparation techniques, input motions, and the different pore fluids used.

The response of the single pile system during these same events is illustrated by bending moment time histories at depths of 3.8 and 5.3 m in Figure 4-13. Bending moments were normalized by the peak superstructure acceleration because the peak superstructure acceleration in Csp1 was about 50% greater than in Csp3. The difference in superstructure accelerations is due to both a 20% difference in the peak base input motion and the previously described differences in the soil profile ARS at the natural period of the structure (about one second). Normalized bending moments for this single pile system in Csp1 and Csp3 show very little difference during shaking, but do show interesting, although inconsequential, differences developing after shaking because of the different dissipation rates for excess pore pressures. Comparing bending moment time histories at other depths and other levels of shaking also gave very similar results, and thus the bending moment distributions at any time were essentially the same in Csp1 and Csp3. These results suggest that changing pore fluid viscosity by a factor of

10 had only minor effects on the soil-pile interaction.

4.3.5 Effect of Upper Soil Layer

The effect of the upper soil layer on structural response and bending moment distribution is illustrated by a comparison of results from Csp2, 3, and 4 (Table 4-1). Results from these tests are described in detail in later sections of this report, while select results are used here to illustrate issues related to the centrifuge modeling techniques. In Figure 4-14(a), the bending moment distributions versus depth are shown for an identical single pile system in Csp2, 3, and 4 during a Kobe event with $a_{max,base} \approx 0.23$ g. In Figure 4-14(b), these bending moments are normalized to a ground surface moment of unity. Note that liquefaction was more extensive in Csp2 than in Csp3 during these events, as evidenced by pore pressure time histories showing that pore pressures increased much quicker, and dissipated slower, in the $D_r \approx 35\%$ sand layer of Csp2 than in the $D_r \approx 55\%$ sand layer of Csp3 (Figure 4-15). The looser condition of the upper layer in Csp2, relative to Csp3, resulted in generally lower ground surface accelerations, lower peak superstructure accelerations, and a greater apparent softening of the liquefied soil's p-y resistance (Boulanger et al. 1997); these aspects of behavior are shown by the smaller bending moment at the ground surface [Figure 4-14(a)], but a greater depth to peak bending moment [Figure 4-14(b)]. In Csp4 (upper layer of soft clay), the peak superstructure acceleration was lower than that of Csp2 and 3, and the depth to peak bending moment was comparable to that of Csp2. These data are consistent with the expected effects of soil conditions on site response and soil-pile-superstructure interaction for the input motion used in these tests.

4.3.6 Behavior of the Container and Soil Column System

The dynamic characteristics of a model container and its interaction with the soil column must be clearly understood if reliable interpretations of test results are to be made. Container effects on the soil column response have been studied using several different measurements of response (e.g., Fiegel et al. 1994, Van Laak et al. 1994, Whitman and Lambe 1986). In this study, the interaction is evaluated in terms of the coherency of horizontal motions and differential vertical displacements in the soil near the container ends.

The coherency of horizontal motions across the soil column and container rings indicates whether the container and soil are moving in unison during shaking. To measure coherency, accelerometers were attached to the individual rings of the FSB1 container and at corresponding depths near the center and corners of the soil profile. Accelerometer records were high-pass filtered and double integrated to get displacements. The accuracy and reliability of these procedures were demonstrated by placing accelerometers on opposite sites of displacement transducers and comparing the calculated and recorded relative displacement time histories. Results for several shaking events on each container show that horizontal acceleration and displacement time histories are nearly identical (i.e., highly coherent) at any given elevation in the soil column and on the corresponding container ring for tests involving nonliquefied sand or low shaking levels with soft clay.

Horizontal motions at shallow depths in Csp1 during a Kobe event ($a_{max,\,base} \approx 0.23$ g) causing liquefaction of the $D_r \approx 55\%$ layer late in shaking are shown in Figure 4-16. Accelerations at the soil surface near the center and one end of the model, and on the top ring, are seen to have similar waveforms but with differing high frequency contents later in shaking.

In particular, several large high-frequency acceleration spikes were recorded near the end of the container. However, horizontal displacements relative to the container base at these three points were relatively uniform (bottom of Figure 4-16).

Spikes in acceleration records from centrifuge tests with liquefied soils have been observed by several investigators, while they have been less obvious in field data. In our tests, acceleration spikes have been observed throughout liquefied layers, near the middle and ends of the container, and in horizontal and vertical directions. Acceleration spikes have not been observed when the excess pore pressure ratio is less than about 70%. Acceleration spikes coincide with rapid pore pressure drops, and thus are likely due to the uniform soil profile "locking" up all at once as the sand goes through a phase transformation (i.e., the transition from contractant to dilatant behavior). Additional research, however, is needed to evaluate potential instrumentation effects, such as a local interaction between the instrument and liquefied soil. It should also be noted that these high frequency acceleration spikes have a lesser effect on the velocities, displacements and kinetic energy in the soil profile and structural models.

Horizontal motions at shallow depths in Csp2 during a Kobe event ($a_{max, base}$≈0.23 g) causing liquefaction of the D_r≈35% layer are shown in Figure 4-17. Accelerations at the surface of the soil near the center of the container were very different than the acceleration of the top ring. Furthermore, the displacements of the top ring and the soil relative to the container base were very different, at times nearly 180° out of phase. In this case, when r_u was high and D_r was low, the soil column became much softer than the container, as shown by the predominant frequency content of recorded motions in the profile and on the container. As a result, the container restricted lateral movements near its edge. While this is not ideal, it is physically difficult to avoid and may be incorporated into numerical analyses if necessary. Coherency of horizontal motions, however, improved with depth in the liquefied soil layer. This is illustrated at the bottom of Figure 4-17 by the horizontal displacements relative to the container base for two locations at the same elevation deeper in the liquefied layer.

A similar set of plots from Csp4 for a Kobe event ($a_{max,base}$≈0.23 g), where the upper soil was normally consolidated clay, are shown in Figure 4-18. In this case, however, the top ring was empty and the soil surface was level with the second ring. The upper plot shows the difference between displacements at the surface center of the soil profile and the second ring relative to the container base. The lower plot, however, shows that by the third ring, the container and the soil are moving mostly together.

In addition to the container moving with the soil, the soil profile should also deform in shear as opposed to column bending. In shear, there is no vertical strain when the soil profile deforms horizontally, while column bending will cause one side to compress and the other to extend. The container should help minimize column bending by providing complementary shear stresses at the end interfaces between the soil and the container. Discussions of the role of complementary shear stresses and rocking in centrifuge modeling can be found in Whitman and Lambe (1986) and Scott (1994).

In Csp2 (D_r≈35% upper layer), vertical accelerometers were included at the north and south ends of the model container base and top ring, and near the bottom and top of the soil profile (total eight transducers), in order to quantify rocking of the container and soil column. Figure 4-19 is a summary plot of the recorded peak accelerations and integrated peak absolute displacements from these transducers. The peak vertical accelerations were typically 20 to 30% of the peak horizontal accelerations at all locations other than the upper soil profile, and the peak vertical displacements were typically less than about 10% of the peak horizontals, again other

than in the upper soil profile. Note that these data are for the ends of the container, while vertical motions within the central portion of the container are expected to be much smaller. These data show that the shaking table and FSB1 container do not introduce significant rocking or pitching motions, and that the lower halves of the soil profile have similarly low levels of vertical motion. However, the vertical accelerations and displacements in the upper soil profile are comparable to their horizontal counterparts, indicating that motions are not uniform within the upper soil profile. Note, however, that liquefaction occurred in all but the smallest events in Csp2. For the smallest events, the vertical accelerations and displacements recorded in the upper soil profile appear to be consistent with the magnitude of the other vertical recordings. This indicates that the large vertical motions near the ends of the upper soil profile were due to liquefaction effects, as discussed below.

There are at least two simple modes of vertical displacement for the soil near the ends of the container. In the first scenario, the soil profile deforms as a column, as shown schematically in Figure 4-20(a). As shown, when the base accelerates to the north, the relative displacement of the surface will be to the south. The vertical displacement at the south end of the container will be down, and the opposite will occur at the north end. In the second scenario, the liquefied soil "sloshes" in a relatively rigid container, as shown schematically in Figure 4-20(b). Here, when the base accelerates to the north and the relative displacement of the surface is to the south, the soil at the south end of the container is likely to slosh upward, and the vertical displacement at the north end will be negative.

Vertical and horizontal displacements of the ground surface relative to the container base in Csp2 ($D_r \approx 35\%$ upper layer) are summarized in Figure 4-21 for both (a) a non-liquefaction and (b) a liquefaction event. The convention used in Figure 4-21 is that positive horizontal displacement is a displacement to the south, and positive vertical displacement is upward. In Figure 4-21(a), the horizontal displacement and the north vertical displacement are nearly in phase, while the south vertical is nearly 180° out of phase. This is consistent with the expected behavior for bending of the soil column, as previously described. Also, the vertical displacements are on the order of 10% of the horizontals. In Figure 4-21(b), the opposite phasing occurs, with the south vertical moving in phase with the horizontal and the north nearly 180° out. This would be consistent with the sloshing mode previously described, and is consistent with Figure 4-17 where we saw the effects of the soil profile becoming softer than the container. Also, in Figure 4-21(b) we see that the vertical displacements are of the same magnitude as the horizontals. Although this is a greatly simplified analysis, it is consistent with the argument that the large vertical displacements are not due to a lack of complementary shear stresses, but due to the difference in stiffness between the soil and the container. While not ideal, an appreciation of this limitation is necessary for realistic interpretations or analyses of the centrifuge data.

4.3.7 Pore Pressures Near Structures

The influence of the pile foundation on the excess pore pressures in the upper sand layer of Csp1-3 was evaluated by placing pore pressure transducers both near and far from the structures. Figure 4-22 shows excess pore pressure ratios (r_u) at depths of 3.7 m in the $D_r \approx 35\%$ layer of Csp2: (a) at a "free field" location, (b) about 0.3 m prototype from a single pile, and (c) about 3 m prototype from a 2x2 pile group. Pore pressures near the single pile system show a cyclic component at the predominant period of the single pile system (e.g., compare Figures 4-15

and 4-22). Pore pressures near the 2x2 pile group also show a significant cyclic component corresponding to the horizontal motions of the pile cap. While pore pressures near foundations are clearly not equal to those in the free field, these data show very similar trends in their mean values over time.

4.3.8 Conclusions Related to Modeling Techniques and Systems

Results from dynamic centrifuge tests of pile-supported structures in soft or liquefied soils were used to evaluate several aspects of the centrifuge modeling system that could potentially affect subsequent interpretations and analyses. Detailed examination of the centrifuge modeling system was necessary because of the newness of the shaking table, and since recent reviews have highlighted important limitations that can exist in dynamic centrifuge systems (Scott 1994, Arulanandan et al. 1994).

Signal processing procedures and methods for calculating displacement time histories from accelerometer records were evaluated. Test results showed that the transient displacement time histories could be reliable calculated using the established procedures, but that permanent displacements could not (as expected). It was also noted that the "default corner frequency" used to mass-process all acceleration time histories may not be the best choice for an individual recording (either passing too much noise or removing too much real signal). Thus detailed interpretation of individual records is required when reliable transient displacement time histories are desired.

Performance of the shaking table on the large centrifuge at UC Davis was shown to be satisfactory. Full frequency spectra of desired input motions (including real earthquake records) were recreated, with the motions being scaleable and repeatable. Dynamic vertical displacements at the ends of the container base were limited to about 10% of the dynamic horizontal displacements, indicating that rocking of the container base was reasonably small over the full operating range of the shaker.

The FSB1 container produced satisfactorily uniform and coherent horizontal motions, with relatively little rocking of the soil column, in tests on nonliquefied sand or even liquefied D_r~55% Nevada sand. Incoherent horizontal motions and differential vertical displacements developed at shallow depths in upper layers of liquefied D_r~35% Nevada sand or strongly-shaken soft clay, indicating that the soil column had become effectively "softer" than the FSB1 container in these tests.

Changing pore fluid viscosity by a factor of ten between two containers had negligible effect on the soil-pile interaction, with or without liquefaction of the upper soil layer. Furthermore, the nearly identical dynamic pore pressures and bending moment distributions obtained in these two tests showed that reasonably repeatable test results could be obtained nearly a year apart.

Bending moment distribution versus depth was found to be highly dependent on the soil stiffness. In tests with liquefied sand at low D_r and in tests with soft clay the maximum bending moment occurred much deeper than in tests with liquefied sand at higher D_r. The apparent p-y resistance of liquefied sand was shown to be strongly dependent on its D_r (Boulanger et al. 1997).

4.4 DISSEMINATION OF CENTRIFUGE DATA

Each centrifuge tests has been documented with an individual hard-copy data report and a diskette (100 Megabyte "Zip" disk) containing all recorded time histories. These data reports and diskettes have been submitted to Caltrans, and been made available to other researchers, including the geotechnical group at U.C. Berkeley and Professor W. D. L. Finn at the University of British Columbia. We will continue to disseminate these data, and expect that their use by other researchers will benefit Caltrans in the long-term.

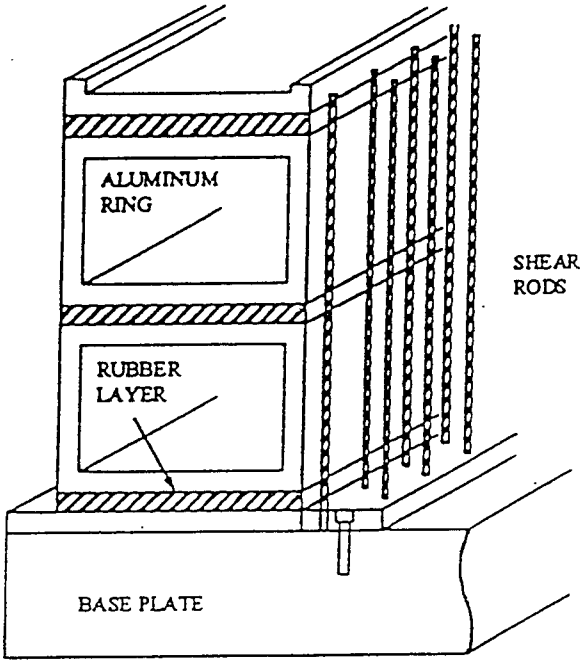

Fig. 4-1: Schematic of rings and shear rods at the container ends (from Divis et al. 1997)

Fig. 4-3: Model layout Csp2

Fig. 4-2: Model layout Csp1

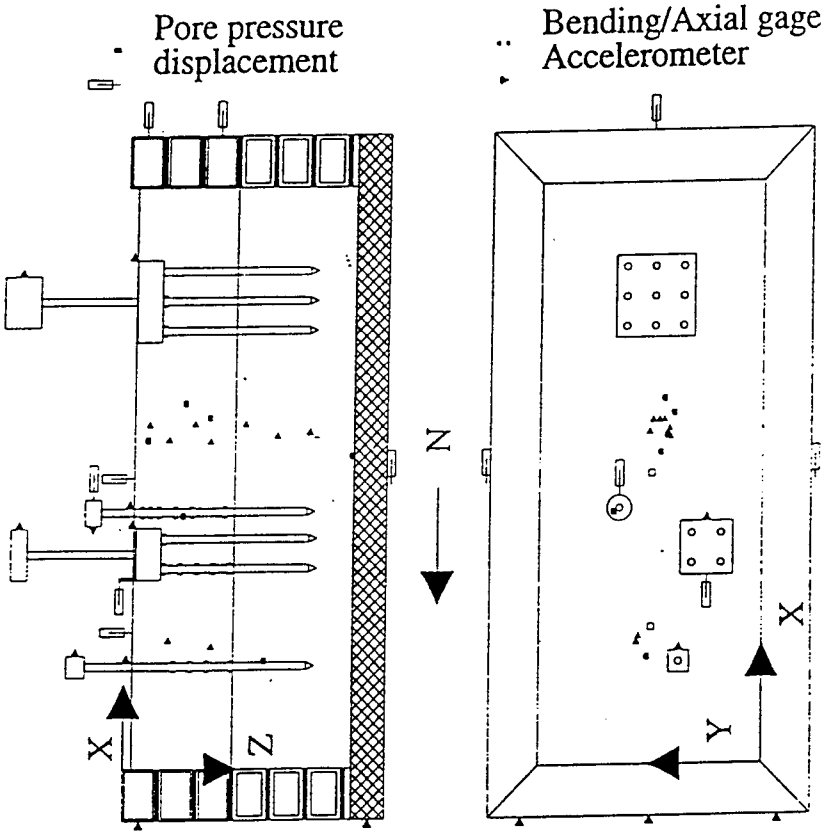

Fig. 4-4: Model layout Csp3

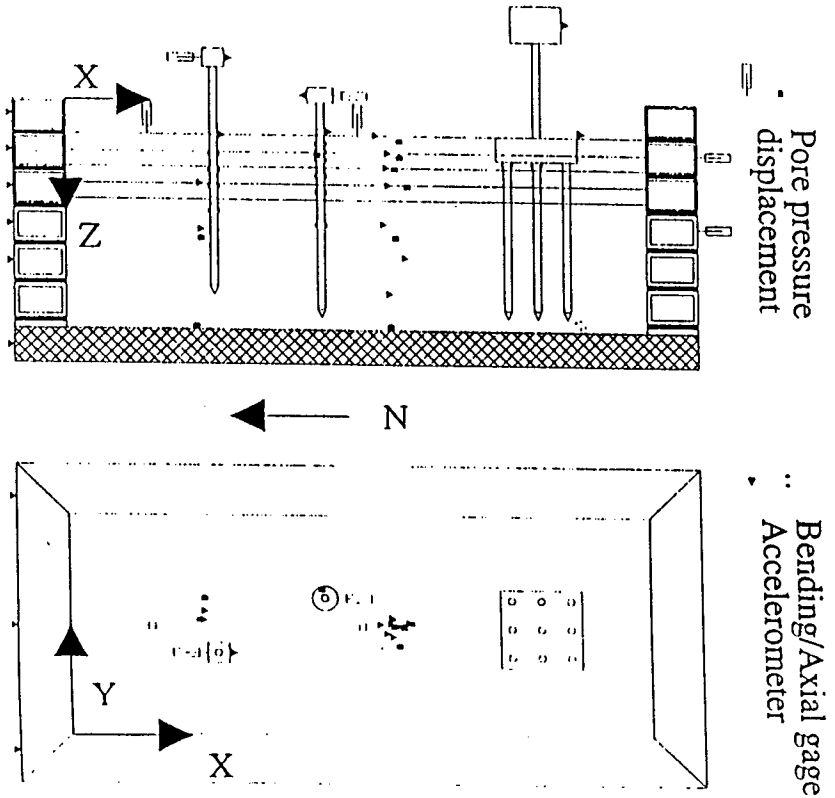

Fig. 4-5: Model layout Csp4

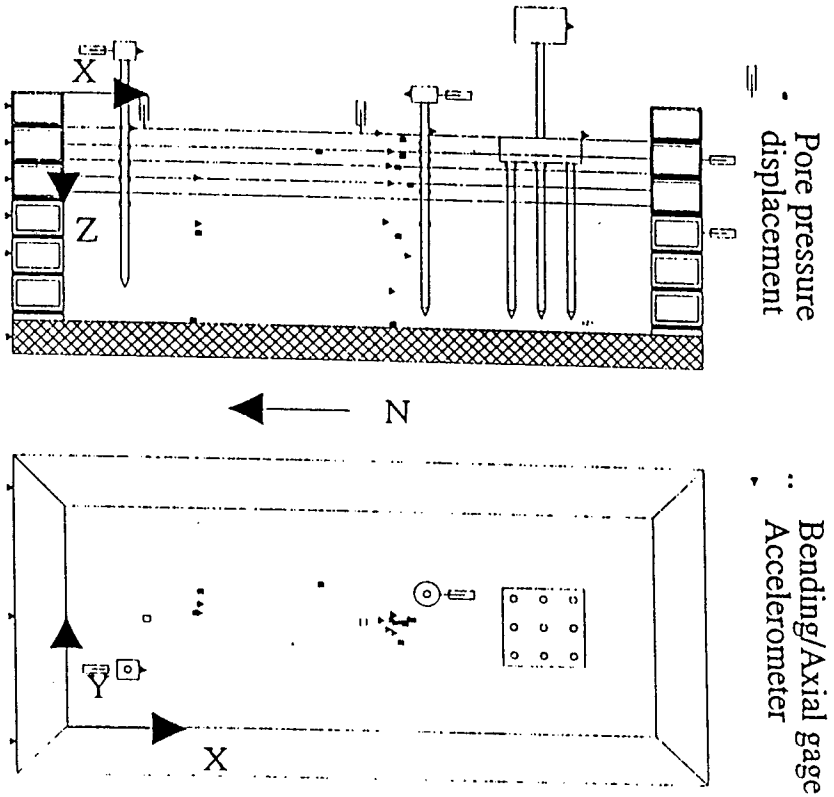

Fig. 4-6: Model layout Csp5

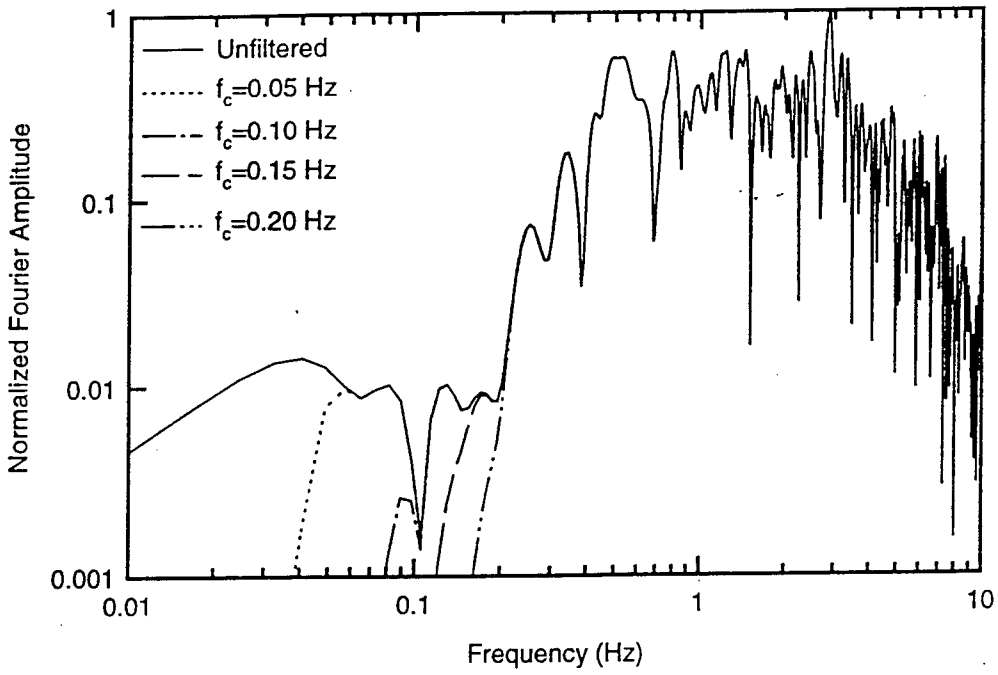

Fig. 4-7(a): Fourier spectrum of base acceleration in Csp2 event F filtered with 10^{th} order IIR Butterworth filter with f_c=0.15 Hz

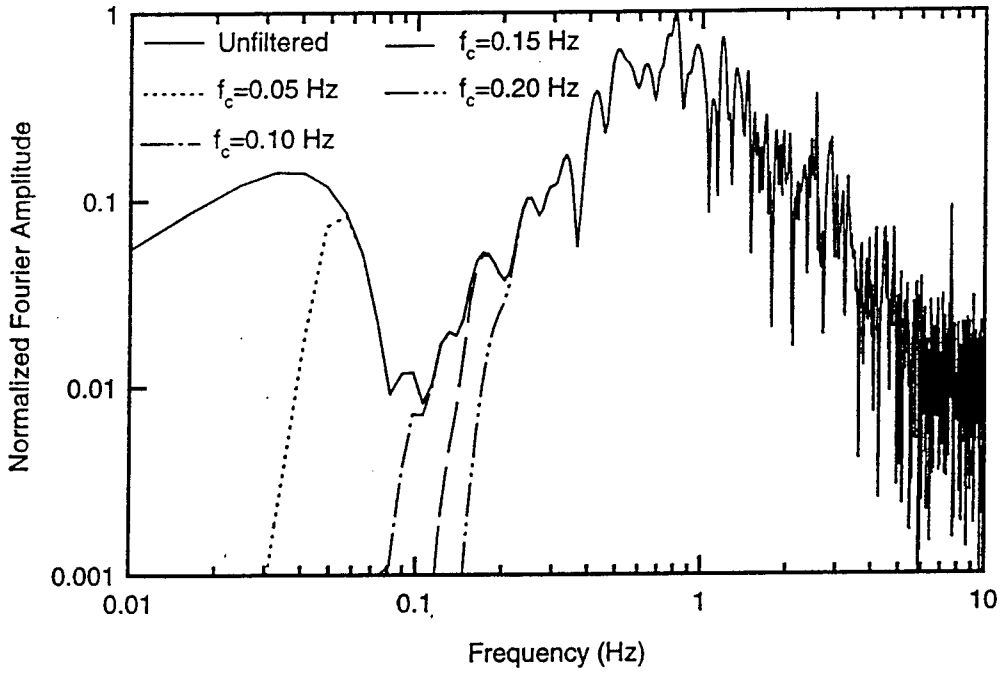

Fig. 4-7(b): Fourier spectrum of superstructure acceleration in Csp2 event F filtered with 10^{th} order IIR Butterworth filter with f_c=0.15 Hz

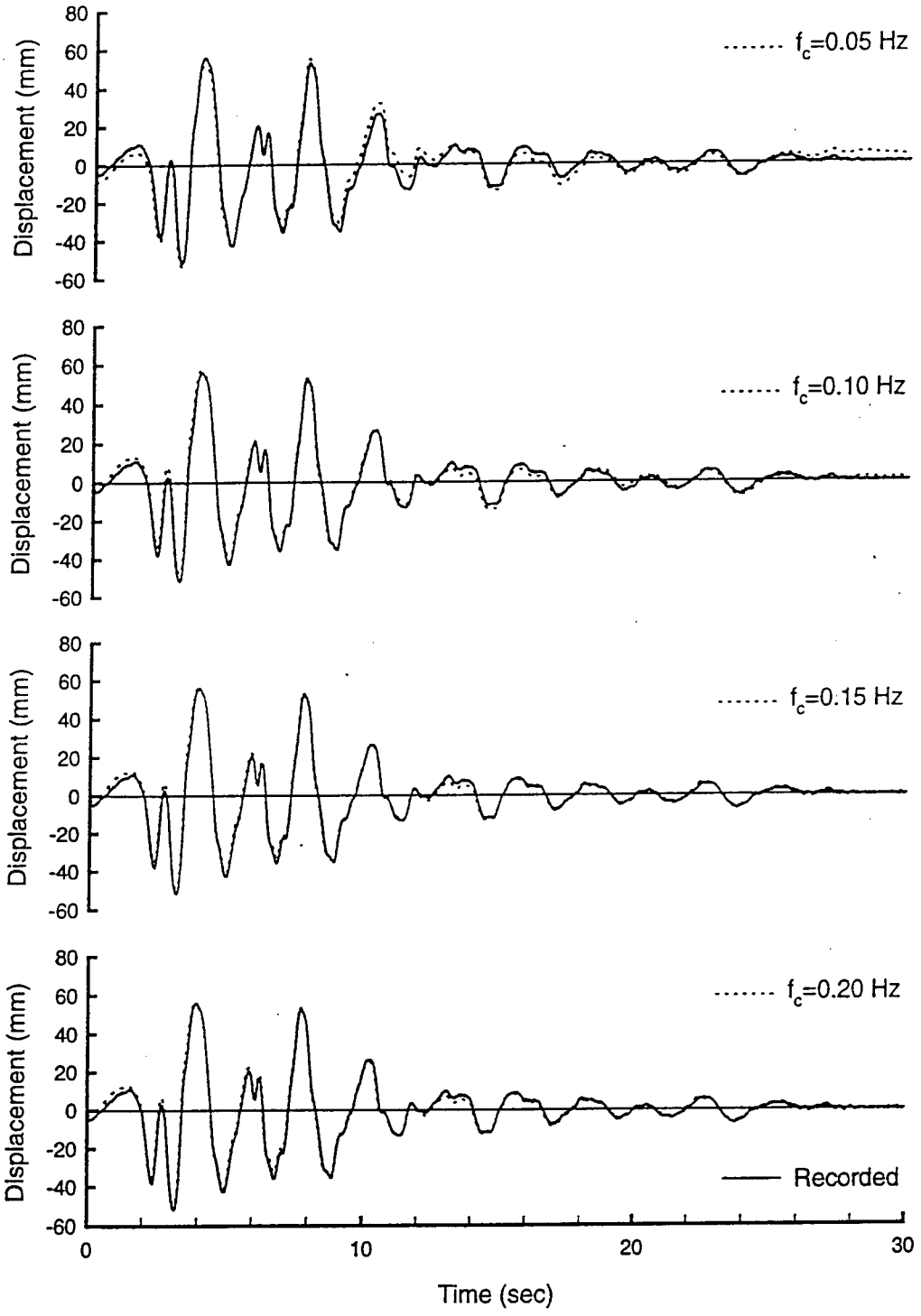

Fig. 4-8: Effect of corner frequency on calculating displacement of the base relative to the manifold in Csp2 event F using 10^{th} order FIR Butterworth filter

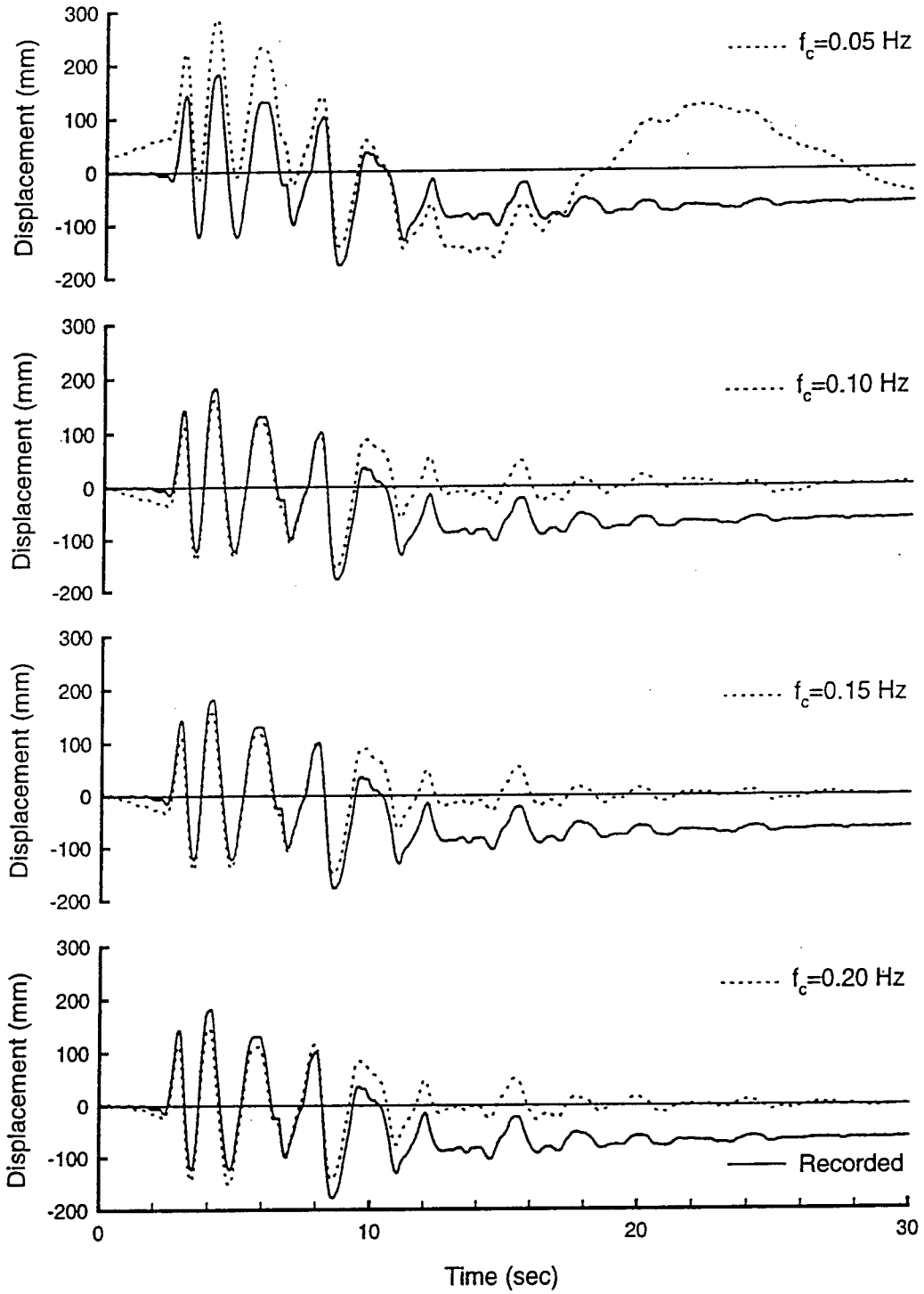

Fig. 4-9: Effect of corner frequency on calculating displacement of the superstructure relative to the top ring in Csp2 event F using 10^{th} order FIR Butterworth filter

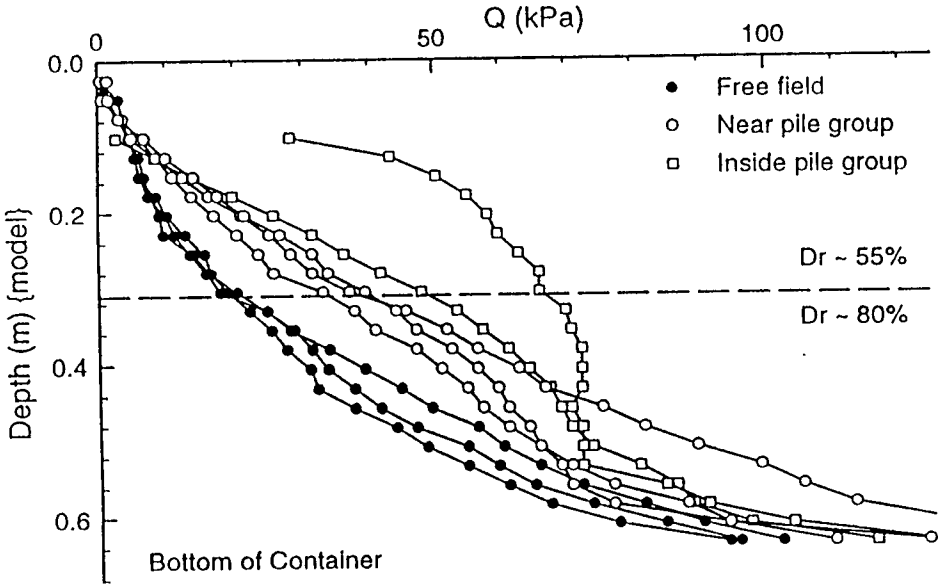

Fig. 4-10: Results of penetration tests Csp3

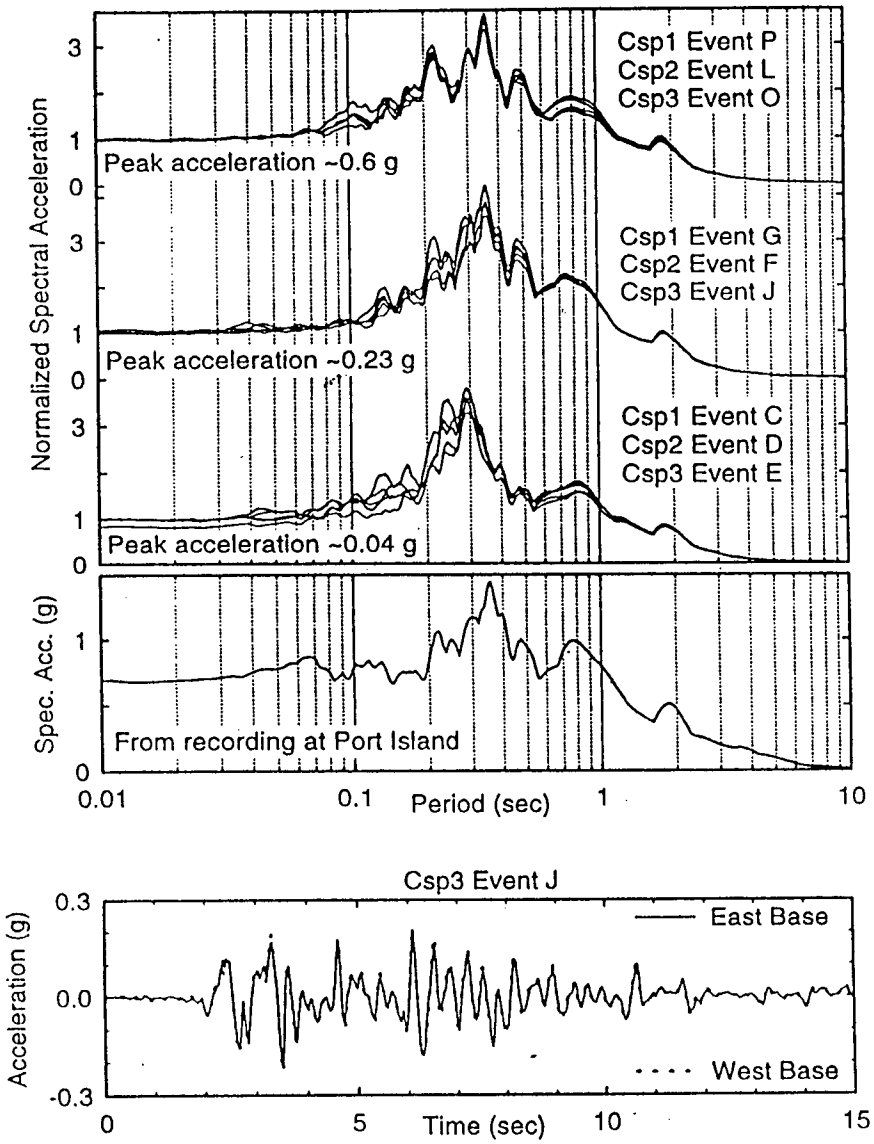

Fig. 4-11: Repeatability of input motions
(all spectra at 5% damping)

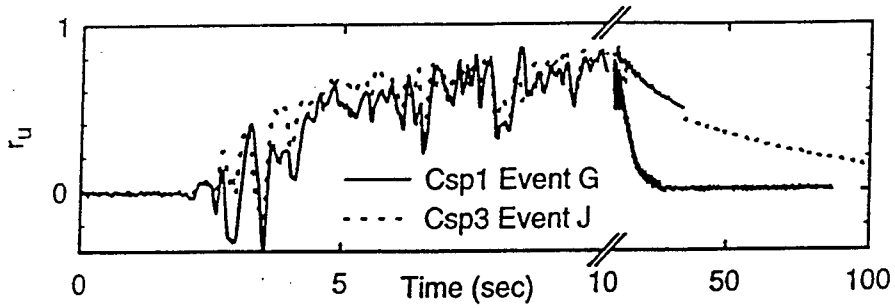

Fig. 4-12: Effect of pore fluid viscosity on generation and dissipation of pore pressure in Csp1 (water) and Csp3 (HPMC-water)

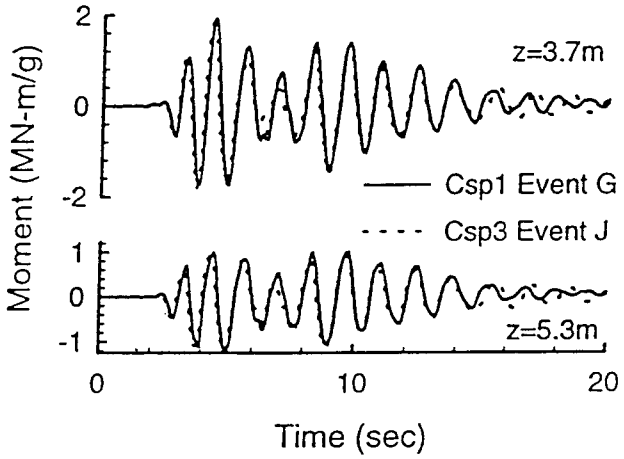

Fig. 4-13: Effect of pore fluid viscosity on bending moments (pile diameter D=0.67m)

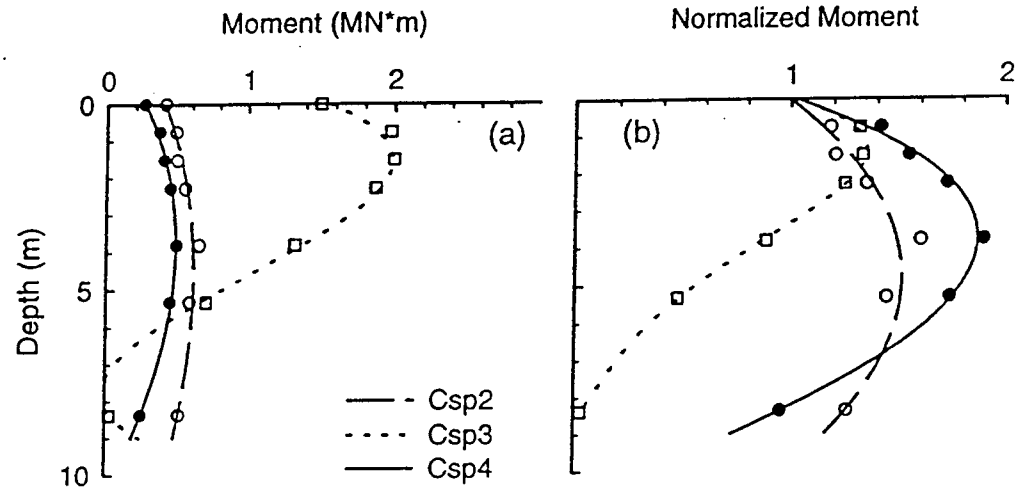

Fig. 4-14: Bending moment distribution with varying soil types for Kobe events with $a_{max,base} \approx 0.23g$

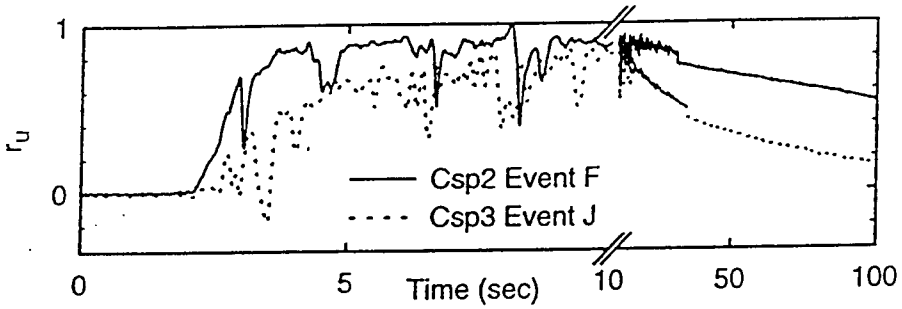

Fig. 4-15: Generation and dissipation of pore pressure in 35% D_r soil (Csp2) and 55% D_r soil (Csp3)

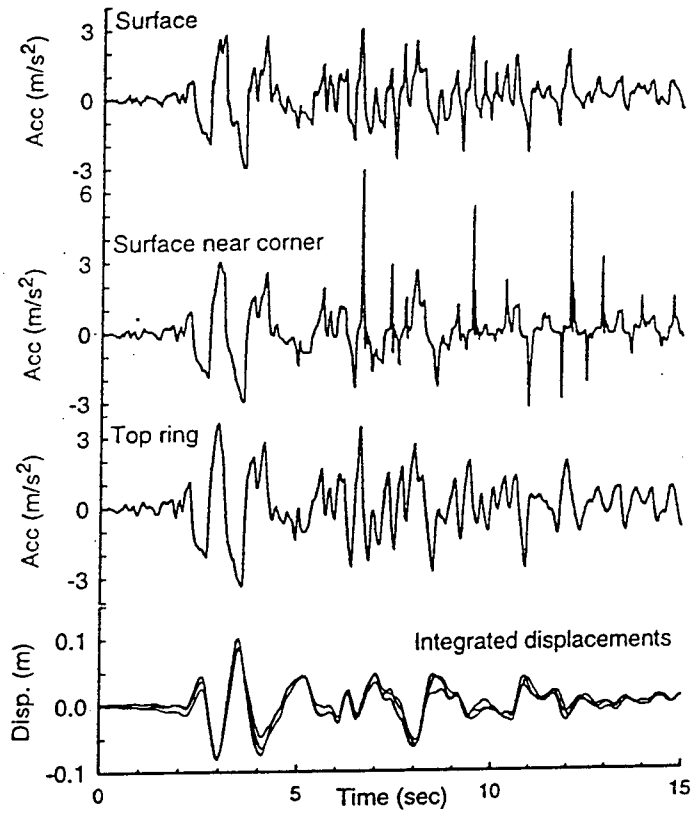

Fig. 4-16: Coherency of motion near top of container Csp1 Event G (Kobe, $a_{max,base}$≈0.23g)

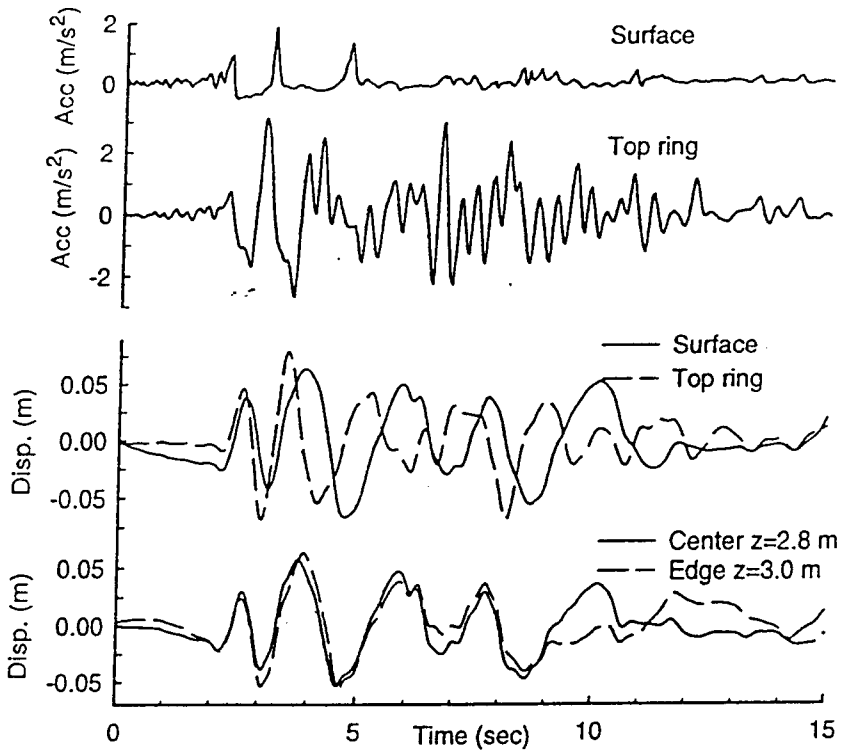

Fig. 4-17: Coherency of motion in liquefied sand - Csp2 Event F
(Kobe, $a_{max,base}$≈0.23g)

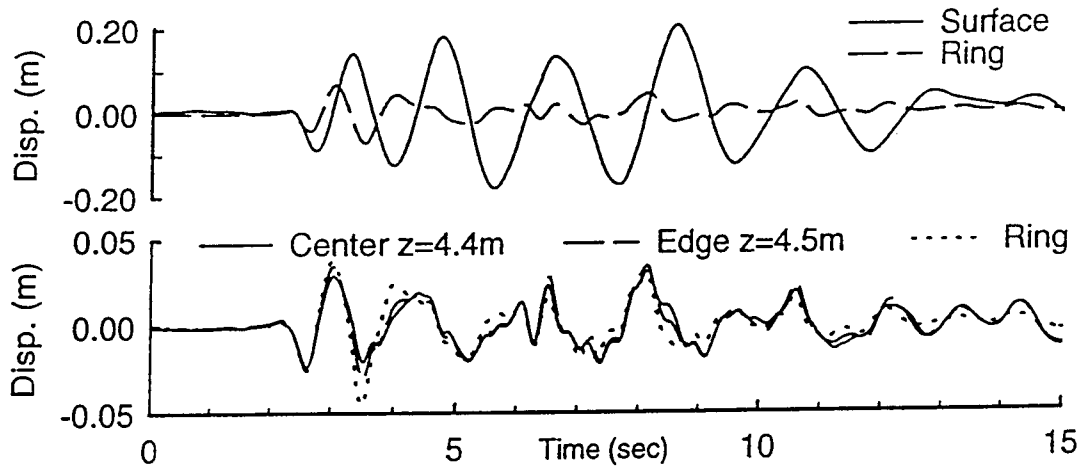

Fig. 4-18: Coherency of motion in clay - Csp4 Event D
(Kobe, $a_{max,base}$≈0.23g)

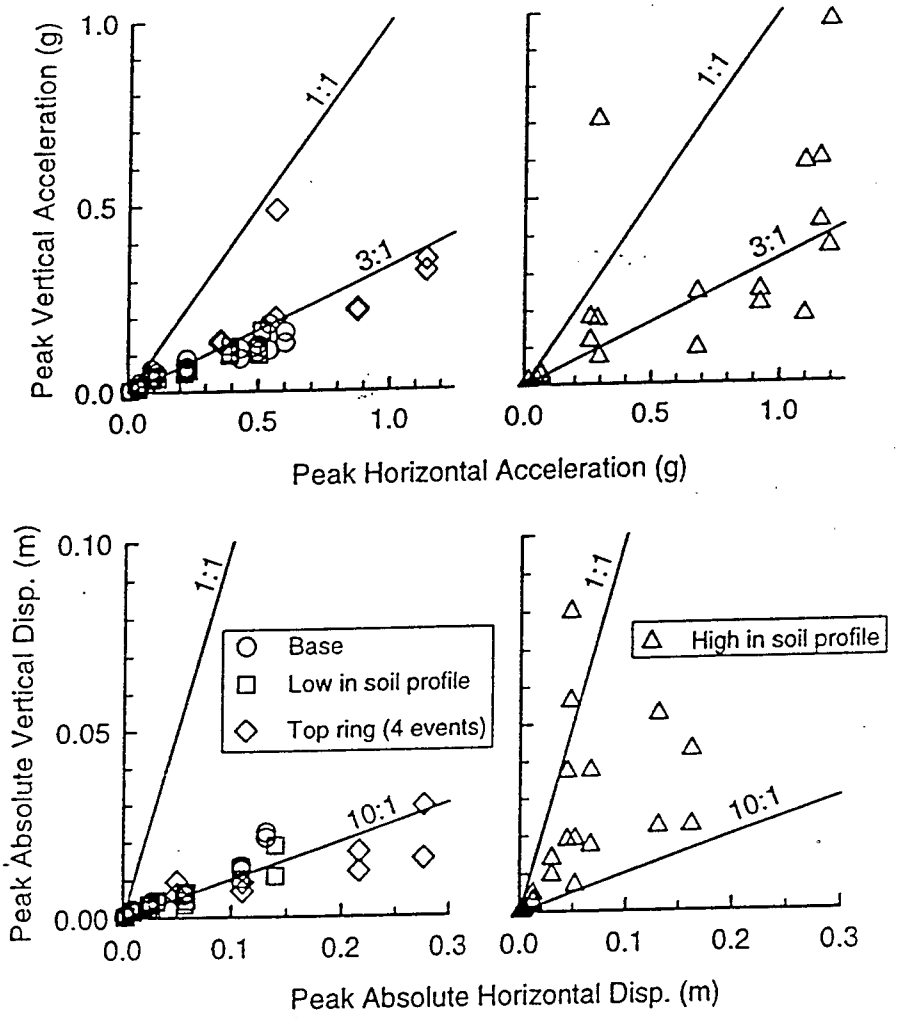

Fig. 4-19: Peak vertical vs. peak horizontal accelerations and displacements throughout model

(a) Column bending (b) Sloshing

Fig. 4-20: Two possible modes of deformation (greatly exaggerated)

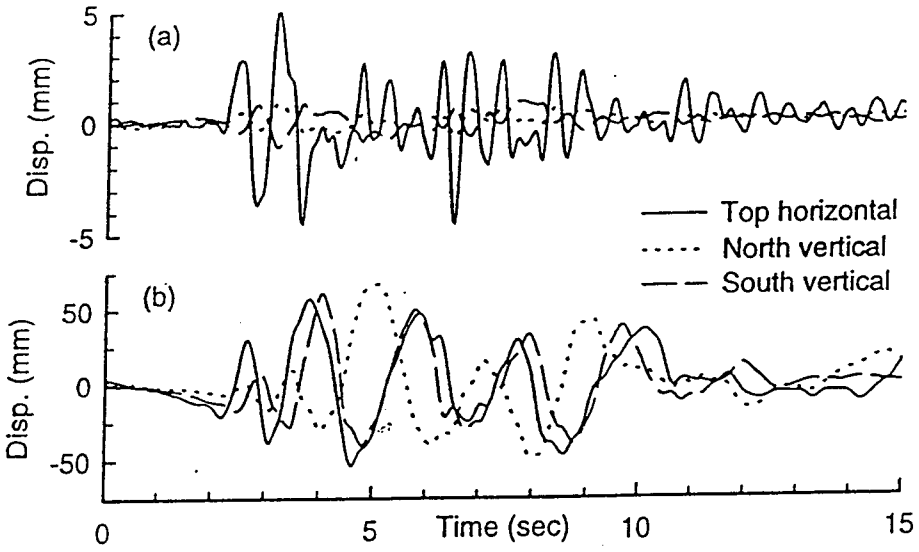

Fig. 4-21: Relative displacements at the top of the FSB1 container showing (a) column bending, and (b) sloshing of liquefied soil

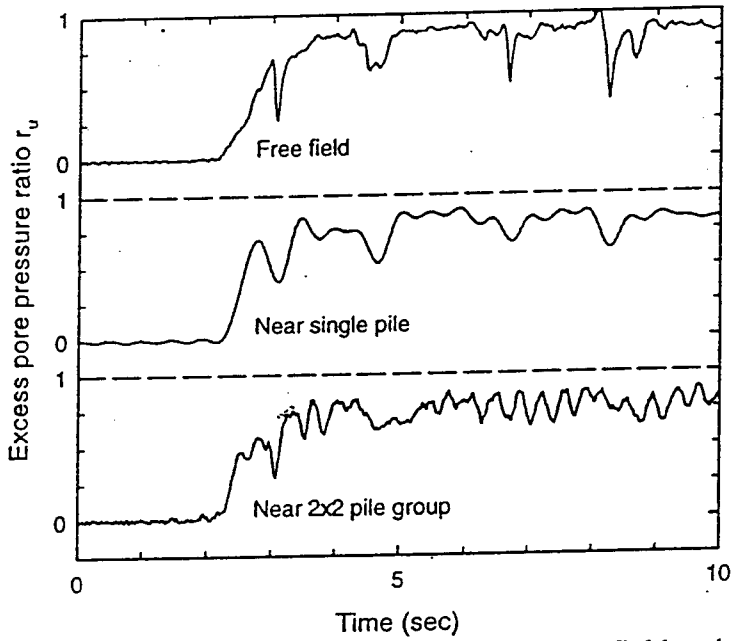

Fig. 4-22: Excess pore pressure ratio in free field and near structure

5 DYNAMIC ANALYSIS OF PILES

5.1 INTRODUCTION

In this study, four different implementations of the Beam on a Nonlinear Winkler Foundation (BNWF) approach were evaluated:

1. PAR Pile Analysis Routine, PMB Engineering Inc. (1988).

2. NONSPS NONlinear Soil-Pile-Structure, Kagawa (1983).

3. DRAIN-2D Dynamic Response Analysis of INelastic 2D structures, Version 1.10, Prakash and Powell (1993).

4. GeoFEAP Geotechnical Finite Element Analysis Program (Bray et al. 1997).

PAR is a commercial code with a user interface, options for automatic generation of p-y curves, a simple gap model, and cyclic degradation of p-y curves. NONSPS is a research code that can account for effective stresses, pore pressure generation, and cyclic degradation of p-y curves. Both PAR and NONSPS use "parallel radiation damping" (hysteretic and viscous damping components in parallel) as default, but can be made to use "series radiation damping" (hysteretic and viscous damping components in series) by experienced users; the use of series versus parallel radiation damping was discussed in Section 3-2. DRAIN-2D is a more general structural engineering code; it is well documented, has a rich element library, and the source code is available. Analyses with "parallel radiation damping" were performed using PAR, NONSPS and DRAIN-2D to verify the consistency of the three computer programs. Then, DRAIN-2D was used to demonstrate the advantages of "series radiation damping" over "parallel radiation damping". While this section will focus on comparisons of NONSPS, PAR and DRAIN-2D, it will be shown that in the absence of liquefaction, existing BNWF codes can be suitably adapted to analyze the soil-pile-structure interaction problem if care is taken in the representation of radiation damping.

Looking to the future, the program GeoFEAP seems to offer the most flexibility for modifying new elements to account for the effects of liquefaction on soil-pile-structure interaction, and has thus been adopted in our continuing efforts. Subsequently, we have developed some new p-y element subroutines based on bounding surface plasticity concepts for GeoFEAP (Wang 1997).

The computer programs used to analyze the free-field dynamic site response in this study were:

1. SHAKE (Schnabel et al. 1972),

2. SRANG (Kagawa 1980), and

3. SUMDES (Li et al. 1992).

These different analysis methods were compared to results obtained from the centrifuge

experiments (Chacko 1995, Wang et al. 1997). The version of NONSPS used for this study is linked to SRANG (Kagawa, 1980b). SRANG assumes either hyperbolic or Ramberg-Osgood stress strain relations, and the shape of the p-y curves in NONSPS is related to the shape of the stress-strain curves in SRANG. The free-field ground motion inputs for PAR and DRAIN-2D were calculated by the program SHAKE (Schnabel et al. 1972), which uses the equivalent linear procedure to approximate nonlinear soil behavior.

5.2 CENTRIFUGE TESTS ANALYZED

The centrifuge model tests analyzed in this section were performed using the servo-hydraulic shaker (Chang, 1990) on the Schaevitz centrifuge at UC Davis. The hinged plate container (Fiegel et al. 1994) was used to provide shear beam boundary conditions to the soil. Tests were performed on samples of normally consolidated San Francisco Bay Mud with a "crust" of dense sand on the surface of the clay. These models were first subjected to several shaking events as part of a site response study by Fiegel (1995). After these initial shakes, the model was spun down and a model pile consisting of an aluminum tube was inserted through the clay layer. A mass, representing the superstructure, was attached to an extension of the pile. Installation of the model piles at 1g does not accurately model the effects of method of pile installation on soil behavior. In terms of the lateral stress state around the pile, a pile driven at 1g probably acts more like drilled shaft than a driven prototype pile.

Accelerometers were mounted on the pile near the ground surface (pile head) and on the model superstructure. The centrifuge was spun up to 50 g and the clay was allowed to consolidate. Several earthquake events were then applied to the base of the centrifuge container with sufficient time between events for any induced excess pore pressures to dissipate. Consequently, the clay developed an apparent overconsolidation as it progressively compressed after each shaking event. A summary of these centrifuge test results and subsequent numerical analyses were presented by Chacko (1994).

For brevity, this section presents detailed results for a typical shaking event for one of the pile models. Table 5-1 summarizes the centrifuge scaling laws used to convert model dimensions to prototype dimensions. For the model test presented herein, a scale factor N=50 was used. The reader is referred to Kutter (1992) for an explanation of the principles of centrifuge modeling. The dimensions of this model and the instrumentation layout are shown in Figure 5-1. In prototype terms, this model represents a superstructure mass of 1.44 tonne and pile head mass 1.12 tonne, supported by a 317 mm diameter pipe pile with an equivalent "steel" wall thickness of 10 mm, and a fixed base fundamental period of 0.35 seconds. In the chosen shaking event, shown in Figure 5-2, a scaled version of the ground motion recorded at Santa Cruz during the 1989 Loma Prieta Earthquake was used to excite the base of the centrifuge model. Select recordings of acceleration response are shown in Figure 5-2. For this event, the ground surface motion shows a slight amplification of peak acceleration and a lower frequency content than the input base motion. The superstructure shows additional amplification while responding at a fundamental period of about 0.85 s. The frequency content of the pile head accelerations shows an influence of both the soil-pile-structure system motion and free field ground motions. The difference between the observed fundamental period (0.85 s) and the calculated fixed base period (0.35 s) is due to the flexibility of the pile foundation.

Table 5-1. Scale Factors for Dynamic Centrifuge Modeling

Quantity	Scale Factor
Length	N^{-1}
Acceleration	N
Time	N^{-1}
Frequency	N
Volume	N^{-3}
Density	1
Mass	N^{-3}
Stress	1

5.3 Numerical Simulations with Existing Programs

Three computer codes (PAR, NONSPS, and DRAIN-2D) are used to simulate the response of the soil-pile-structure system shown in Figure 5-1 to the base motion presented in Figure 5-2. All of the calculations neglected gap formation, cyclic degradation of p-y curves, and pore water pressure generation. Excess pore pressures in the soil profile measured in the centrifuge tests were generally small during this event. The sensitivity of the calculations to possible variations in the p-y curves will be evaluated in a subsequent parametric study.

In the BNWF method, four types of input data need to be specified: (1) free field response as a function of depth along the pile; (2) description of nonlinear p-y relationships for the soil-pile interaction; (3) description of the radiation damping; and (4) description of the structural components. The specification of these items is described below.

5.3.1 Free Field Motion

In these analyses, the input motions to the p-y springs are approximated as the free field displacement time histories. For DRAIN and PAR analyses, the input motions were obtained using SHAKE. The input data for SHAKE includes the base motion of the centrifuge model container, the maximum shear modulus profile, and the modulus reduction and damping curves. Shear wave velocity profiles for the clay were derived using the procedure presented by Dickenson (1994) as:

$$v_s = 10.9\left(\frac{m/\sec}{\sqrt{kN/m^2}}\right)\sqrt{\sigma'_p} \qquad (1)$$

where v_s is the shear wave velocity and σ'_p is the preconsolidation pressure. The maximum shear modulus, G_{max} is then calculated by $G_{\max} = \rho v_s^2$, where ρ is the mass density of the soil. Dickenson recommended that the above relationship be used only for soil with σ'_p exceeding 25 kPa, but this restriction was relaxed in the present study. Shear modulus reduction curves for the clay were based on results presented by Sun et al. (1988) and the damping was obtained from Fiegel (1995).

G_{max} for the sand was determined using the equation presented by Seed and Idriss (1970):

$$G_{max} = 219\sqrt{kPa}\,K_2\sqrt{\sigma_m'} \qquad (2)$$

where K_2, the soil modulus coefficient, was chosen as 70 based on the relative density of the sand layer (90%) and σ_m' is mean effective stress.

For sand, the modulus reduction curve was chosen from the upper range of data given by Seed and Idriss (1970), while the damping curve was chosen from the lower range of data given by Seed and Idriss (1970).

The ground motion time histories for input to NONSPS were obtained using the program SRANG (Kagawa 1980b) because the programs are linked together. SRANG uses either a hyperbolic model or a Ramberg-Osgood model for the site response analysis. To facilitate cross-comparisons based on SHAKE and SRANG analyses, SRANG was run in the total stress mode and the parameters of the hyperbolic model were adjusted to provide a "best fit" approximation to the modulus reduction curves used in SHAKE. The procedure for adjusting the hyperbolic model parameters is described in detail by Chacko (1994).

5.3.2 Description of p-y Relationships

In analysis of laterally loaded single piles under horizontal shaking, axial deformations are relatively unimportant; therefore, t-z behavior was neglected. For all three programs, PAR, NONSPS, and DRAIN, p-y curves were based on recommendations by Matlock (1970) for soft clay, and by Reese et al. (1974) for sand. For PAR, piecewise linear segments approximated the Matlock p-y curves; the automatic p-y curve generation features of PAR were not used. In PAR, unloading of p-y elements is assumed to be linear elastic. For NONSPS, the hyperbolic model was used and the backbone curve was adjusted to make a "best fit" (Chacko 1994) approximation to the Matlock (1970) recommendations. NONSPS uses a Masing criterion to describe unloading and reloading. DRAIN-2D had no direct provisions for nonlinear p-y springs, but the element library was used to create a series of bi-linear springs that approximated the p-y curve by piecewise linear segments. By this method, plastic deformation during unloading was also permitted in the p-y curves. Examples of calculated cyclic p-y relationships are presented later.

The Matlock (1970) procedure to construct p-y relations for piles in soft clay is described briefly below. The pre-plastic region is represented by

$$\frac{p_s}{p_{ult}} = 0.5\left(\frac{y}{y_c}\right)^{\frac{1}{3}} \qquad (y < 8\,y_c) \qquad (3)$$

$$\frac{p_s}{p_{ult}} = 1 \qquad (y > 8\,y_c) \qquad (4)$$

where
$y_c = 2.5\ B\ \varepsilon_c$
B = pile diameter

ε_c = strain at half of the maximum stress of a laboratory stress-strain curve for soil
p_s = soil reaction per unit pile length
y = displacement of pile relative to the soil
p_{ult} = static ultimate resistance per unit pile length

The static ultimate resistance in clay may be expressed as

$$p_{ult} = N_p \, c_u B \tag{5}$$

where N_p is a non-dimensional ultimate resistance coefficient and c_u is the undrained shear strength. N_p varies from 3 near the surface to 9 at the depth $x = x_r$:

$$N_p = 3 + \frac{\sigma'_v}{c_u} + \frac{J\,x}{B} \qquad (x < x_r) \tag{6}$$

$$N_p = 9 \qquad (x > x_r) \tag{7}$$

x_r is obtained by setting $N_p = 9$ in equation 6. J was taken as 0.5. The undrained shear strength (c_u) was estimated using a ratio of c_u / σ'_v selected to represent the effects of stress path, loading rate effects, and prior shaking-induced consolidation. As a lower bound on the possible range of c_u / σ'_v, a set of analyses used $c_u / \sigma'_v = 0.3$ (i.e., normally consolidated condition) to generate the p-y curves. In a second set of analyses the p-y curves were scaled upwards (stiffer and stronger) by a factor of two to investigate sensitivity.

The initial stiffness that is implied by Matlock's p-y curve (equation (3)) is infinite. For static analysis, this may not be important. But for a dynamic calculation, a finite stiffness is needed. For DRAIN-2D analyses in this study, the initial elastic stiffness k^e of the p-y curve is obtained from Vesic (1961):

$$k^e = 0.65 \sqrt[12]{\frac{E_s D^4}{EI}} \frac{E_s}{1 - \nu^2} \tag{8}$$

where

E_s = Young's modulus of the soil
ν = Soil's Poisson's ratio (0.5 is assumed in this case)
D = pile diameter
EI = bending stiffness of the pile

The initial portion of the Matlock's curve was replaced by k^e up to the point of intersection implied by equation (3) and equation (8). Typically this intersection occurred at a load P of about 35% of P_{ult}.

5.3.3 Radiation Damping

In NONSPS, "parallel radiation damping" is used (damper in parallel with nonlinear

element), with the value of the dashpot coefficient determined according to the 1-D Berger model:

$$c = 2B\rho\left(v_p + v_s\right) \tag{9}$$

For undrained analyses of clay, the soil is nearly incompressible, and the P-wave velocity can become large, leading to excessive damping calculated from the above equation. To avoid this, the Berger model is modified in PAR to:

$$c = 4B\rho v_s \tag{10}$$

For the DRAIN-2D analyses, the values of damping coefficient used were the same as those used in PAR (equation 10). However, DRAIN-2D analyses were performed using both "parallel radiation damping" and "series radiation damping" arrangements.

5.4 Comparison of Numerical Simulations with Existing Programs

Table 5-2 summarizes the conditions and methods of determining the input parameters for six different simulations of the centrifuge model test results shown in Figure 5-2. NONSPS, PAR, and DRAIN-2D Case I, were conducted to cross-check numerical simulations from different codes using input properties that were as similar as possible. DRAIN-2D Case II was run to investigate, by comparing with Case I, the effect of varying the strength and stiffness of the p-y element by a factor of 2. DRAIN-2D Cases III and IV were similar to Cases I and II respectively, but "series radiation damping" was used instead of "parallel radiation damping". Figure 5-3 a-f shows time histories of motions calculated at the pile head and superstructure for all six cases listed in Table 5-2.

Table 5-2. Conditions and Input Information for Each Analysis Case

	NONSPS	PAR	DRAIN-2D Case I	DRAIN-2D Case II	DRAIN-2D Case III	DRAIN-2D Case IV
Damping Model	Parallel	Parallel	Parallel	Parallel	Series	Series
Damping Coefficient	$2B\rho(v_s+v_p)$	$4\ B\rho v_s$	$4\ B\rho v_s$	$4\ B\rho v_s$	$4\ B\rho v_s$	$4\ B\rho v_s$
Free Field Analysis	SRANG	SHAKE	SHAKE	SHAKE	SHAKE	SHAKE
p-y curves for clay	Hyperbolic "best fit" to Matlock	Piecewise Linear Matlock	Piecewise Linear Matlock	Piecewise Linear Matlock x 2	Piecewise Linear Matlock	Piecewise Linear Matlock x 2
p-y strength	1 x p_{ult} from eq. (5)	1 x p_{ult} from eq.(5)	1 x p_{ult} from eq. (5)	2 x p_{ult} from eq. (5)	1 x p_{ult} from eq. (5)	2 x p_{ult} from eq. (5)

Figure 5-4a shows comparisons between response spectra measured in the centrifuge test and those calculated by NONSPS for the superstructure and pile head, and by SRANG for the ground surface and mid-depth in the soil profile. Figure 5-4b shows comparisons between the centrifuge test and calculations by PAR and SHAKE. For the level of shaking in this model test, SHAKE does an excellent job of predicting the ground motions. This observation is consistent with findings by Fiegel (1995), who did an extensive comparison between SHAKE and centrifuge data. For low to moderate levels of shaking, he found that SHAKE performed well. For very large levels of shaking, however, Fiegel (1995) found that nonlinear time-domain site response calculations can perform better than SHAKE.

Figure 5-4a and b show that while the peak acceleration of the superstructure and pile head are reasonably predicted by PAR and NONSPS, the frequency content of the motions are not well predicted. The predictions of PAR and NONSPS are quite similar to each other.

Spectral accelerations for predictions from DRAIN Cases I-IV are shown in Figures 5-5a-d. Case I was intended to mimic PAR, and this exercise was successful. DRAIN, Case I shows slightly smaller peak acceleration than PAR, and a smaller peak in the spectral acceleration, but the peak is almost at the same frequency as for PAR. Pile head accelerations predicted by PAR show an erroneous short period component at about 0.1 s in the acceleration spectrum. This peak is attributable to numerical noise, and it does not appear to affect the superstructure accelerations.

DRAIN Case II was conducted to determine (by comparison with CASE I) the effect of altering the p-y curve on the predicted response. For Case II, the stiffness and strengths of each p-y curve were doubled. Surprisingly, doubling the p-y curve had negligible effect on the frequency content and amplitude of predicted superstructure accelerations; Figure 5-5a is nearly identical to Figure 5-5b, and likewise, Figure 5-3c is very similar to Figure 5-3d. Chacko (1994) came to a similar conclusion based on parameter studies using the program NONSPS.

Figure 5-6 shows the plastic components of the calculated p-y curves for all four DRAIN-2D analyses; the plastic components can be separated from the dashpot forces in a consistent manner for all cases and thus provide a good basis for comparisons. Figure 5-6 shows that larger forces were transmitted to the pile for the cases with stiffer soil springs. Why then is the predicted response for Case I so similar to that for Case II? The reason is that the viscous dashpots for the cases of "parallel radiation damping" dominate the calculated responses. Figure 5-7a illustrates the dominance of the dashpot forces over the plastic p-y spring forces for DRAIN-2D Case I. This figure shows the envelope of peak forces in the plastic p-y spring and dashpot elements as a function of depth. Near the soil surface, the dashpot forces are seen to be much larger than the forces in the plastic p-y springs. This explains why a change in the p-y spring can have little effect; the response is governed by the dashpot, placed in parallel with the non-linear spring. Comparing the response spectra for Cases I and III (Figures 5-5a and 5-5c), it is clear that the "parallel radiation damping" acted to restrict the lateral movement of the pile head, and therefore resulted in a stiffer system response (e.g., higher frequency content in the response spectra).

DRAIN-2D Cases III and IV (Figures 5-5c and 5-5d), using "series radiation damping" show a dramatic improvement in the predicted frequency content of the pile head and superstructure. Case III is the case with the p-y relationship obtained according to Matlock (1970), while Case IV is the case with the p-y curve stiffened and strengthened by a factor of 2. Using "series radiation damping", the predicted response is sensitive to the stiffness of the p-y curve. Figures 5-6c and 5-6d show the p-y spring force calculated for the two cases using "series radiation damping". As expected, the predicted displacement for the stiffened p-y curve is

smaller than the displacement for the softer p-y curve. Figure 5-7b illustrates that if "series radiation damping" is used, the envelope of dashpot forces is always smaller than the envelope of plastic p-y spring forces; the dashpot does not dominate over the p-y springs. Overall, the response of the pile head and superstructure calculated using "series radiation damping" (Cases III and IV) show significantly improved agreement with the responses measured in the centrifuge test.

Maximum bending moments along the pile length are shown in Figure 5-8 for DRAIN-2D Cases I and III. The difference in the highest peak moments was about 29% for these two analyses, but it should be noted that "parallel radiation damping" is not always conservative. The peak moment at the ground surface depends primarily on the acceleration of the superstructure, which depends on the coincidence of the natural period of the system and the predominant period of shaking. "Parallel radiation damping" is likely to produces a stiffer system than "series radiation damping"; it allows forces to bypass the hysteretic system through a parallel dashpot. Therefore, "parallel radiation damping" results in bending moments decreasing more rapidly with depth than calculated using "series radiation damping" in Case III. It is not possible to generalize about which method will produce greater bending moments, however, because this depends on the characteristics of the ground motions and the soil-pile-superstructure system.

The use of Matlock (1970) p-y curves for soft clay to predict the results of centrifuge tests is quite simplistic. Strain-rate effects and the seismic history of the centrifuge model would be expected to alter the p-y relationships to be different from those recommended by Matlock (1970). More rigorous accounting for rate effects, seismic stress history, cyclic degradation, and gapping could reduce discrepancies between theoretical and experimentally measured soil-pile-structure response.

Another obvious and straightforward improvement to the calculations would be to use multiple spring-dashpot pairs to emulate the correct frequency dependent nature of far field radiation damping (Nogami and Konagai 1986). This aspect was not evaluated in this study to reduce the number of variables involved in the comparison between parallel and series damping.

5.5 New p-y Elements Based on Bounding Surface Plasticity

5.5.1 Basic p-y Element Without Gapping

In this section, two new simple p-y elements based on bounding surface plasticity concepts are presented. These new p-y elements were developed for clays with and without gapping, and were implemented in the finite element program GeoFEAP (Bray et al. 1995). As discussed previously, GeoFEAP offers the most flexibility for modifying new elements and thus was selected for our ongoing research efforts. The implementation of a single element to represent the nonlinear p-y resistance provides a much simpler-to-use tool than the use of combinations of spring and friction elements to simulate nonlinear behavior.

The following model simulates p-y behavior by separating it into elastic ($p\text{-}y^e$) and plastic ($p\text{-}y^p$) components or springs. The complete cyclic p-y curve is thus obtained by combining the elastic and plastic springs. Elastic stiffness was obtained using the equations recommended by Vesic (1961). The parameters of the bounding surface $p\text{-}y^p$ model can be obtained by fitting the backbone curves of empirical p-y curves, as will be shown later.

A simple formulation of deformation dependent plastic modulus recommended by Dafalias (1986) is used in this study, with an exponential parameter "n" added to control the

sharpness of the transition from elasticity to plasticity. The plastic modulus k_p is defined as:

$$k_p = h\left(\frac{\delta}{\delta_{in} - \delta}\right)^n$$

in which,

h = a scalar parameter controlling shape hardening
n = a scalar parameter controlling the sharpness of the plastic transition
δ = distance between the current stress state (p/p_{ult}) and the corresponding bounding ("image") stress state. The bounding stress states are $p/p_{ult} = -1$ and $+1$.
δ_{in} = the initial value of δ along a loading path.

Four parameters are needed to define the bounding surface plastic p-y^p curve: (a) the maximum resistance p_{ult}; (b) the elastic range ratio "elast," which is the ratio of the elastic range of p to its maximum value during virgin loading; (c) the hardening parameter "h"; and (d) the exponential term "n."

The definition of the δ and δ_{in} are shown in Figure 5-9. The cyclic feature of the p-y^p relationship is automatically built in by the bounding surface formulation. When the plastic p-y^p is in the plastic range (e.g., point C) and loaded in the positive direction, the value of δ is taken as the distance from the current normalized load (p/p_{max}) to the upper bound load ($p/p_{max}=1$). When the plastic p-y^p is unloading from point D for example, the behavior is elastic for a range of 2 times "elast" (Bauschinger effect) to point E, where plastic deformation begins to occur. Beyond point E (for example, point F), the measure of δ is the distance of the current normalized load to the lower bound load ($p/p_{max}=-1$), and the δ_{in} is the distance from point E to the lower bound load. Kinematic hardening is evident in Figure 5-9, while no isotropic hardening is considered.

Undesired "overshooting" is introduced by the above formulation as seen in Figure 5-9 at point A, where a small reversal of the previous loading erases memory of the previous δ_{in}. Subsequent reloading of the p-y curve will overshoot the previous plastic loading curve, which is contradictory to experimental observations. A remedy recommended by Dafalias (1986) is to set a threshold of reverse plastic strain accumulation. When the current plastic reversal strain exceeds the threshold value, then the current δ_{in} is updated to produce a desirable response of unloading/reloading (e.g., points B and C). If the current plastic reversal strain does not exceed the threshold value, then the value of δ_{in} would not be updated, thereby avoiding the overshooting. This improved description of loading/unloading/reloading was not coded into GeoFEAP at this time.

The behavior of the bounding surface p-y^p element is illustrated by the following comparisons. The influence of the "n" and "elast" parameters on p-y^p curves are shown in Figure 5-10. The combined behavior of the p-y^e and p-y^p curves are shown in Figure 5-11(a). Lastly, the bounding surface p-y^p curve is compared to the plastic component of the empirical curve for soft clay recommended by Matlock (1970) in Figure 5-11(b). Radiation damping is accounted for using the modified Berger et al. model as described in Section 3-2.

5.5.2 p-y Element With Gapping

Formation of a gap between the pile shaft and surrounding soil under cyclic lateral loading has been observed in many field cases. Studies of the importance of gap formation to seismic soil-pile-superstructure interaction can be traced back to Matlock et al. (1978), in which experimental results showed that a zone of reduced resistance tended to form under cyclic loading. This behavior is most pronounced near the ground surface.

In this section, formation of a gap was included in the bounding surface plasticity p-y^p curve previously described. A slack zone is defined in the model that simulates the drag resistance on a pile when a gap is formed. The formulation of the slack zone will be described by referring to the typical hysteretic behavior with gap formation shown in Figure 5-12.

A gap is formed when unloading of the p-y^p curve reaches the opposite slack zone. For example, if the pile is at point D after unloading from point A, there will be gaps to the left of the pile (points D to K) and to the right of the pile (points D to C). Positive loading from point D will cause the gap to close (point D to E to F), followed by elastic behavior to point G and inelastic behavior to point H.

The drag resistance within the slack zone can be explained as a friction force provided against the sides of the pile when a gap is open. When the pile moves within the slack zone, the soil will provide a constant resistance to movement; the direction of the drag resistance is always opposite to the direction pile movement relative to the soil (e.g., loop of points I, J, K, and L in Figure 5-12). This drag resistance is specified by a drag resistance ratio parameter "frict," which is defined as the ratio of the drag force when the gap is open to the maximum soil resistance (p_{ult}). The value of "frict" was taken as 0.1 throughout this study.

This p-y^p element with gapping uses the same parameters as the previously described p-y^p element, except with the addition of the drag resistance ratio "frict." The complete bounding surface p-y curve can be obtained by combining the plastic p-y^p with gapping element and the elastic p-y^e element, as illustrated in Figure 5-13.

5.6 Numerical Simulations with New p-y Elements

The new bounding surface p-y elements, as implemented in GeoFEAP, were evaluated by performing analyses of the centrifuge model test results previously analyzed using DRAIN-2D, PAR, and NONSPS. In this section, select results obtained using GeoFEAP and the new p-y elements are compared to both the centrifuge data and the results obtained using DRAIN-2D with series radiation damping.

The first result shown here is for GeoFEAP Case I, which used the new bounding surface p-y element without gapping. The conditions adopted were the same as used for DRAIN-2D Case III (Table 5-2). Figure 5-14 shows satisfactory agreement between the results obtained using GeoFEAP and DRAIN-2D (Wang 1998), except for the presence of some high frequency numerical noise at the pile head for the GeoFEAP results. Recent GeoFEAP analyses of other model test data have shown that numerical damping can effectively remove this high frequency noise while having negligible effect on the main features of structural response (superstructure accelerations, pile bending moments) for these single-pile systems.

The effect of radiation damping on the GeoFEAP Case I results was also evaluated. Figure 5-15 shows the acceleration time history at the superstructure and pile head with and without radiation damping, while Figure 5-16 shows the acceleration response spectra at the superstructure and pile head with and without radiation damping. The influence of radiation

damping at longer periods is small, while the effect is greater at shorter periods (higher frequencies). This is reasonable since the energy dissipated by nonlinear soil response dominates over radiation damping at low frequencies. As frequency increases, more energy is radiated away from the pile and its contribution to energy dissipation is greater. Comparing these numerical analyses with the centrifuge data suggests that the analysis method still seems to be overestimating damping (Figure 5-16).

The plastic p-y^p hysteretic loops at different depths with radiation damping is shown in Figure 5-17. The nonlinearity of the soil reaction is most pronounced near the ground surface, with the soil below about three pile-diameters depth behaving more or less elastically.

GeoFEAP Case II repeats the Case I analysis but with the new p-y element with gapping. The acceleration time histories of the superstructure and pile head when gap formation is included are shown in Figure 5-18: (a) for the case without radiation damping, and (b) for the case with series radiation damping. Figure 5-19 shows the acceleration response spectra of the superstructure and pile head corresponding to these two cases. Figure 5-20 shows the plastic hysteretic p-y^p loops of the soil spring near the ground surface with the radiation damping taken into account.

Inclusion of the gap formation resulted in improved agreement between the measured and calculated responses. The formation of the gap had two main effects: (1) it slightly softened the response of the soil-pile-superstructure system, and (2) it reduced the amount of hysteretic energy dissipated by the p-y^p springs, thereby reducing the amount of damping in the system. The effect of turning off the radiation damping was an increase in the dynamic response but with little effect on the system's fundamental period. The nonlinearity of the soil reaction remained significant down to a depth of six to seven pile diameters, which is considerably deeper than was calculated without gap formation.

5.7 Significance of Damping Details

It has been shown that series radiation damping is technically superior to parallel radiation damping because it avoids the possibility of unrealistically large damping forces. The possibility of unrealistically large damping forces was demonstrated by the analyses presented herein for a single pile in soft clay with an elevated superstructure mass that imposed large lateral loads and bending moments on the pile head. Consequently, there was significant yielding of soil near the pile (near-field) such that the relative soil-pile displacement (y) greatly exceeded the elastic range of behavior. Under these conditions, the use of parallel hysteretic and viscous (radiation) damping components, with the dashpot coefficients derived for elastic conditions, resulted in unrealistically large damping forces. These large damping forces then had a significant effect on the natural period of the structural system, thereby affecting its dynamic response. Badoni and Makris (1996) also recognized that parallel radiation damping could produce excessive damping forces, and chose to circumvent this possibility by limiting the magnitude of the parallel radiation damping force.

It should be noted, however, that there are many situations for which the error introduced by use of parallel radiation damping has been found to be small. For example, a pile group embedded in stiff soils may experience relative soil-pile displacements that only slightly exceed the elastic range, such that the overestimation of damping forces is not excessive. Furthermore, a pile group in competent soils is often stiff enough that marginal changes in its stiffness have only a small effect on the predominant period of any relatively long-period structure. It follows that in such cases, the dynamic response of the structural system may be relatively unaffected by the use

of parallel radiation damping.

A recommended method for checking the importance of radiation damping in a nonlinear dynamic analysis is to conduct at least a limited parametric study of how the linear damping coefficients affect important predicted quantities. It is appropriate to run one analysis with the linear radiation damping set to zero for those p-y elements that are loaded into the nonlinear range to see how important it is. If there is a significant difference between these two predictions, one must be careful to check that radiation damping is being properly implemented.

5.8 Conclusions From Dynamic Response Comparisons

Radiation damping, and the details of how it is implemented, can have a significant impact on the calculated response of nonlinear systems. In dynamic BNWF analyses, energy loss through radiation damping is modeled by viscous dashpots that are derived for linear elastic conditions. Viscous dashpots in parallel with a hysteretic element ("parallel radiation damping") can provide a mechanism for unrealistically large forces to be transmitted around the hysteretic element. This problem can be avoided by placing the linear viscous dashpot in parallel with only the linear component of the hysteretic element, and in series with the hysteretic element ("series radiation damping"). The importance of these damping details is relevant to other nonlinear soil dynamics and structural dynamics problems.

By separating the soil into two zones, near field and far field, soil behavior under soil-pile-structure interaction can be more reasonably modeled. This macroscopic model comes from the understanding of the interaction mechanism, i.e. strong soil nonlinearity in the near field and elastic wave radiation into the far field. The contributions of the two parts to the response of the whole system depend on the seismic input (level of shaking, frequency contents etc.) and characteristics of the soil-structure system. A complete mathematical model should address both parts.

If "parallel radiation damping" is used, shallow p-y elements dynamically loaded past yield can produce dashpot forces that exceed the ultimate capacity of the p-y spring. Thus these numerical models did not capture the lengthening of the single-pile system's fundamental period observed in the centrifuge tests. In fact, the calculated response of the superstructure was insensitive to large changes in the p-y curves.

If "series radiation damping" is used, the calculations are sensibly dependent on the stiffness and strength of the p-y curves. Furthermore, predictions of the pile-head and superstructure response are in reasonable agreement with the preliminary centrifuge results.

The inclusion of gap formation was shown to improve the agreement between the calculated and measured dynamic responses of the centrifuge model tests analyzed in this study. The main effects of gap formation were shown to be: (1) a slight lengthening of the system's fundamental period; and (2) a reduction in the hysteretic energy dissipated by the p-y springs.

The preceding analyses do not account for several aspects that may warrant attention in future studies: frequency dependence of radiation damping; compatibility of the elastic p-y^e resistance with the free-field soil stiffness; degradation of p-y resistance with cyclic loading; and extension of the analysis method to pile groups.

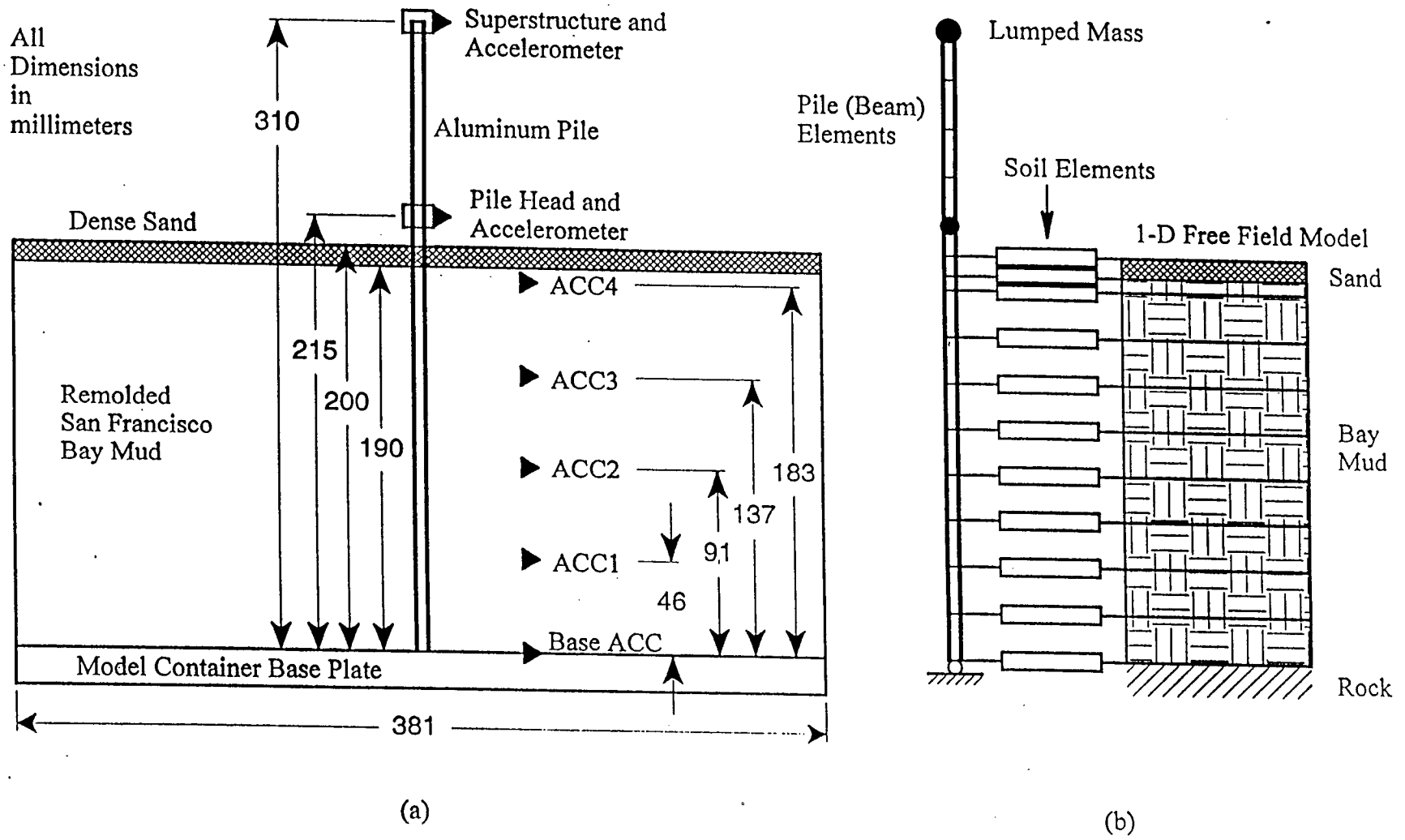

Fig. 5-1: (a) Configuration of Centrifuge Model for test CSPSM7
(b) Configuration of Numerical Model of test CSPSM7

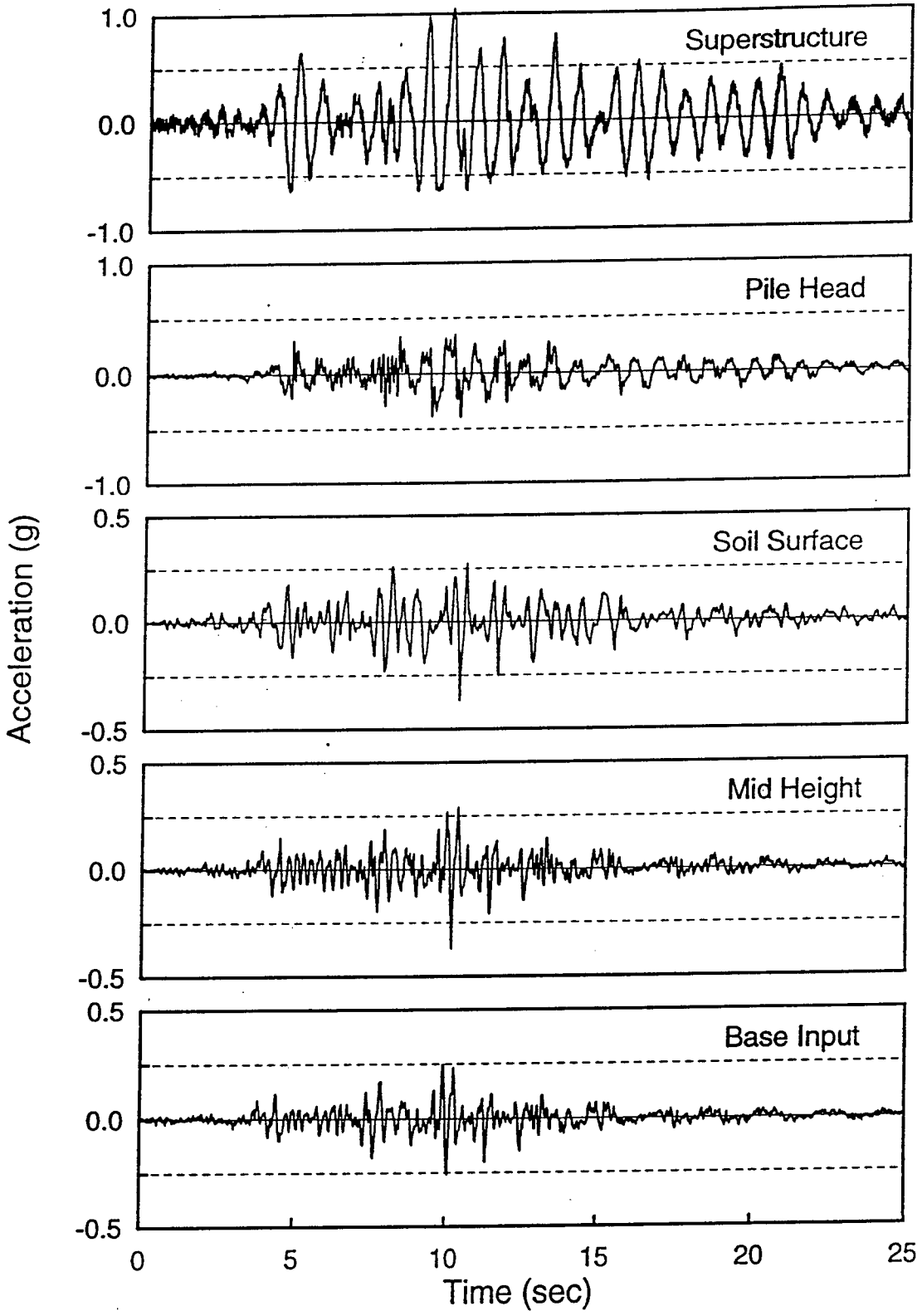

Fig. 5-2: Acceleration time histories (centrifuge)

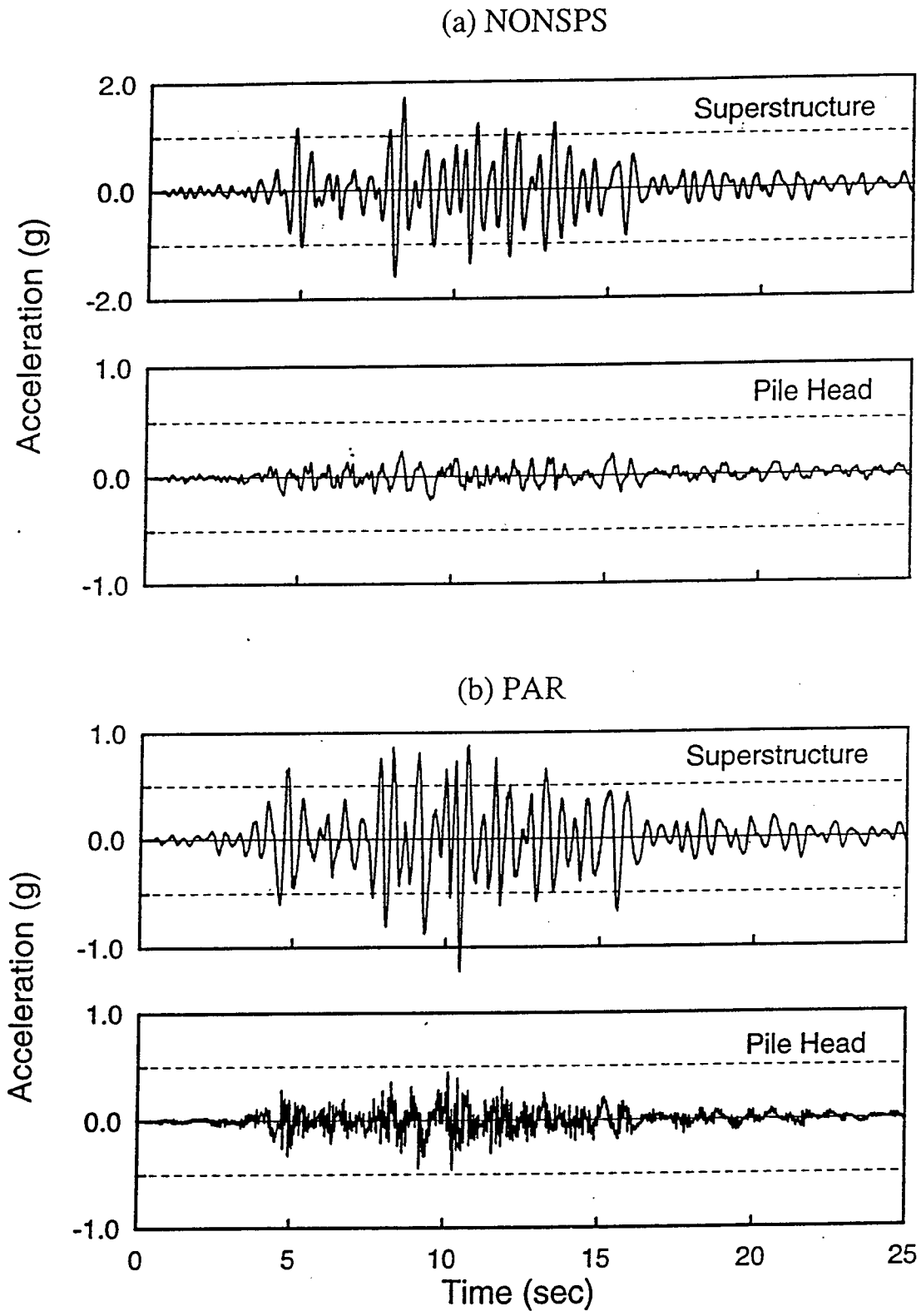

Fig. 5-3: Acceleration time histories (numerical)

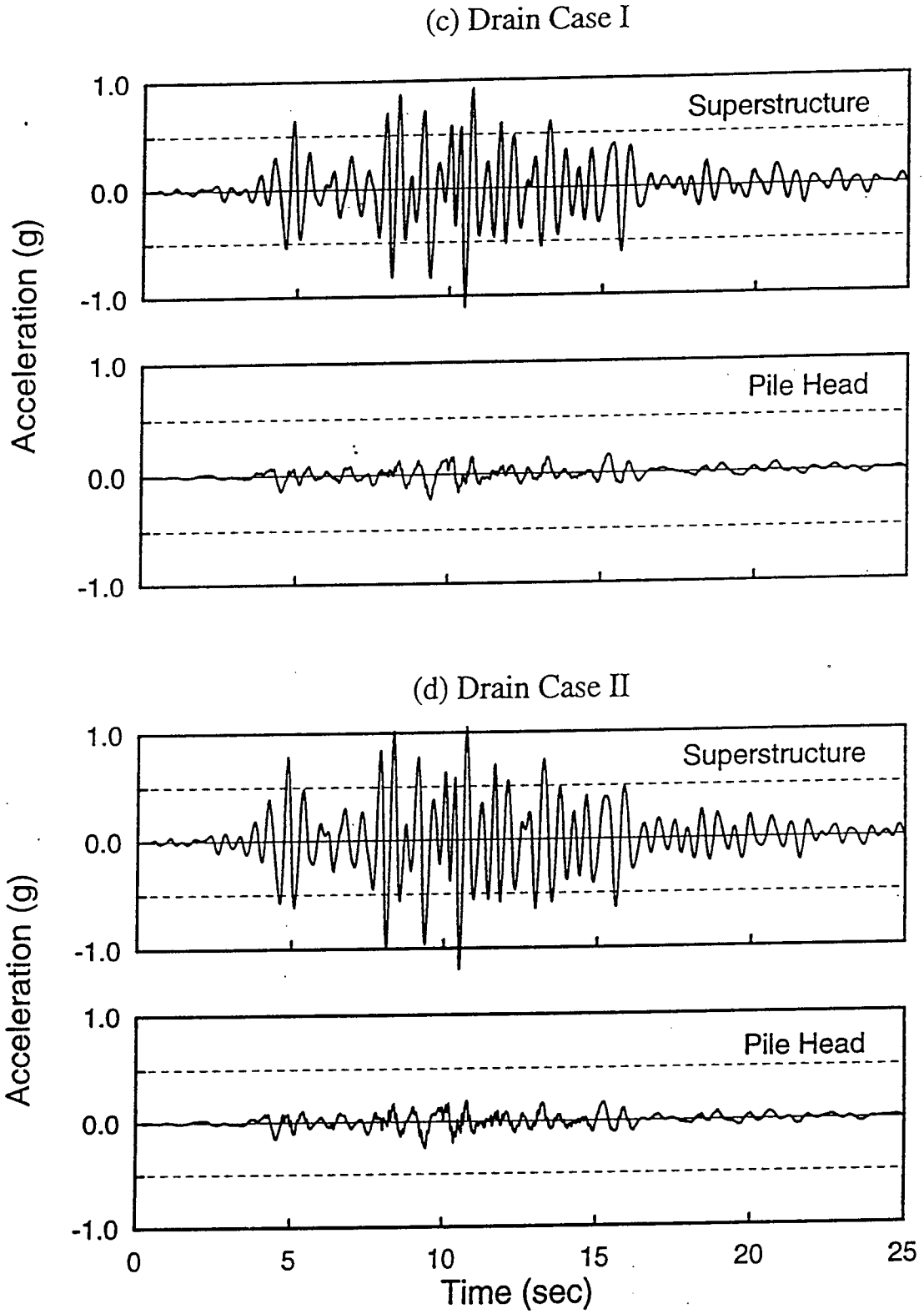

Fig. 5-3: Acceleration time histories (numerical)

(e) Drain Case III

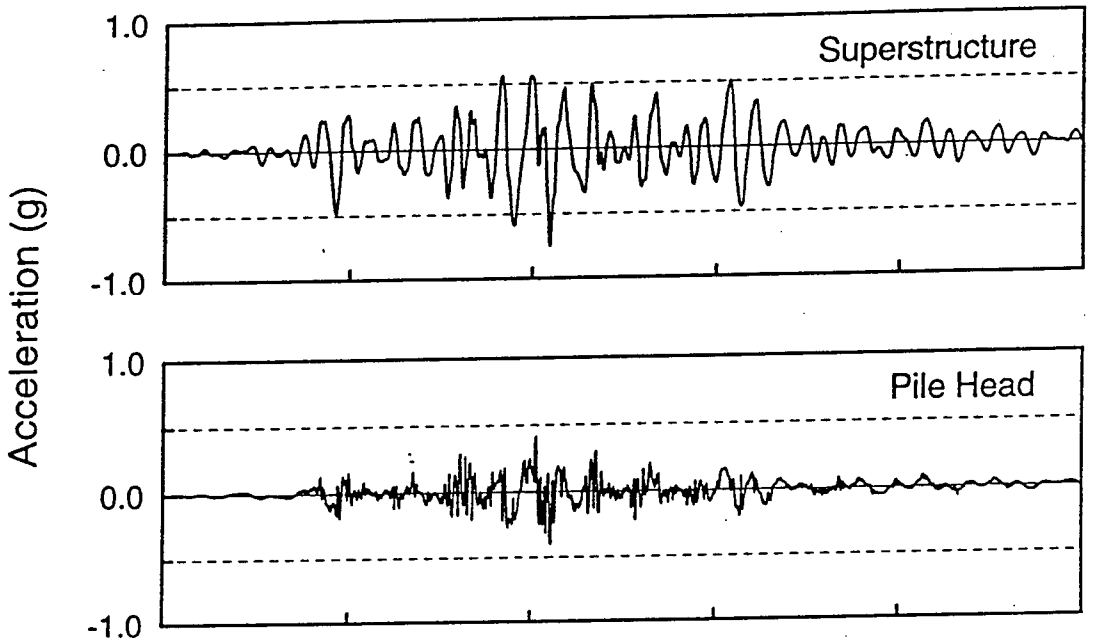

(f) Drain Case IV

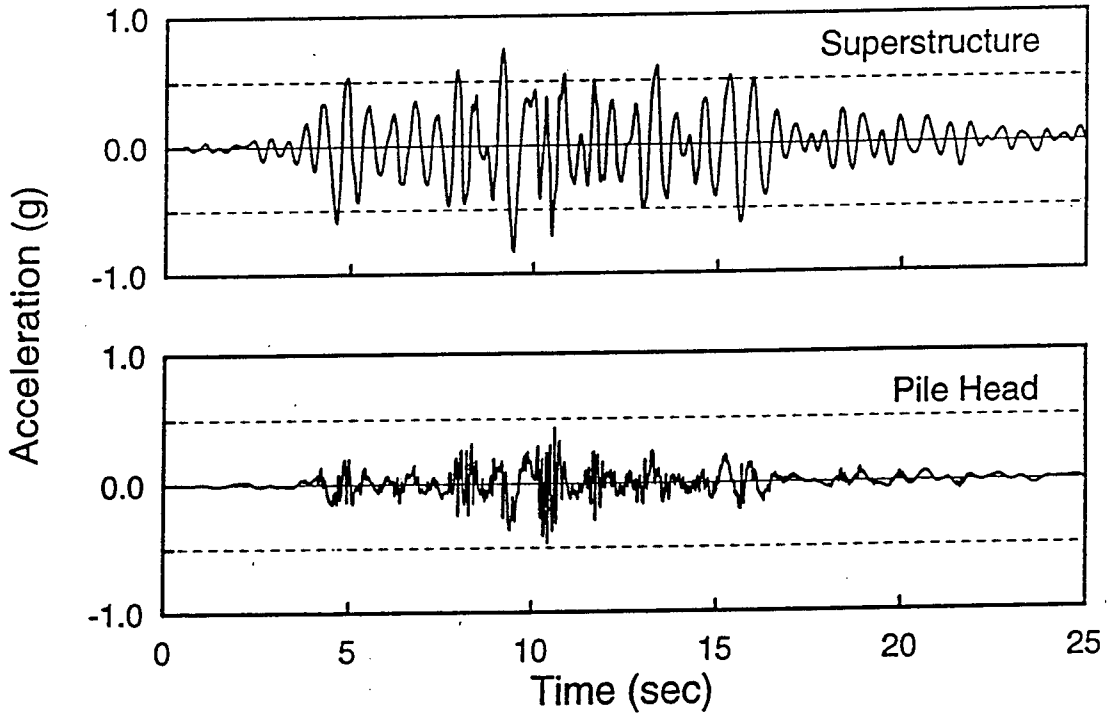

Fig. 5-3: Acceleration time histories (numerical)

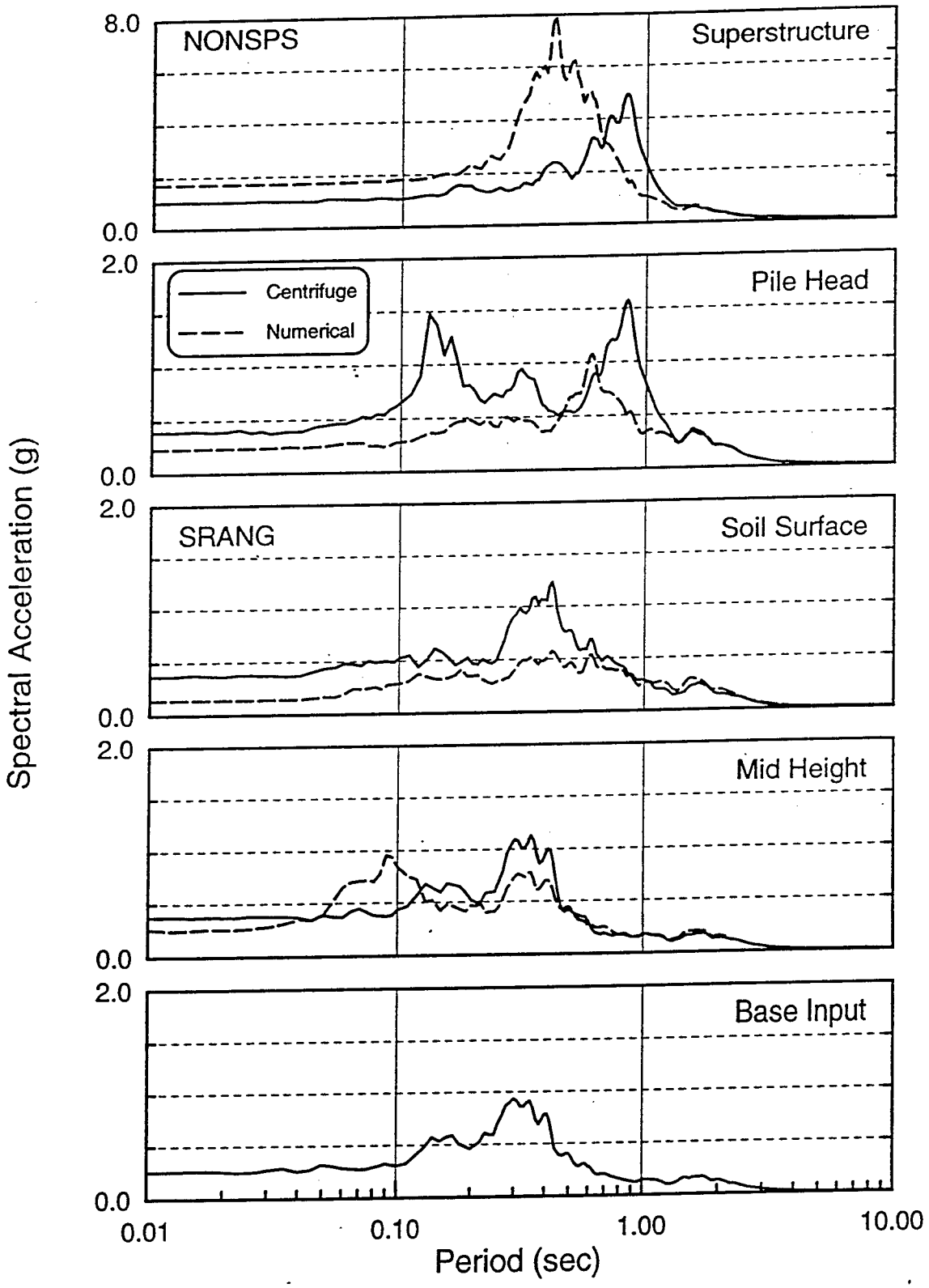

Fig. 5-4(a): Comparison of recorded and computed acceleration response spectra on the pile and free field by NONSPS and SRANG

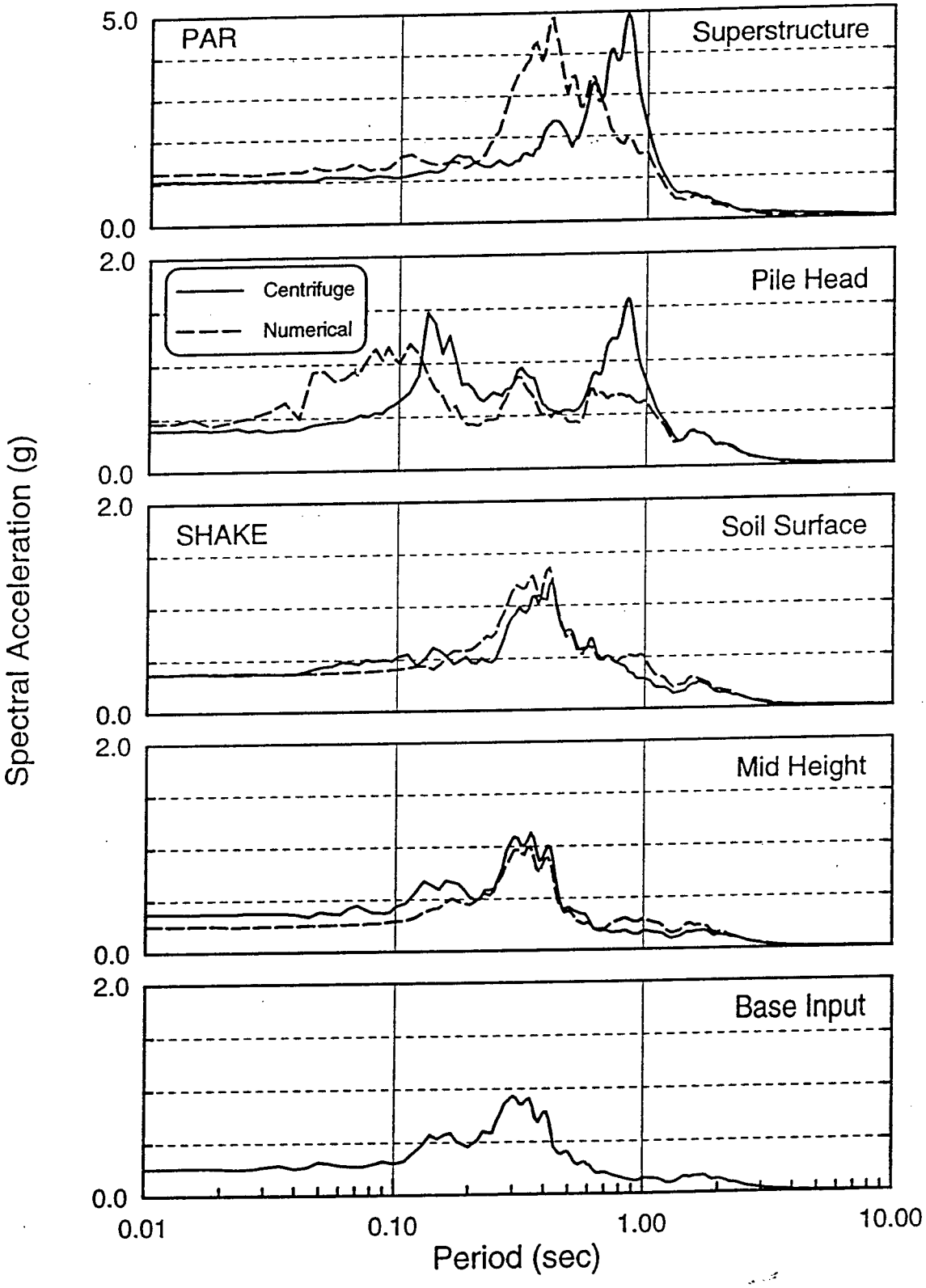

Fig. 5-4(b): Comparison of recorded and computed acceleration response spectra on the pile and free field by PAR and SHAKE

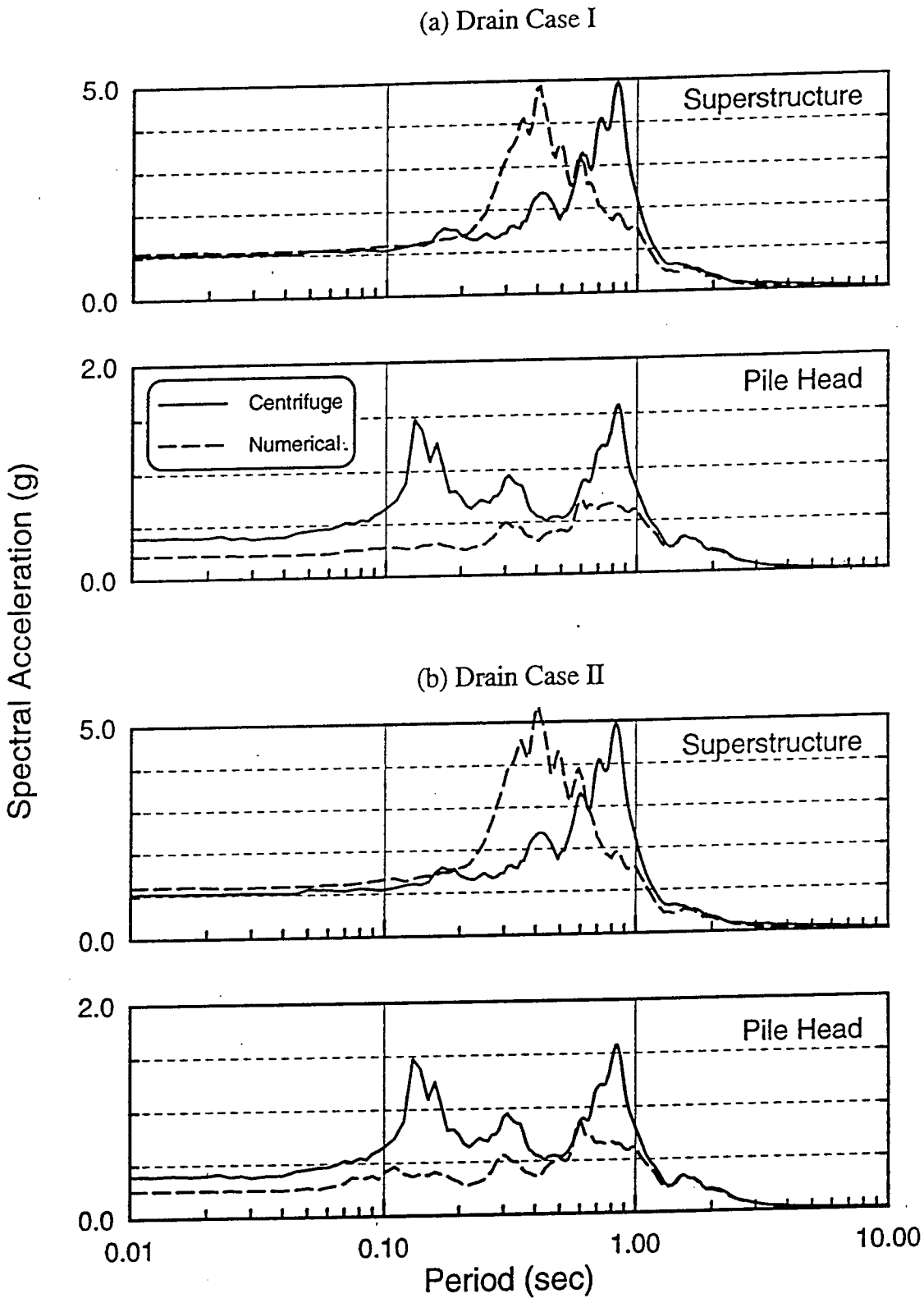

Fig. 5-5: Comparison of recorded and computed acceleration response spectra on the pile head and superstructure by DRAIN

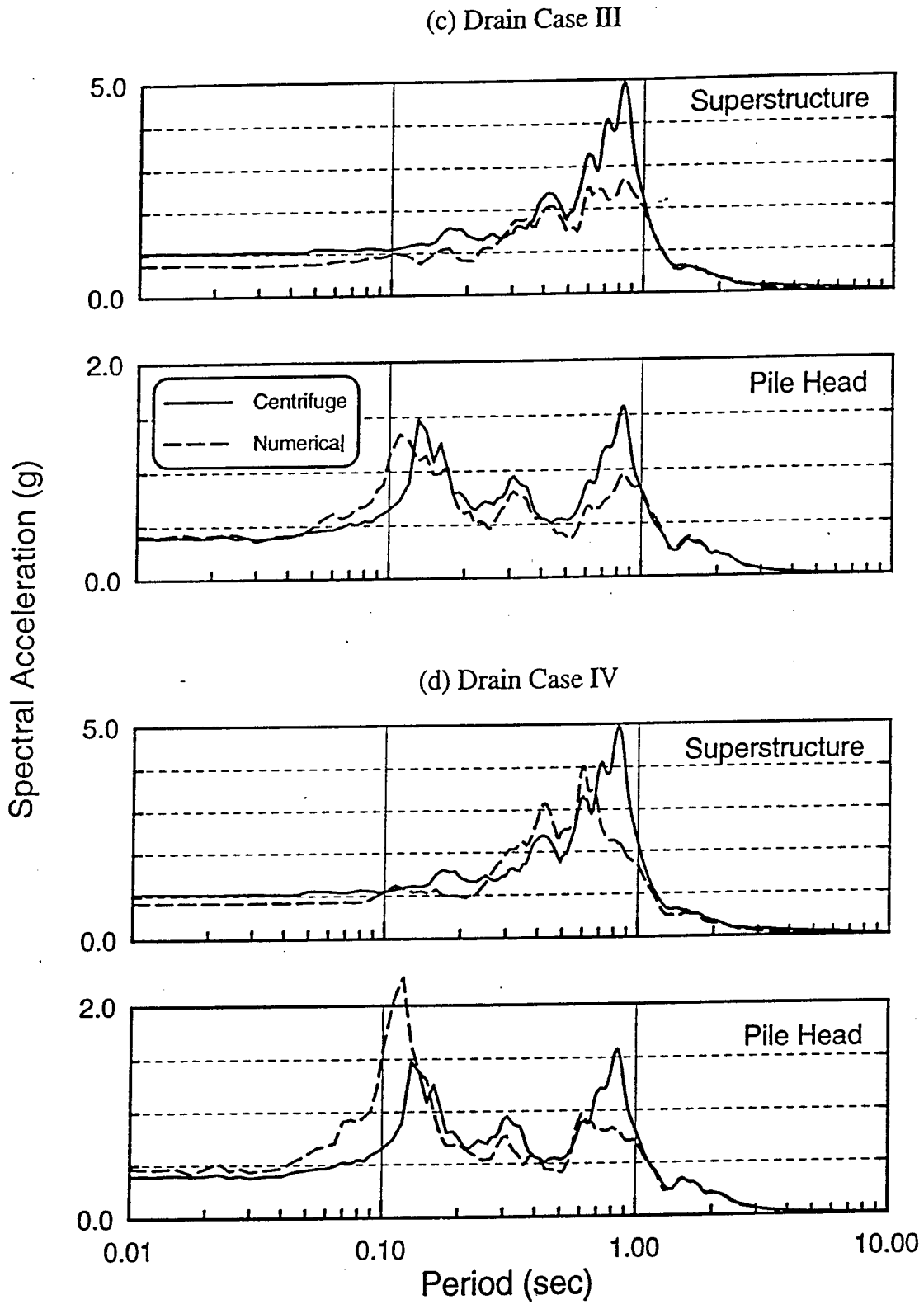

Fig. 5-5: Comparison of recorded and computed acceleration response spectra on the pile head and superstructure by DRAIN

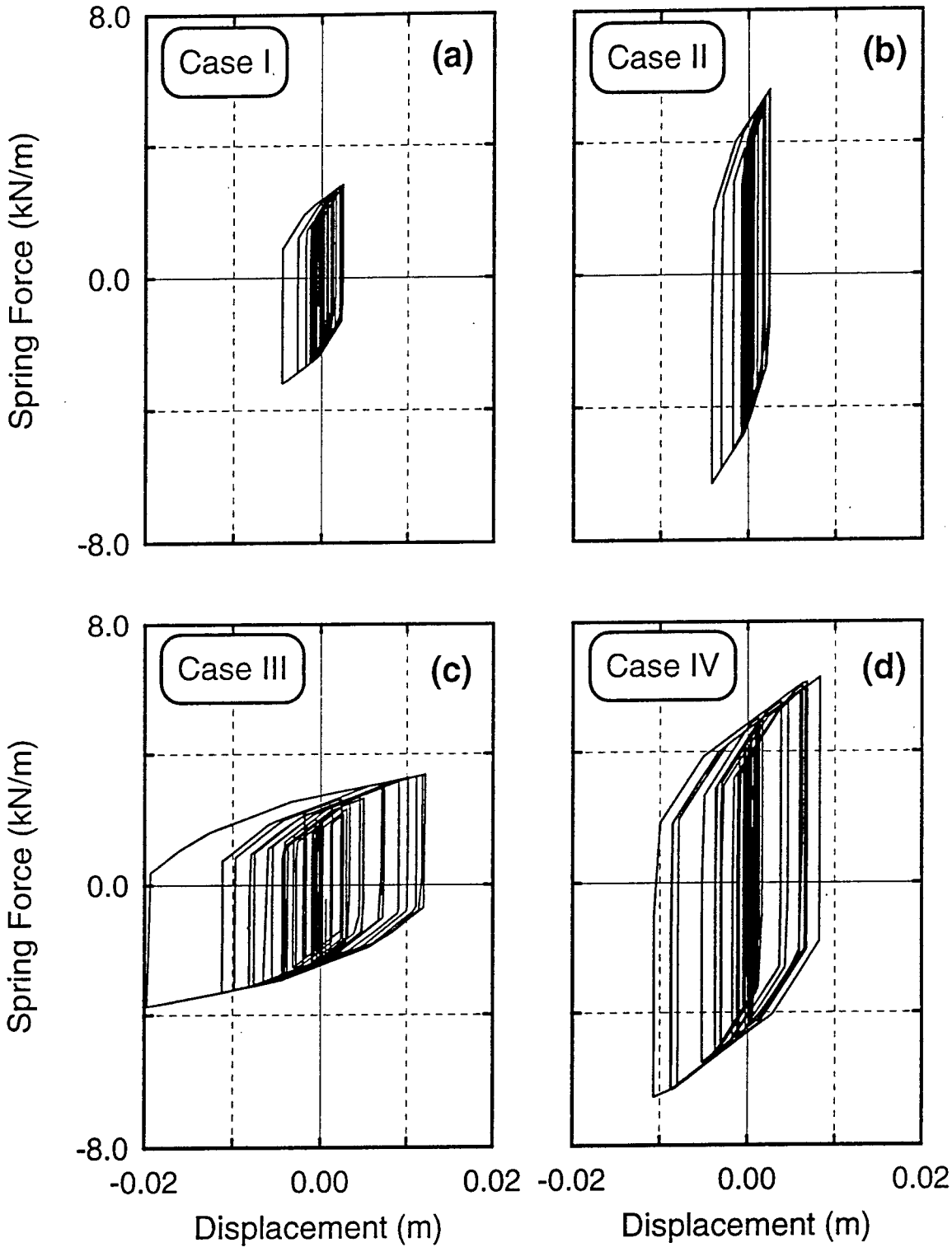

Fig. 5-6: Plastic hysteretic loops in the clay at a depth of 0.508 m for DRAIN analyses

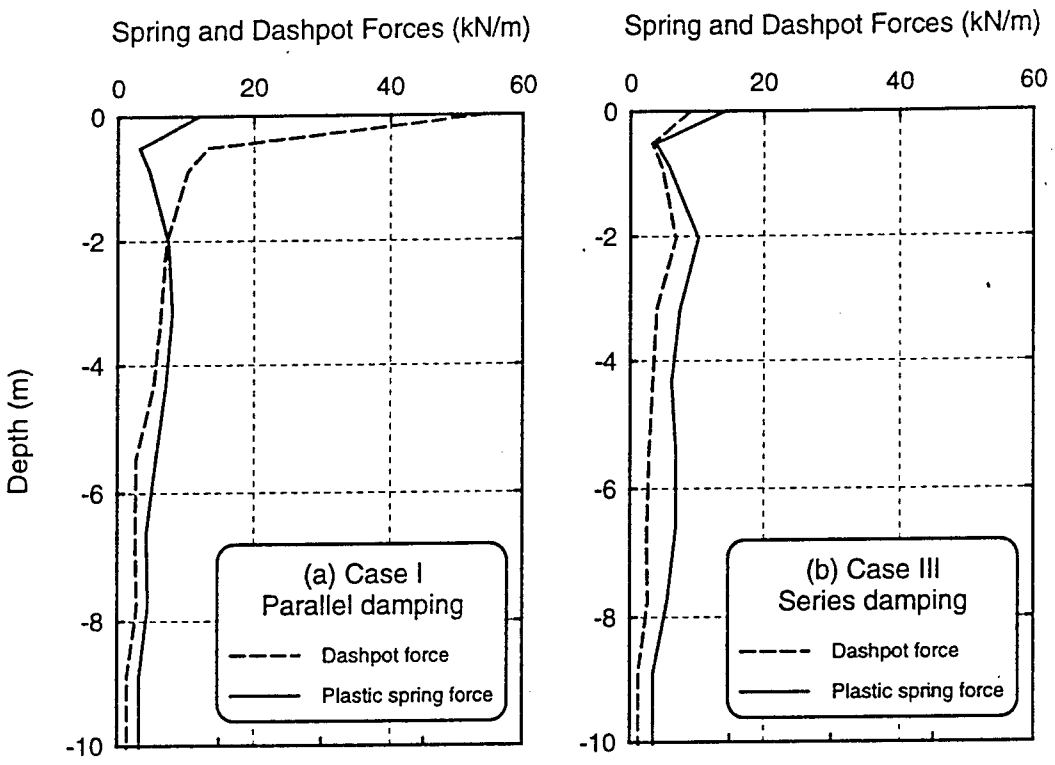

Fig. 5-7: Envelopes of plastic p-y spring force and dashpot force

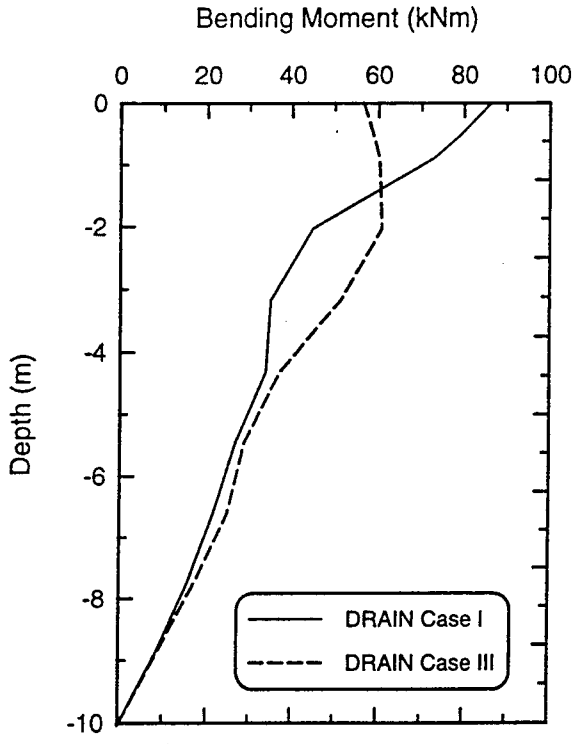

Fig. 5-8: Envelopes of pile bending moments
for DRAIN Case I and Case III

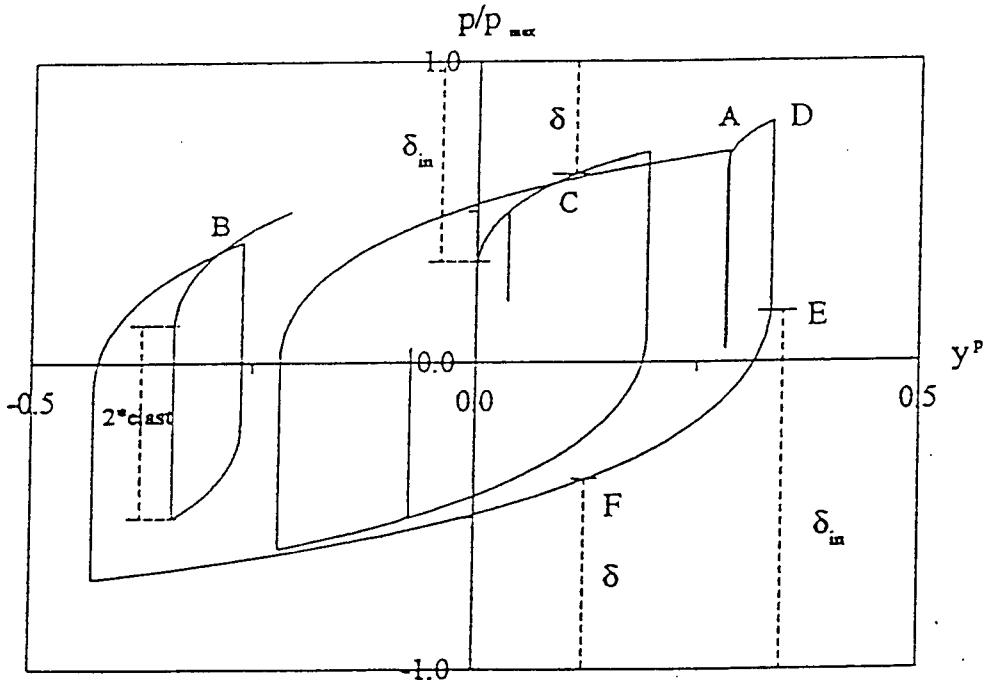

Fig. 5-9: Bounding surface plastic $p - y^p$

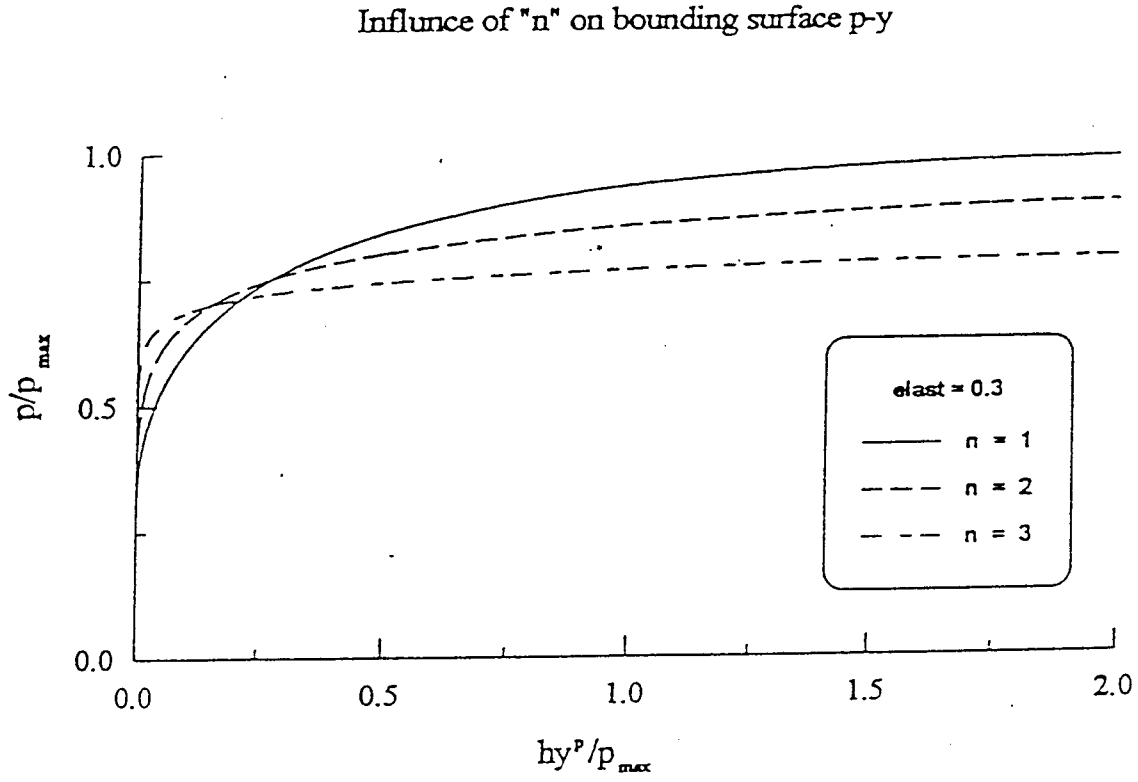

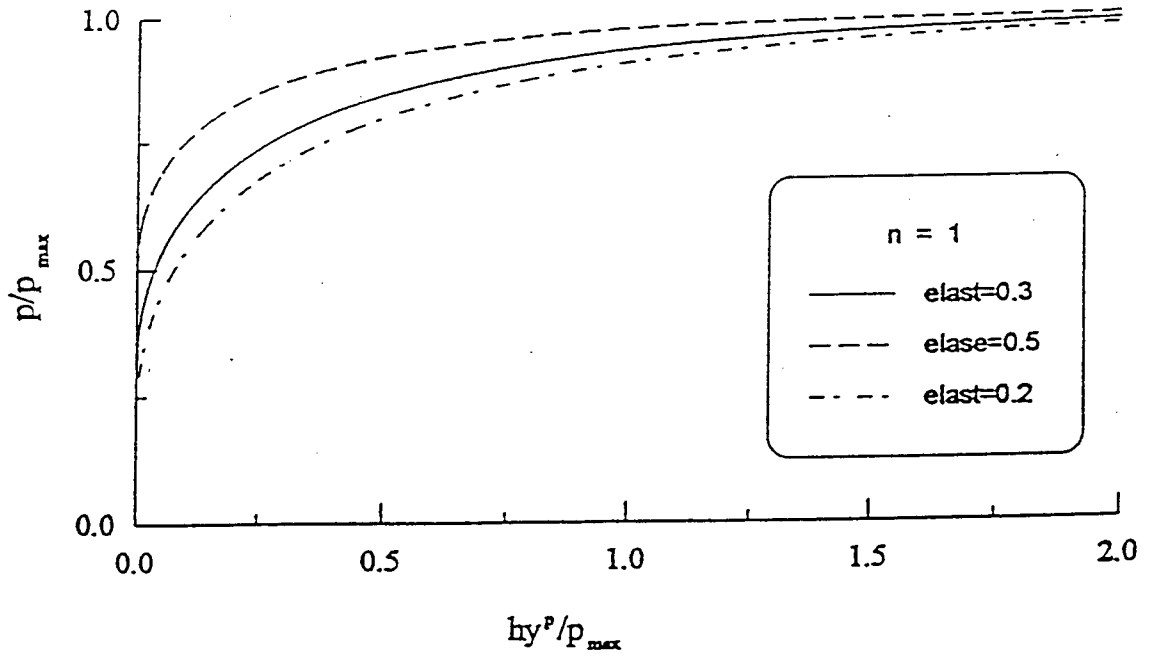

Fig. 5-10: Influence of 'n' and 'elast' on bounding surface plastic $p - y^p$

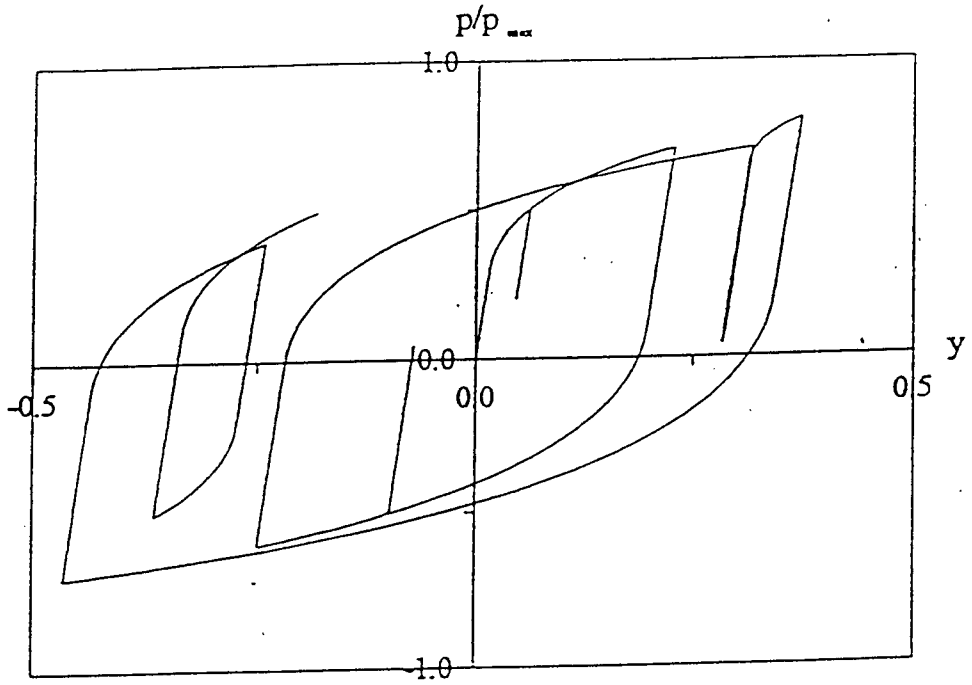

Fig. 5-11(a): Bounding surface p-y: combination of plastic $p - y^p$ and elastic $p - y^e$

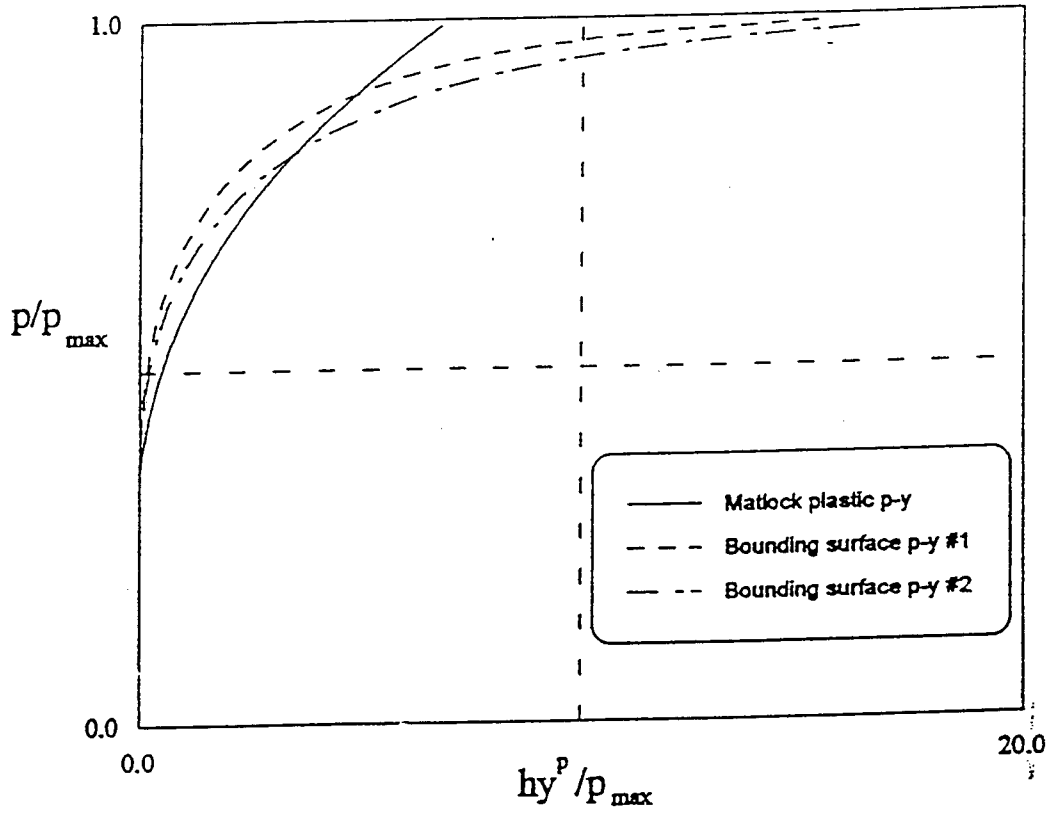

Fig. 5-11(b): Fitting of the Bounding Surface Model to the Matlock's p-y

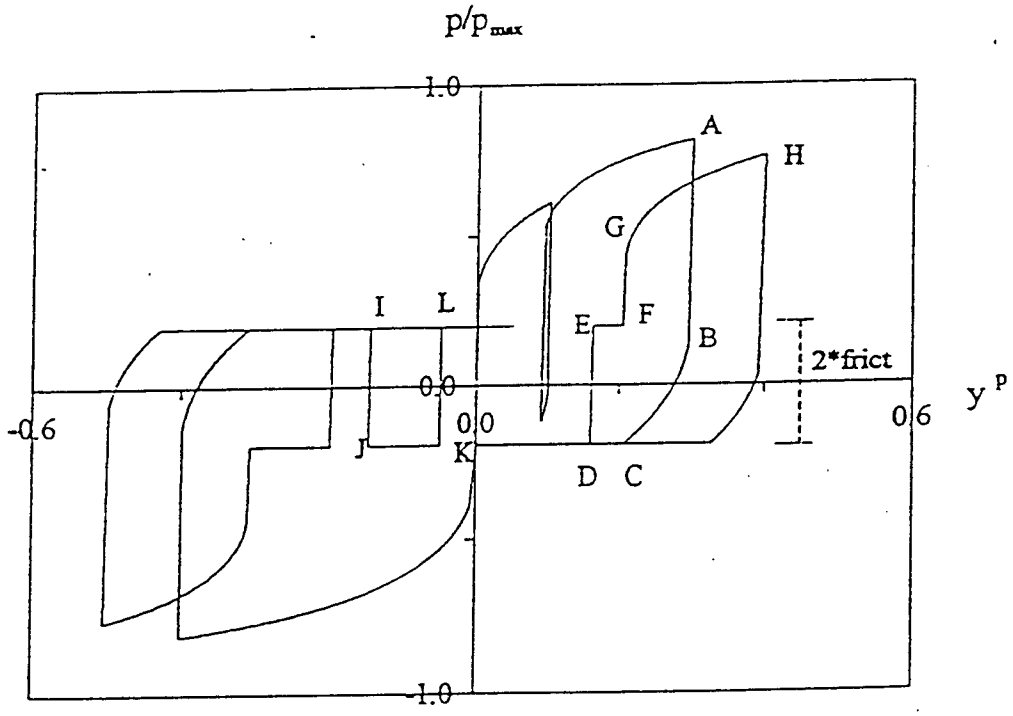

Fig. 5-12: Formation of the gap with a bounding surface plastic p-y^p

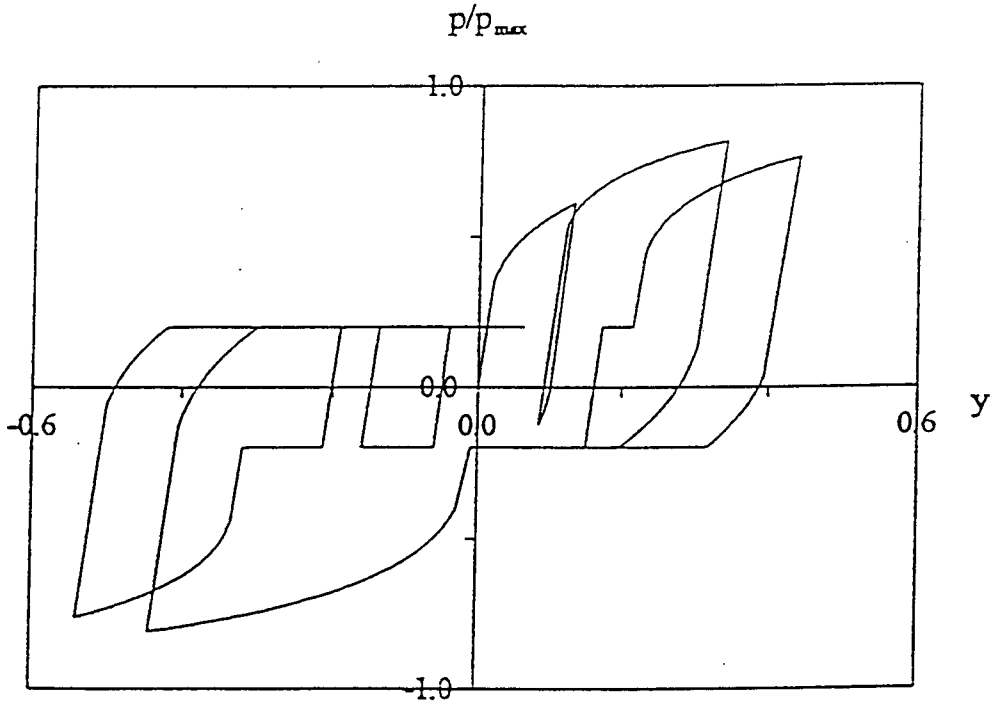

Fig. 5-13: Bounding surface p-y with gap

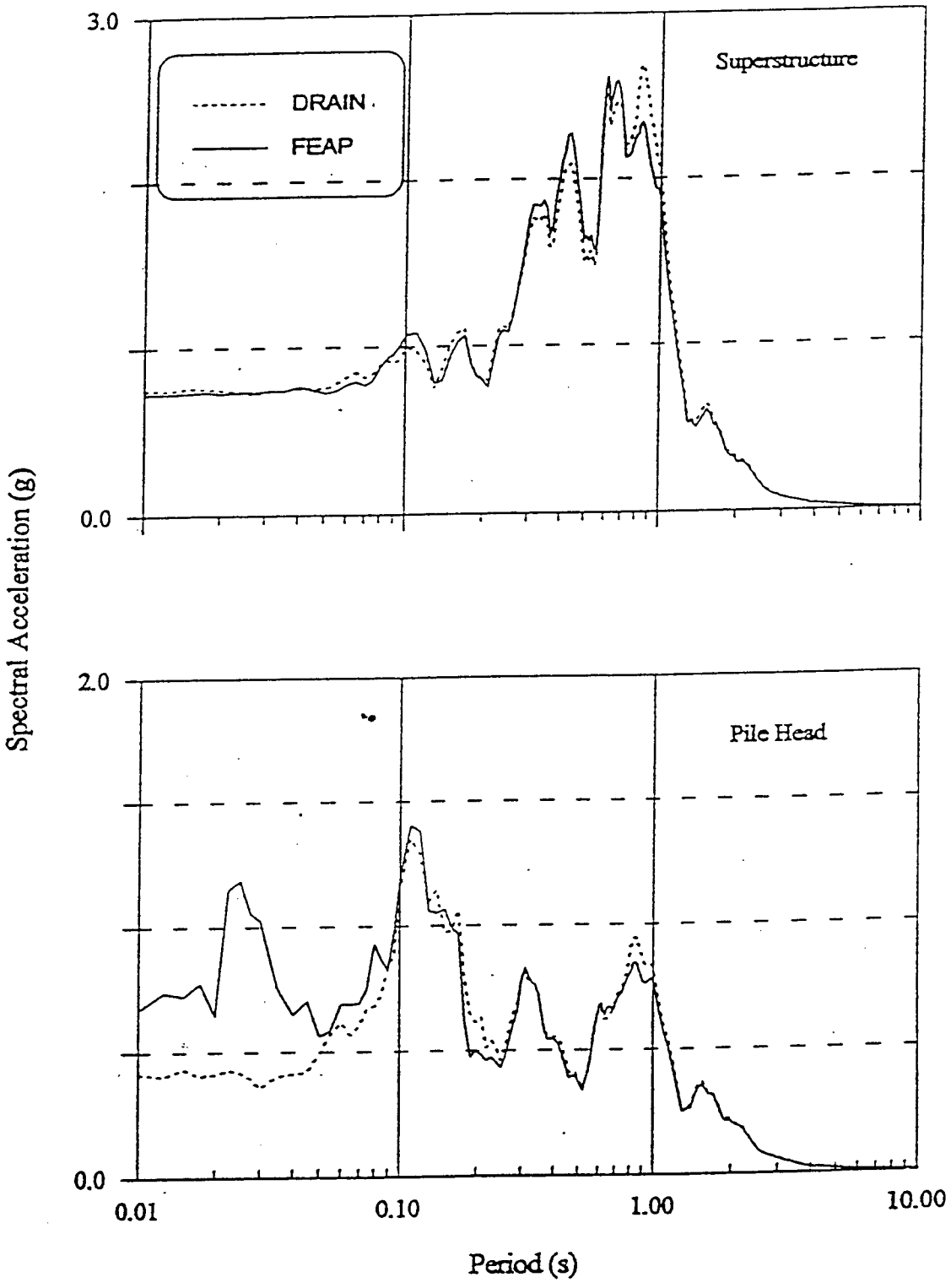

Fig. 5-14: Comparison of computed acceleration response spectra on the pile head and superstructure for DRAIN Case III and GeoFEAP Case I

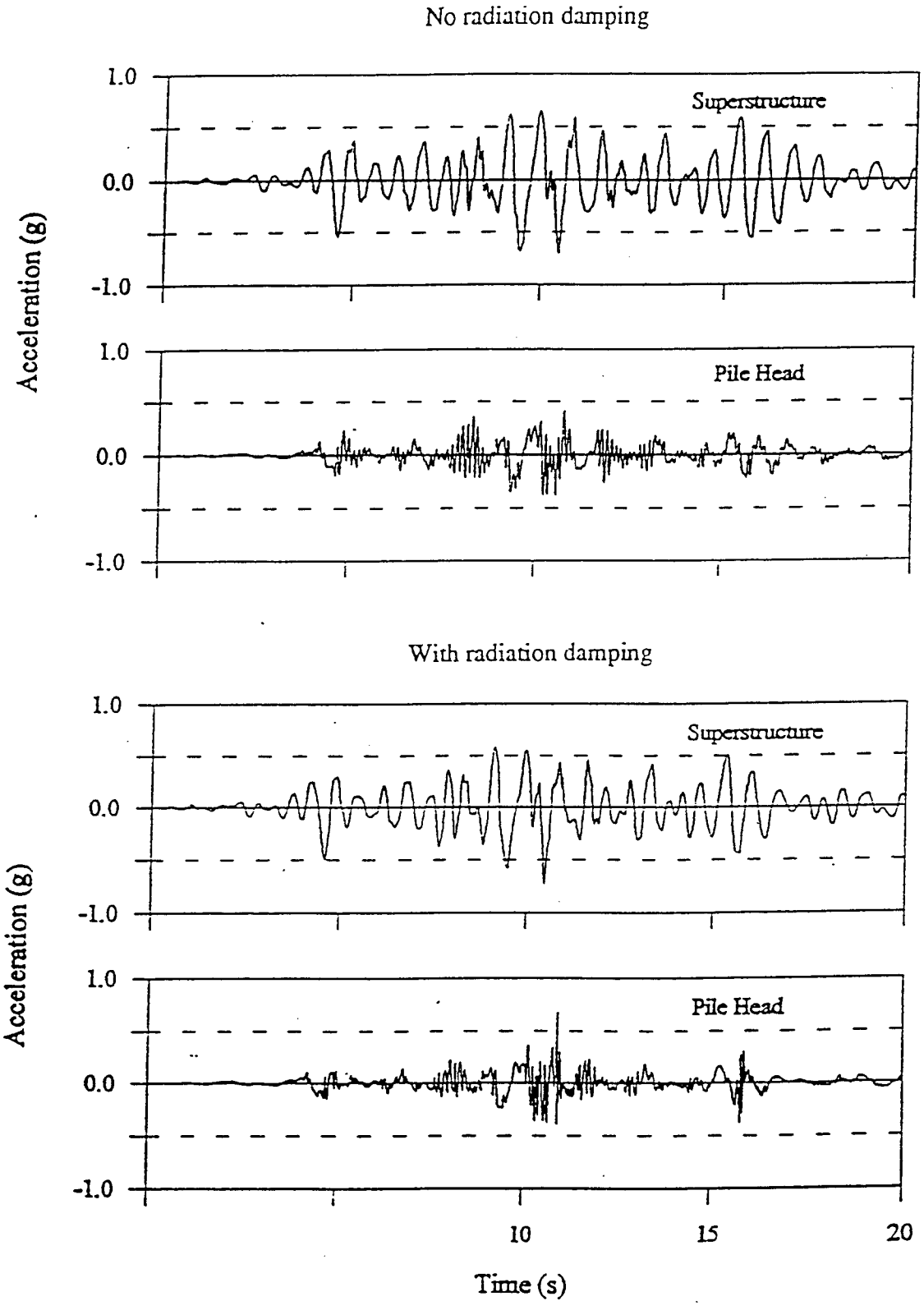

Fig. 5-15: Acceleration time history for GeoFEAP Case I

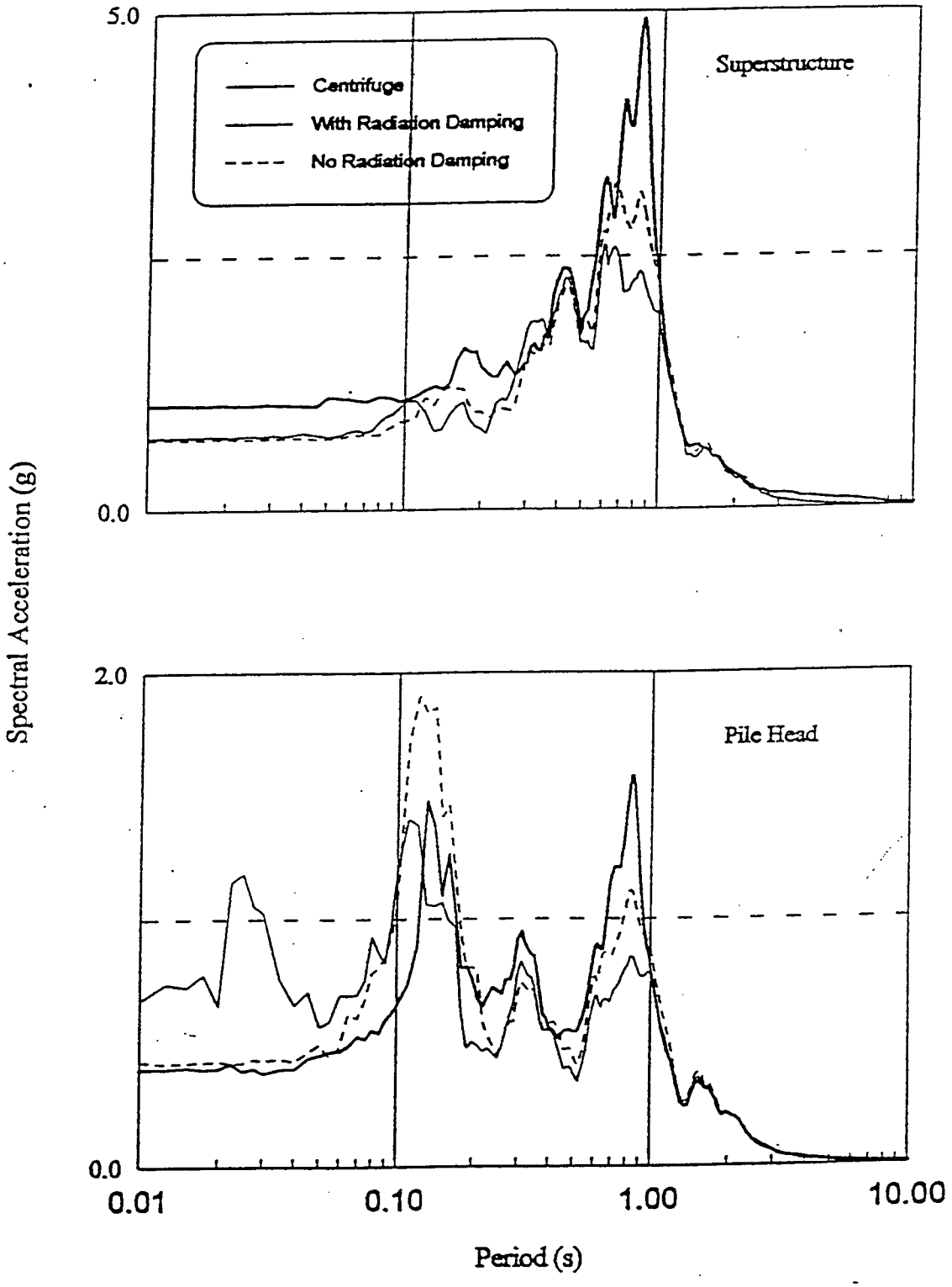

Fig. 5-16: Acceleration response spectra for GeoFEAP Case I

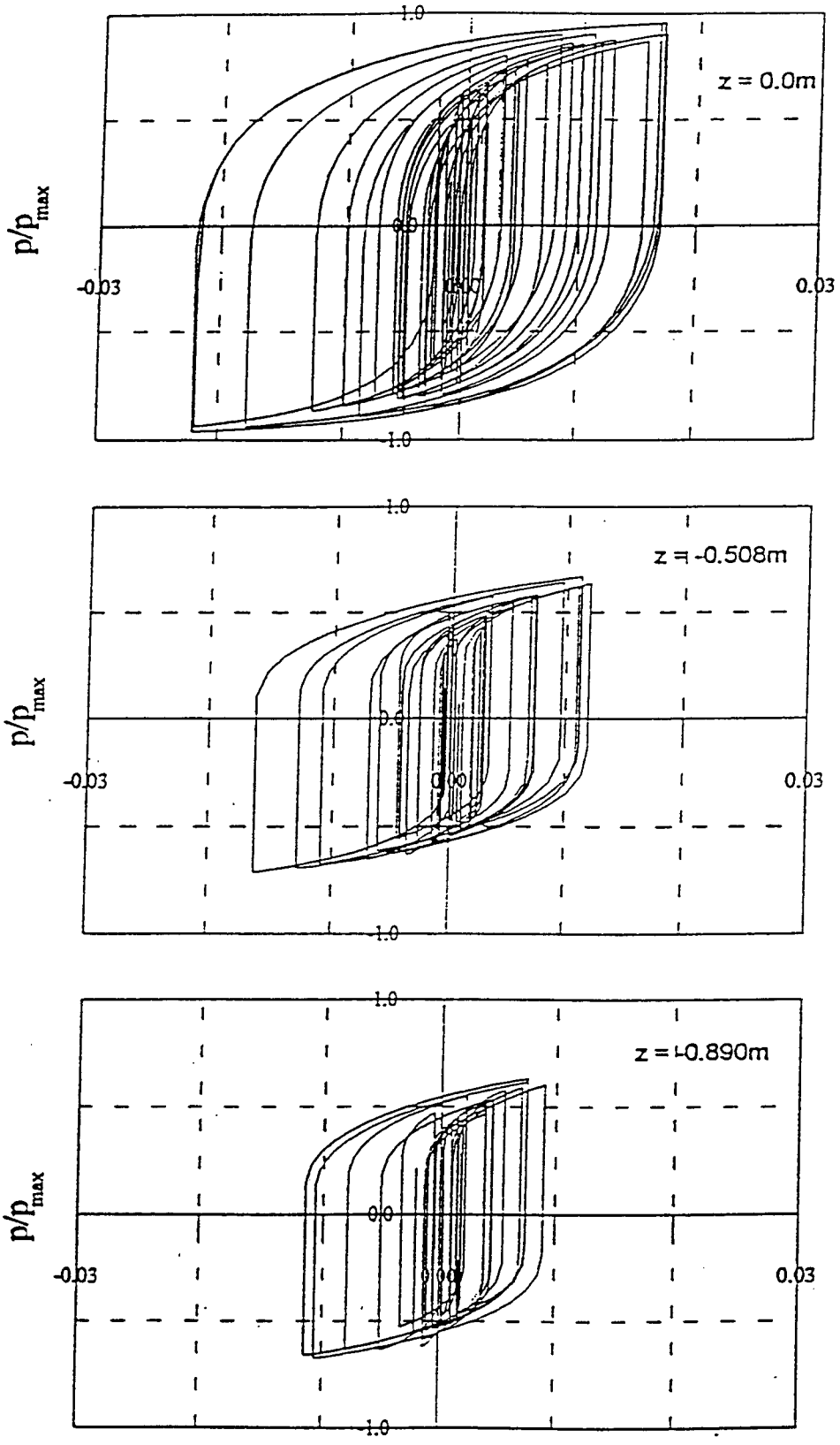

Fig. 5-17: Plastic p-y for soil springs at different depths for GeoFEAP Case I

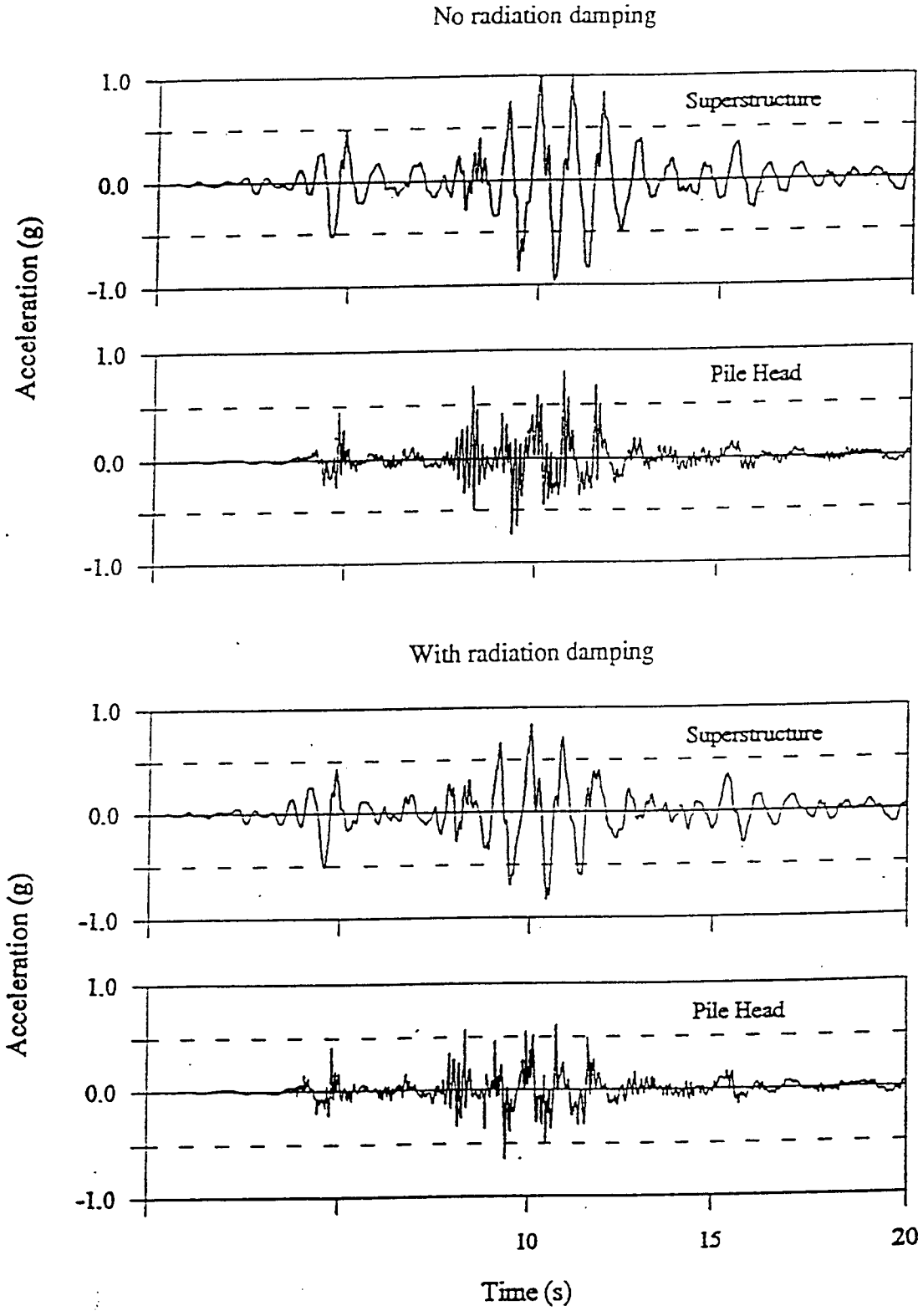

Fig. 5-18: Acceleration time history for GeoFEAP Case II

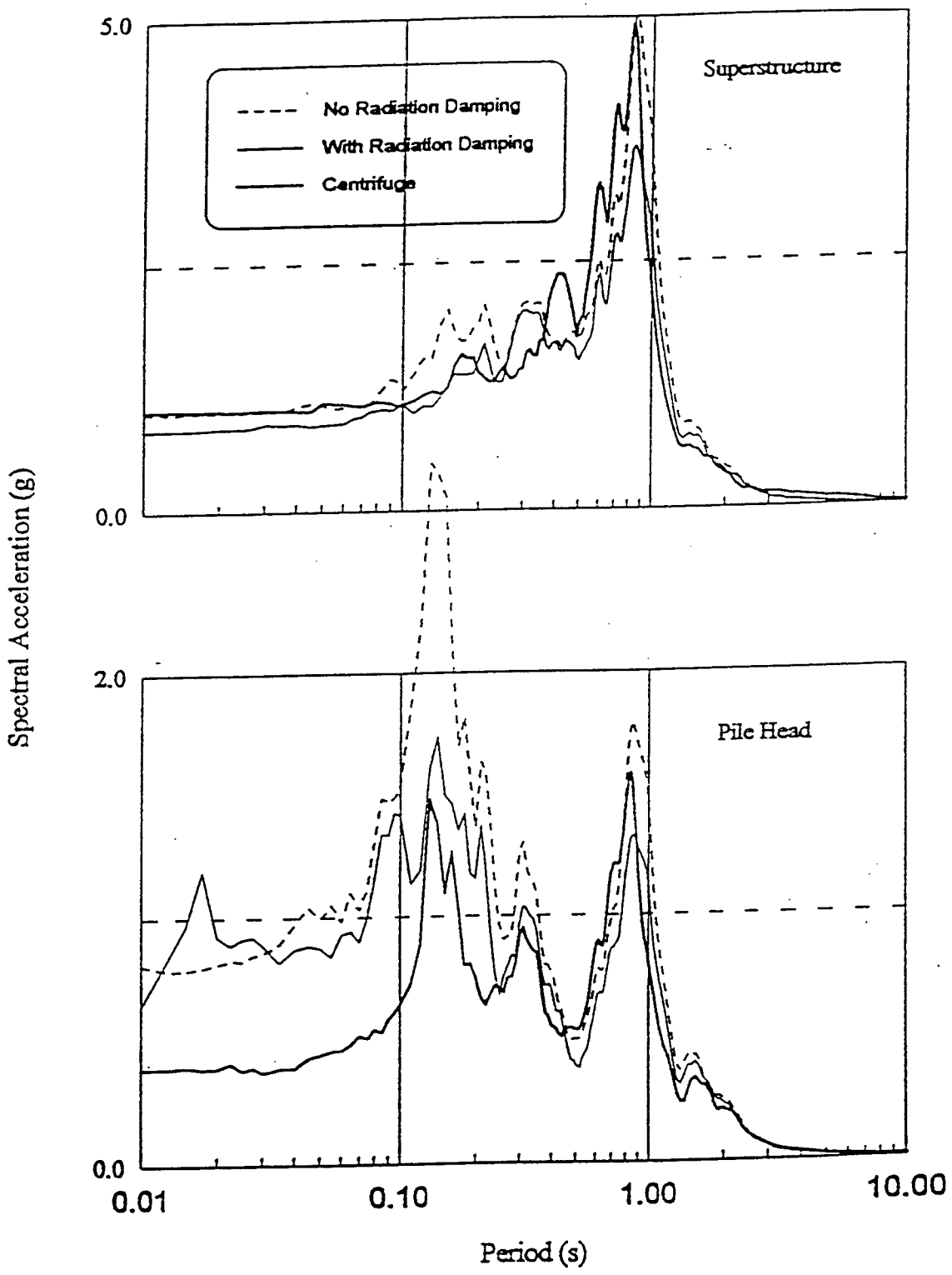

Fig. 5-19: Acceleration response spectra for GeoFEAP Case II

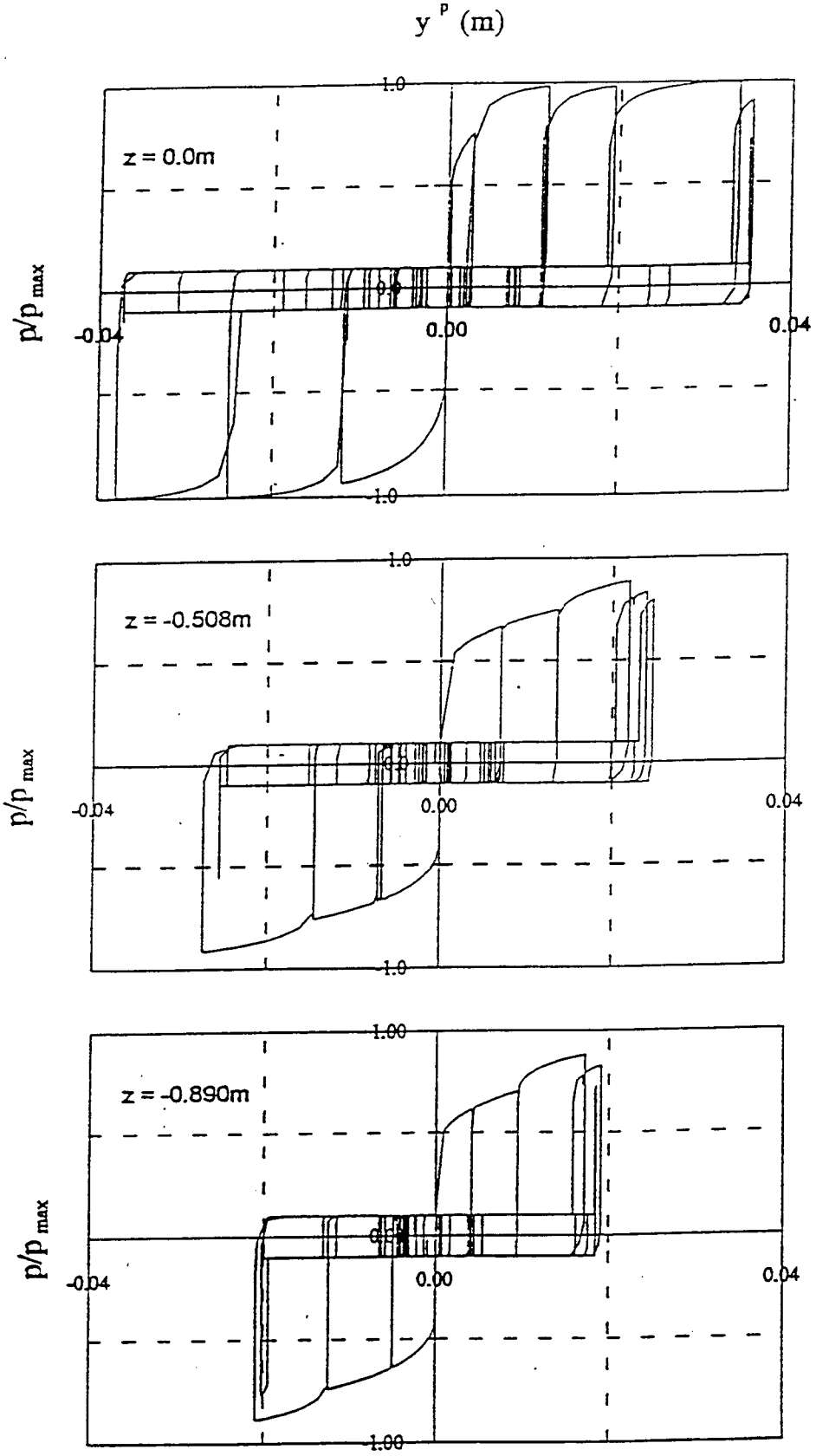

Fig. 5-20: Plastic p-y for soil springs at different depths for GeoFEAP Case II

6 PILES IN LIQUEFIABLE SOILS

6.1 INTRODUCTION

In this section, select recordings from the dynamic centrifuge tests of pile-supported structures in liquefiable sand are presented as examples of the behavior with and without liquefaction in the sand. All recorded data are available in Wilson et al. [1997(b)-(f)], and aspects of the observed behavior have been discussed by Wilson et al. (1995) and Boulanger et al. (1997). As previously described, the structural model components were designed to be representative of select Caltrans bridge structures.

Pseudo-static analyses of the peak loading conditions for single pile systems are then used to back-calculate an apparent reduction in the p-y curves of the sand when it liquefies. Discussion of these results includes a comparison with the recent findings of Liu and Dobry (1995) and other investigators.

6.2 CONSTRUCTION AND TESTING OF MODEL CONTAINER 2

The model container layouts, soil properties, and structural systems were described earlier in this report, and thus the following description focuses on aspects related specifically to Container 2. Recall that the soil profile consisted of two level layers of Nevada sand, each approximately 0.30 m thick. The sand was air pluviated to relative densities (D_r) of about 75-85% in the lower layer and about 35-40% in the upper layer. The pore fluid was a hydroxy-propyl methyl-cellulose (HPMC)-water mixture that has 10 times the viscosity of water alone. Three structural systems were tested: one supported by a single pile (SP), one supported by a 2 by 2 pile group (PG22), and one supported by a 3 by 3 group (PG33). In this report, all measurements are given in prototype dimensions unless otherwise noted. Each model pile simulates a steel pipe pile 0.67 m in diameter, 14-17 m long, with a 19 mm wall thickness. Superstructure masses for each system simulated a weight of about 445 kN per pile. The fundamental period of each system at very low shaking levels was about 0.7-0.8 sec.

System SP was impact driven into the saturated sand at 1 g. Systems PG22 and PG33 were impact driven into the dense sand layer prior to placing the loose sand layer. Air pluviation of the loose sand layer then proceeded around the piles for PG22 and PG33.

Penetration resistances for a conical probe were about 5-10 times greater in the dense layer than the loose layer, and were consistent across the container. Penetration resistances adjacent to the sides of PG22 and PG33 were slightly lower than free-field values, indicating pluviation around the pile groups resulted in a slightly lower density than in the free-field.

Model container 2 was shaken with 1 step wave event and 16 simulated earthquake events, sequentially identified as events A-Q. Earthquake input motions were scaled or modified versions of recordings from Port Island in the Kobe Earthquake (recorded at a depth of 83 m) or from Santa Cruz in the Loma Prieta Earthquake. Each shaking event was separated by 15-20 minutes, which was at least 10 times greater than the time required for excess pore pressures to fully dissipate.

6.3 TYPICAL BEHAVIOR WITH AND WITHOUT LIQUEFACTION: EVENTS D AND F

Results for events D and F are presented as examples of non-liquefaction and liquefaction events, respectively. Results are only shown for select instruments in the soil profile, on the single pile system (SP), and on the pile group PG22. Additional data is available on: axial stresses in the piles within PG22 and PG33; vertical accelerations on the shaker manifold, soil container, and throughout the soil profile; and accelerations and pore pressures at many other points as indicated in Figure 6-1. Input motions for events D and F were the "Kobe" motion scaled to peak base accelerations of about 0.03 g and 0.20 g, respectively. Event D had been preceded by only smaller shaking levels. Between events D and F there was a Santa Cruz event that produced extensive liquefaction throughout the soil model.

The effects of multiple shaking/liquefaction events on the behavior of these models was evaluated by Wilson et al. (1995) using data from model Container 1. As expected, successive events resulted in a progressive, but moderate, increase in relative density of the sand that appeared to slightly stiffen the soil profile and increase its liquefaction resistance. The results also showed that the lateral loading stiffness of the foundation appeared to decrease slightly with intervening large events, which may possibly be attributed to the large intervening events imposing a large lateral displacement history on the surrounding sand. however, these slight effects of intervening large effects appear to be small relative to the more dominant effects of liquefaction/nonliquefaction, level of shaking, and earthquake motion characteristics.

6.3.1 Soil Profile Response

Response of the soil profile for events D and F are shown by the time histories of select instruments in Figures 6-2 and 6-3. The base acceleration in event F appears to be a nearly scalar multiple of the base acceleration in event D (Figure 6-2). Accelerations at the bottom, middle, and top of the loose sand layer show progressive amplification in event D, compared to progressive and dramatic de-amplification in event F. Excess pore pressure ratios ($r_u=\Delta u/\sigma_{vo}'$) were negligible throughout the soil profile in event D, but reached 100% throughout the loose sand layer early in event F (Figure 6-3). Excess pore pressures in the dense sand layer in event F slowly increased towards a value approximately equal to the excess pore pressure at the base of the liquefied loose sand layer. This suggests that the excess pore pressures in the dense sand layer in event F were primarily due to downward migration of excess pore pressures from the loose sand layer.

6.3.2 Single Pile Response

The response of single pile system SP during events D and F is shown by the time histories of superstructure acceleration, pile-head acceleration, superstructure displacement, and bending moment at various depths in Figures 6-4 and 6-5, respectively. All recordings show that the system's "fundamental" period lengthened considerably in event F relative to its value during event D. The peak superstructure acceleration was about 5 times the peak base acceleration during event D, but only about 1.4 times the peak base acceleration during event F. In both events, the bending moments and lateral displacements were strongly correlated to the superstructure acceleration. Note that superstructure displacements are relative to the top container ring and thus only approximate the displacement relative to the free-field ground surface. As expected, the depth to the largest bending moment increased as a result of

liquefaction: the largest bending moment was recorded at a depth of 0.75 m in event D and a depth of 3.8 m in event F. In event F, there were progressive increases in permanent lateral displacement of the superstructure and residual bending moments in the pile, particularly towards the bottom of the loose layer.

Acceleration response spectra (ARS) for the input (base), ground surface, and superstructure motions for events D and F are shown in Figures 6-6(a) and (b), respectively. Comparing the ARS for events D and F, liquefaction strongly affected the frequency content of the ground surface motion and widened the spectral peak of the single pile system from about 0.8 sec to between 0.9 and 1.2 sec.

6.3.3 Pile Group PG22 Response

The response of pile group PG22 during events D and F is shown by the time histories of superstructure acceleration, pile-cap acceleration, pile-cap displacement, and bending moment at various depths in Figures 6-7 and 6-8, respectively. All recordings show that the system's "fundamental" period lengthened in event F relative to its value during event D. The peak superstructure acceleration was about 5 times the peak base acceleration during event D, but only about 0.9 times the peak base acceleration during event F. In both events, the bending moments and lateral displacements were strongly correlated to both the superstructure and pile-cap accelerations. Note again that pile-cap displacements are relative to the top container ring. Bending moments at the pile-heads (2.5 m depth) of piles 1 and 2 are almost identical during both events. As expected, bending moments at various depths along pile 1 show a slower rate of decrease with depth in event F (due to the liquefaction). The maximum bending moment was always at the pile-head where it is fixed in the pile cap, although it is noted that a fixed-head condition was not maintained since the pile cap did experience some rotation due to rocking.

6.4 Pseudo-Static p-y Analyses of Single Pile System in Container 2

Pseudo-static p-y analyses of the single pile system were performed using the program PAR (1988). This program is one of several programs that have been used in this study to perform dynamic soil-pile-superstructure interaction analyses based on the "Beam on a Nonlinear Winkler Foundation (BNWF)" model (Figure 6-9). These dynamic analyses model the soil-pile interaction by a series of nonlinear p-y springs and dashpots, and input the free-field ground motions at the ends of the p-y springs, as described in Section 3.

The pseudo-static p-y analyses were done at a snapshot in time, with the time corresponding to a peak inertial load (peak superstructure acceleration) and/or peak bending moment. The measured superstructure inertial loads and free-field soil displacements were included as input to PAR. A baseline set of p-y springs was made using standard API curves (American Petroleum Institute 1987). The baseline curves provide a fixed reference and are not implied to be necessarily correct for the static loading condition. Free-field displacements relative to the model base were calculated by double-integration of the acceleration time-histories in the soil profile (8 records at different depths). The signal processing and integration procedure was calibrated against displacement transducer measurements, and shown to give an excellent record of transient displacements while unavoidably filtering out permanent displacements (as described in Section 4.2). In an analysis, the inertial loads and free-field displacements were applied to the numerical model (dashpot forces were zero), and the calculated bending moment distribution and superstructure displacement was compared to

recorded values. The analysis was repeated with different scalar multiples of the baseline p-y springs (scalar multiple applied to the p-values) in the upper sand layer until a reasonable match between calculated and measured responses was obtained.

Inertial force versus calculated and measured superstructure horizontal deflection for the single pile is shown in Figure 6-10. For event D (no liquefaction), the superstructure deflection was matched with about 1.0 times the baseline p-y curves. For event F (with liquefaction), the superstructure deflection was reasonably matched with about 0.1-0.2 times the baseline p-y curves. Bending moment versus depth is shown in Figure 6-11. The bending moment distribution was reasonably matched using about 1.0-2.0 times the baseline p-y curves for event D, and about 0.1-0.3 times the baseline p-y curves for event F. Comparing these analysis results for events D and F, it appears that the effects of liquefaction in the upper sand layer were reasonably represented by reducing the relative p-y curves by a factor of about 0.1-0.2.

Parametric studies showed that the calculated bending moments deep in the upper soil layer were strongly influenced by the soil displacement profile near the contact between the upper and lower soil layers. Thus, the differences between calculated and recorded bending moments at this depth could be due to errors in the calculated soil displacement profile (e.g., long-period components of displacement that were filtered out, or differences in motions at the "free-field" and pile locations), errors in the p-y representation, or other factors. For example, it should be recognized that the initial stiffness of the API curves increases linearly with depth, which is a reasonable approximation for modeling monotonic at the pile head. At depths greater than a few pile diameters, however, the initial p-y stiffness would be better related to shear modulus which increases as the square-root of confining stress. Thus, the API curves are expected to overestimate the stiffness of the p-y curves at larger depths, and hence overestimate the bending moments due to kinematic loading near the interface between the two sand layers.

The relative contributions of kinematic and inertial forces to the calculated bending moments and deflections of the single pile during event F were also evaluated. Figure 6-12 shows the bending moments and lateral displacements versus depth calculated with the baseline p-y curves scaled by a factor of 0.1 and the loads applied three ways: (1) with the superstructure's inertial force only; (b) with the free-field soil displacements only; and (c) with the superstructure's inertial force and the free-field soil displacements. The analysis results illustrate that the inertial force dominates the pile bending moments above depths of 5 to 6 m, and that the free-field soil displacements dominate the pile bending moments at greater depths.

Figure 6-13 shows the calculated bending moments and lateral displacements versus depth for event F with the baseline p-y curves scaled by a factor of 0.2, and using the same three load cases. Comparing Figures 6-12 and 6-13, the increase in p-y scaling factor from 0.1 to 0.2 caused an increase in bending moments below depths of about 5 m in the liquefied layer. The larger scaling factor also caused a slight decrease in the pile-head deflection under inertial loading alone, a slight increase in the pile-head deflection under kinematic loading alone, and thus a negligible effect on the pile-head deflection under the combined loads.

The effect of different p-y spring representations for the liquefied sand was also evaluated in a few analyses. As an example, suppose that the p-y curve for the liquefied sand was derived by treating it as a material having an undrained residual shear strength (S_r with ϕ_u=0) and using the equations recommended for soft clay by Matlock (1970) since no other rational forms are yet available. The calculated bending moments and lateral displacements versus depth for event F using this alternative approach with S_r=25 kPa and ε_c=0.02 are shown in Figure 6-14. The calculated results are very similar to those presented previously despite using a completely different representation of the p-y curves. In essence, these simplified methods for trying to

approximate the effects of liquefaction on p-y resistance are relying on a series of compensating effects, including the relative roles of inertial versus kinematic forces and the relative roles of p-y spring capacity (p_{ult}) versus p-y spring stiffness. Thus, it is emphasized that the analyses presented herein are only intended to evaluate the potential limitations of any such simplified analyses, and not to imply that they in anyway capture the actual p-y behavior of liquefied sand.

It should be noted that measured inertial loads (based on accelerometer records) were used as input to the above analyses, whereas the estimation of inertial loads for design requires that the effects of liquefaction on the dynamic response of the soil-pile-structure system be accounted for. This is a challenging task given continuing questions regarding the reliability of site response analyses for liquefiable soils and the p-y resistance of liquefied soils.

6.5 PSEUDO-STATIC P-Y ANALYSES OF SINGLE PILE SYSTEM IN CONTAINER 1

Pseudo-static p-y analyses were also performed for a single pile system tested in a previous centrifuge model test (Container 1). A description of this prior centrifuge test is given by Wilson et al. (1995). The soil model for Container 1 differed from that of Container 2 as follows: (1) the loose sand layer was at D_r of 55-60%, as opposed to 35-40%; (2) the pore fluid was water, as opposed to a water-methyl cellulose mixture; and (3) for peak ground motions less than about 0.05 g, the single pile system had a fundamental period of about 0.9 sec, as opposed to 0.8 sec. The single pile systems in Containers 1 and 2 had the same pile properties, but slightly different column heights and superstructure masses. For the pseudo-static analyses of Container 1, a new set of baseline p-y curves were developed based upon its higher D_r.

Acceleration response spectra (ARS) for the input (base) motion, the ground surface motion, and the single pile superstructure motion for two events in Container 1 are shown in Figures 6-15(a) and (b), respectively. Input motions for events F and H were the "Kobe" motion scaled to peak base accelerations of about 0.15 g and 0.34 g, respectively. No liquefaction occurred in event F. In event H, r_u was small early in shaking (r_u <40% for time < 5 sec) and increased later in shaking (r_u >70-90% for time > 9 sec). Liquefaction resulted in less attenuation of the ground surface motion and less lengthening of the single pile's predominant period in Container 1 (Figure 6-15) than in Container 2 (Figure 6-6). These differences in behavior between Containers 1 and 2 are consistent with the upper sand layer in Container 1 being denser and able to dissipate excess pore pressures more rapidly (about 10 times more rapidly due to the differences in pore fluid viscosity).

Inertial force versus calculated and measured superstructure horizontal deflection for the single pile is shown in Figure 6-16. For event F (no liquefaction), the superstructure deflection was matched with about 3.0 times the baseline p-y curves. For event H (with liquefaction), the superstructure deflection at 4.4 sec (r_u <40% throughout the upper sand layer) was reasonably matched with about 2.0 times the baseline p-y curves, while the superstructure deflection at 9.9 sec (after liquefaction, with r_u > 70-90% throughout the upper sand layer) was reasonably matched with about 0.5-1.0 times the baseline p-y curves.

Bending moment versus depth in event H is shown in Figure 6-17. While not shown, the bending moment distribution for event F (no liquefaction) was reasonably matched using about 2.0-3.0 times the baseline p-y curves. For event H (with liquefaction), the bending moment distribution at 4.4 sec was reasonably matched with about 2.0-3.0 times the baseline p-y curves (Figure 6-17(a)), while the bending moment deflection at 9.9 sec was reasonably matched with about 0.5-1.0 times the baseline p-y curves (Figure 6-17(b)).

Comparing the analysis results for events F and event H, the effects of liquefaction in the

upper sand layer were reasonably represented by reducing the p-y curves by a factor of about 0.25-0.35 (i.e., 0.5-1.0 times the baseline when $r_u > 70$-90% versus 2.0-3.0 times the baseline when $r_u < 40\%$). It is also important to note that the peak superstructure deflection and peak bending moment during event H occurred early in shaking while r_u values were still low.

The relative contributions of kinematic and inertial forces to the calculated bending moments and deflections of the single pile during events F and H in container 1 were evaluated using the same three load cases described in the previous section: (1) with the superstructure's inertial force only; (b) with the free-field soil displacements only; and (c) with the superstructure's inertial force and the free-field soil displacements. The analysis results showed that the superstructure's inertial force dominated the bending moments and lateral deflections for the pile. Free-field soil displacements, even with $r_u > 70$-90% throughout the upper sand layer, were small enough that their effect on the resulting bending moments and lateral deflections were small relative to effects of the inertial load.

6.6 Back-Calculation of p-y Curves

Back-calculation procedures were developed for obtaining time histories of p-y resistance from the heavily strain-gauged single pile system used in Containers 2, 3, and 4. The soil profile's deformed shape at any given time was defined by an interpolation function that was fitted to the displacement profile obtained by integration of the accelerometer records (following the signal processing procedures previously described). The interpolation function was then used to define the lateral deformations at desired depths, and then solved for every time step to arrive at time histories.

There are two main difficulties with the interpolated soil profile shape. Firstly, the interpolated shape will not include any permanent components of deformation, but will instead only represent the transient deformations. Secondly, incoherent horizontal motions developed at shallow depths in the upper soil layers of liquefied $D_r \approx 35$-40% sand and soft clay (during strong shaking). This incoherency of horizontal motions means that deformed soil profile shape at different locations within the Container will differ at shallow depths. However, since the single pile is close to the vertical array of accelerometers used in defining the soil profile shape, the deformed soil profile shape should be a reasonable representation of the "free-field" conditions near the single pile. Also, several analyses were performed with the uppermost accelerometer omitted from the calculations, as this shallow accelerometer sometimes appeared inconsistent with the other accelerometers. The effect of including or omitting this one accelerometer record had some effect on the calculated relative displacement (y) at very shallow depths, but negligible effect on the other (deeper) p-y curves.

The deformed pile shape was defined by a beam-element interpolation function that was fitted to: (1) the displacements obtained from integration of accelerometer records on the pile head and superstructure; (2) the relative displacements obtained by integration of bending strains along the pile length; and (3) the assumption of zero relative displacement between soil and pile at a 9 m depth. The interpolation function was used to define the lateral displacements and lateral pressures (i.e., p) at desired depths, and then solved for every time step to arrive at time histories. The interpolation function was set up to only need the displacement of the pile head or the superstructure as input. Then, the interpolation function was used to calculate the displacement at the other point (pile head or superstructure) for comparison to the value obtained by integrating the accelerometer record. The results were generally insensitive to the choice of pile head or superstructure displacement as an input to the interpolation function. Two other interpolation

functions for the deformed pile shape were also used, with the effects on the final p-y curves being small (Wilson 1998).

Time histories of p-y curves were then obtained for different depths from the time histories for the soil profile's deformed shape, the pile's deformed shape, and the lateral soil pressures on the pile. Three different interpolation functions for the pile shape and two different functions for the soil profile shape were used to evaluate the robustness of the back-calculation procedure. The back-calculated p-y curves were relatively insensitive to the different combinations of interpolation functions, except in a few difficult cases. Details of the back-calculation procedures, including their sensitivity to the underlying assumptions and interpolation functions, are given in Wilson (1998).

Examples of p-y curves obtained by Wilson (1998) for the soft clay in Container 4 are shown in Figure 6-18. This figure includes time histories of p and y at a depth of 5.5 pile diameters and a pore pressure time history at a similar depth. P-y curves for three different depths are then shown for the time-window marked on the time history plot. Monotonic p-y curves calculated by Matlock's (1970) procedure are shown on these p-y plots for comparison. The back-calculated p-y curves show maximum lateral pressures (p_{ult}) that are reasonably consistent with values calculated by Matlock's procedure. As expected, the hysteresis loops show progressive softening with increasing displacement and number of loading cycles (as shown by the loops for early in the earthquake shaking versus late in the earthquake shaking). The reasonableness of the results for soft clay provides a measure of confidence in the application of these back-calculation procedures to centrifuge test data (Wilson 1998).

Examples of p-y curves obtained by Wilson (1998) for liquefied sand in Container 2 ($D_r \approx 35$-40% upper layer) and Container 3 ($D_r \approx 55$-60% upper layer) are shown in Figures 6-19 and 6-20, respectively. These figures include time histories of p and y at a depth of 3.0 pile diameters and a pore pressure time history at a similar depth. P-y curves for three different depths are then shown for the time-windows marked on the time history plots. Monotonic p-y curves calculated by the API procedure are shown on these p-y plots for comparison. The back-calculated p-y curves show characteristics that are consistent with the expected stress-strain response of liquefied sand. The p-y resistance of the $D_r \approx 35$-40% upper sand layer in Container 2 is much smaller and softer than for the $D_r \approx 55$-60% upper sand layer in Container 1; this observation is consistent with the expected effects of D_r on the undrained shear resistance (or cyclic mobility) of saturated sand. The p-y curves for the $D_r \approx 55$-60% sand show: (1) a stiffening effect as relative displacement (y) increases beyond a certain limit, and (2) maximum lateral resistances that can be significantly greater than expected for drained conditions at depths less than about 3 diameters (as calculated using API recommendations). This behavior for the $D_r \approx 55$-60% sand is consistent with the expectation that a medium dense sand, under the range of confining stresses involved, would be dilatant at large enough shear strains (i.e., large enough to move the sand through a phase transformation). The p-y curves show a memory of past maximum relative displacements (y), and are softest (smallest p-y slope) for deflections less than the maximum past values. The p-y curves are shown to progressively soften with time during the earthquake event (as shown by loops for early in the earthquake shaking versus late in the earthquake shaking). Clearly, the shape and magnitude of the p-y curves for these liquefied sands are not well represented by any scalar multiple of the common static p-y curves used in practice. Detailed descriptions of back-calculated p-y curves for several depths, earthquake shaking events, and different levels of pore pressure generation are presented in Wilson (1998), along with a more in-depth discussion of their implications for practice.

6.7 DISCUSSION

The idea of applying a scaling factor to static p-y curves to account for the effects of liquefaction, as suggested by Liu and Dobry (1995) and investigated herein, has the attraction of being very easy to implement into design. Liu and Dobry (1995) found that the appropriate scaling factor decreased more or less linearly with r_u, and reached a minimum value of about 0.1 when r_u=100%. Liu and Dobry based their conclusions on centrifuge tests for a sand at D_r≈60% and quasi-static cyclic displacement loading of a pile after the sand was liquefied and shaking had stopped.

The dynamic model tests and pseudo-static analyses presented in this report showed apparent p-y scaling factors for liquefied sand that varied from 0.1-0.35, with the appropriate value depending on D_r. This finding is not surprising since the liquefaction behavior of sand is known to depend on D_r, drainage conditions, loading conditions (e.g., strain versus stress controlled), as well as many other factors. For example, the greater reduction of p-y curves and greater attenuation of ground surface motions obtained for Container 2 (D_r≈35-40% in upper layer) as compared to Container 1 (D_r≈55-60% in upper layer) is consistent with the expected effects of D_r on the cyclic mobility of liquefied sand.

The apparent p-y scaling factor for liquefied sand at D_r≈55-60% in these experiments was larger than the apparent p-y scaling factor obtained by Liu and Dobry (1995) for sand at a similar D_r. This difference in results may simply reflect differences in loading conditions, displacement levels, loading rates, pore pressure levels, or other factors not yet understood.

The back-calculated p-y curves for liquefied sand (Wilson 1998) clearly demonstrate that the use of an apparent p-y scaling factor for liquefied sand is a simplistic approximation to a complex phenomenon, and that more research is needed to evaluate whether this concept can be reliably applied in design or used in dynamic soil-pile-superstructure interaction analyses.

The dynamic centrifuge test data illustrate some important points that should be considered in design. Effects of liquefaction on both the free-field site response and the soil-pile-superstructure interaction must be modeled in a compatible fashion, or the combined results may be unreasonable. A major uncertainty in a dynamic soil-pile-superstructure analysis for a site with liquefiable soils is estimating the free-field site response. Peak bending moments or peak superstructure displacements may occur before or after liquefaction develops, and thus both conditions need to be considered. The depth to peak bending moment may increase greatly as a result of liquefaction and the associated ground displacements, and thus the variation with depth of reinforcing details in concrete piles should consider this effect.

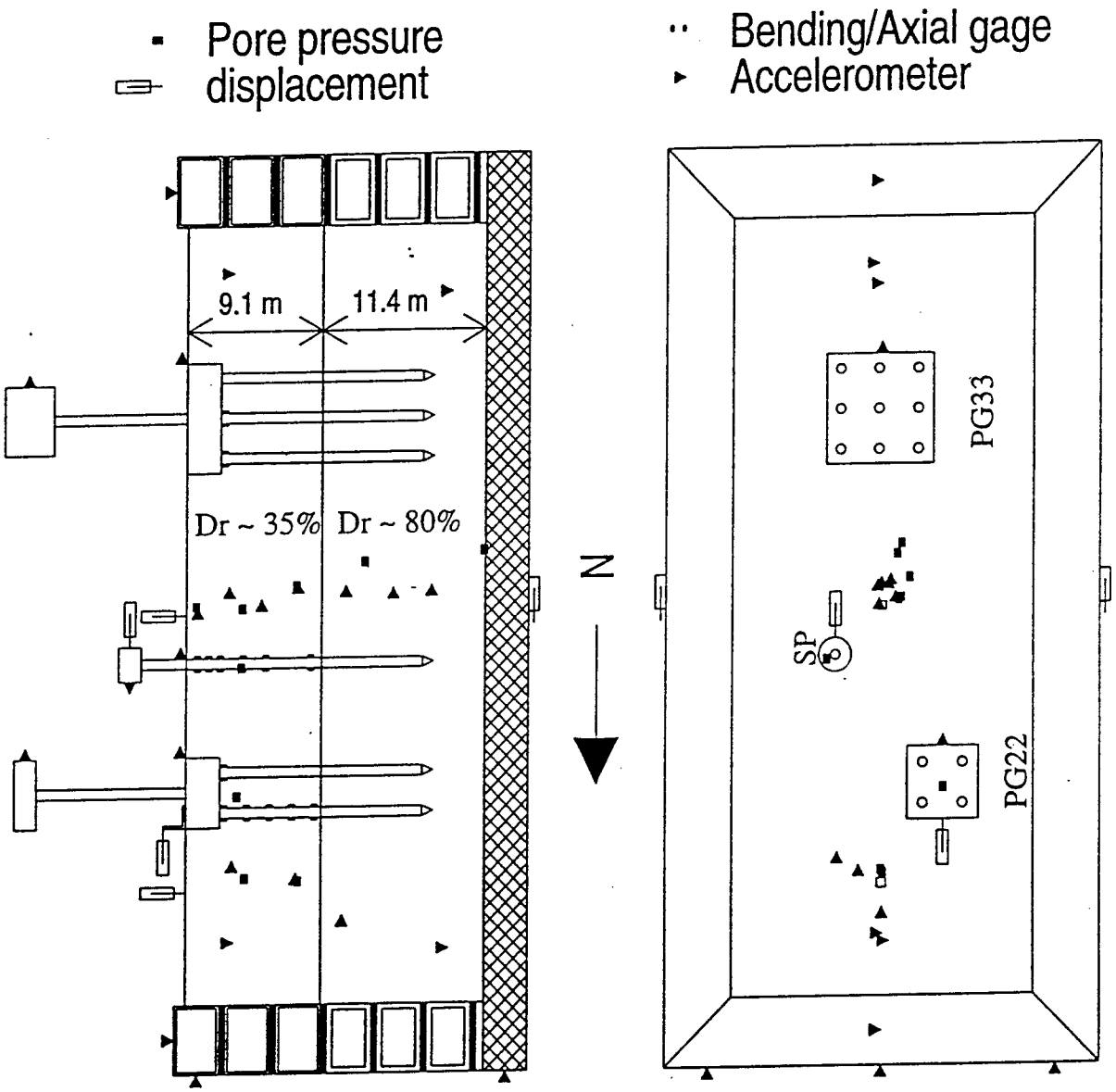

Note: some instruments not included in diagram

Fig. 6-1: Model Layout for Container 2

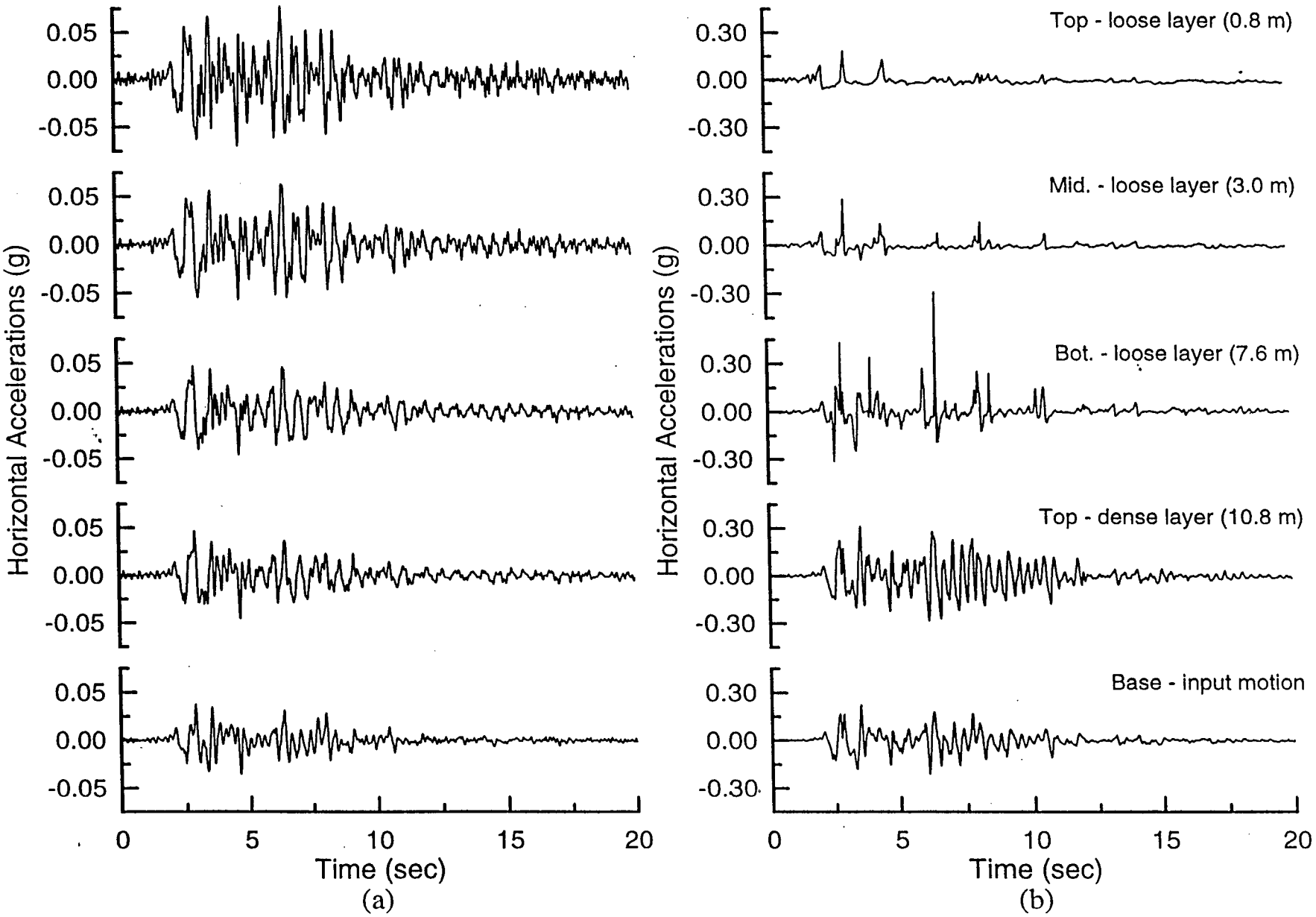

Fig. 6-2: Horizontal Acceleration in Soil Profile: (a) Event D; (b) Event F.

j2.grf

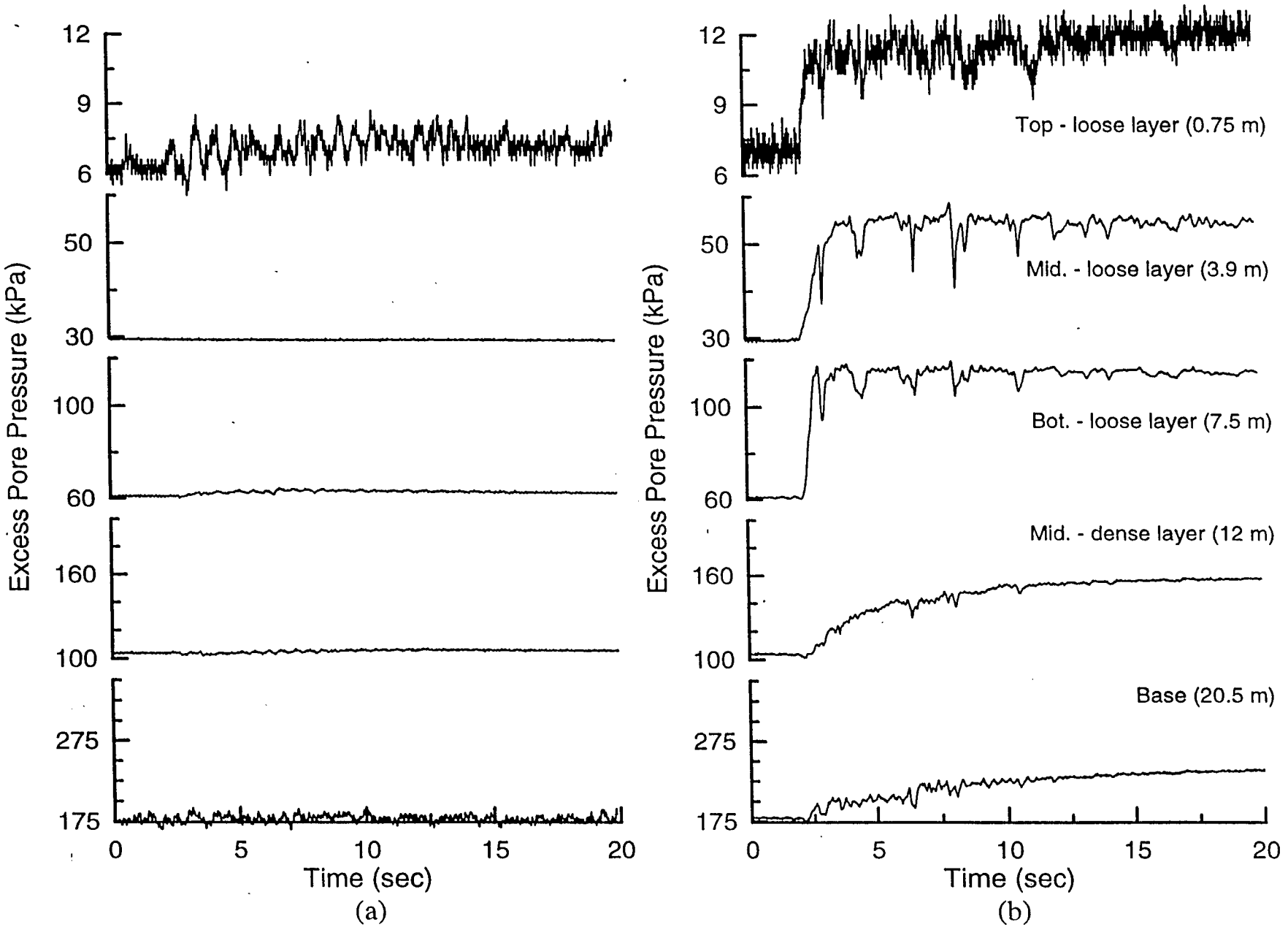

Fig. 6-3: Excess Pore Pressures in Soil Profile: (a) Event D; (b) Event F.

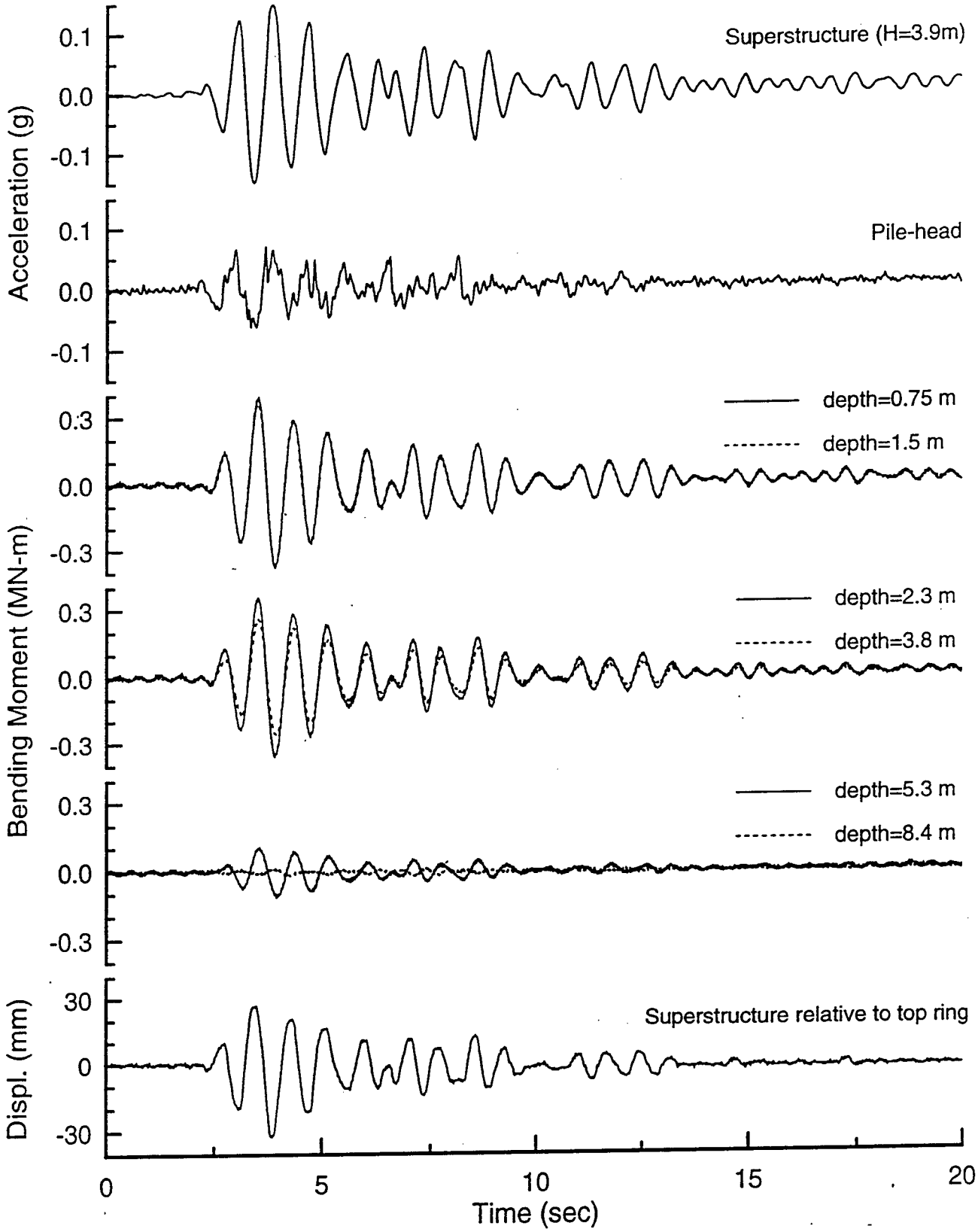

Fig. 6-4: Response of Single Pile - Event D

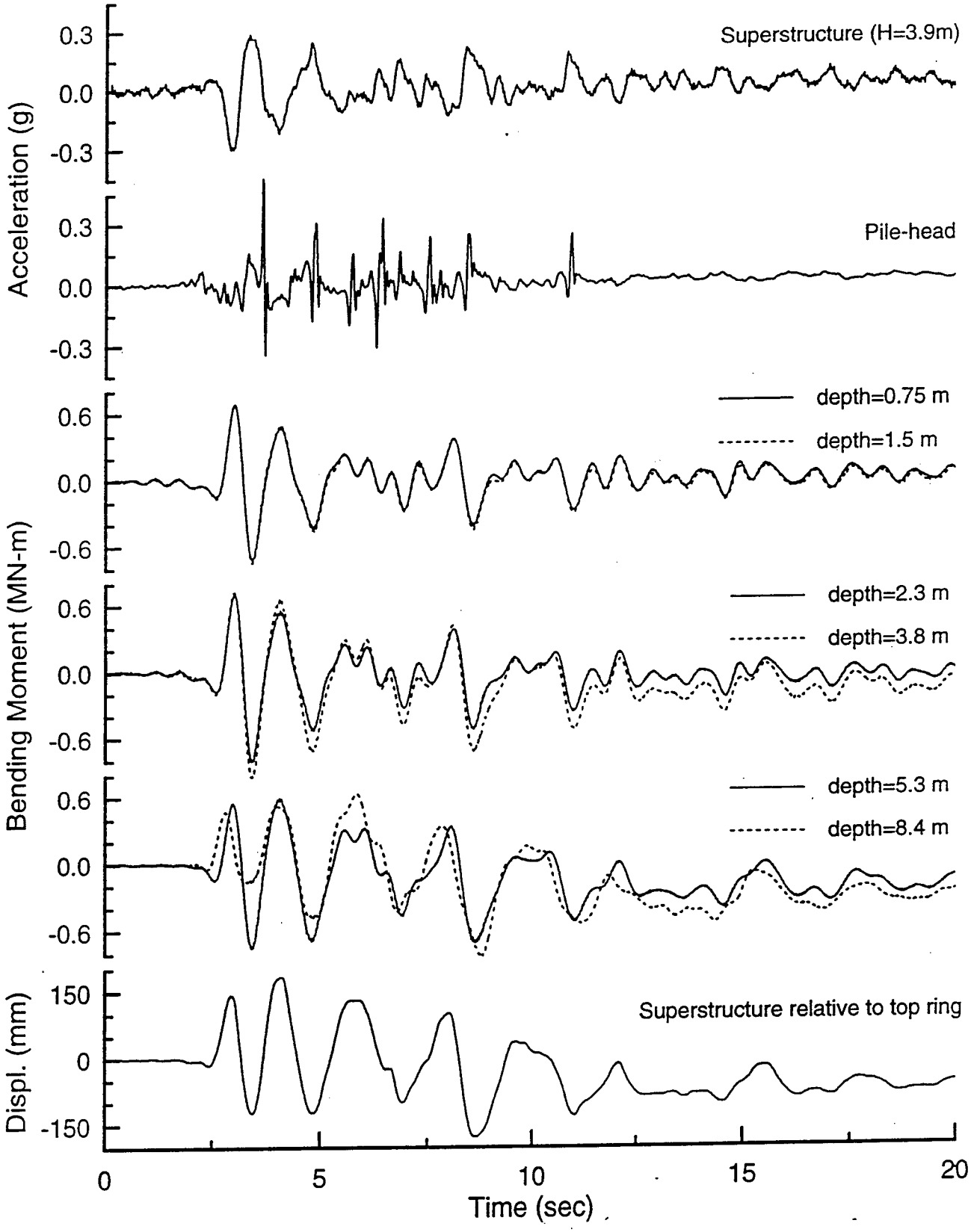

Fig. 6-5: Response of Single Pile - Event F

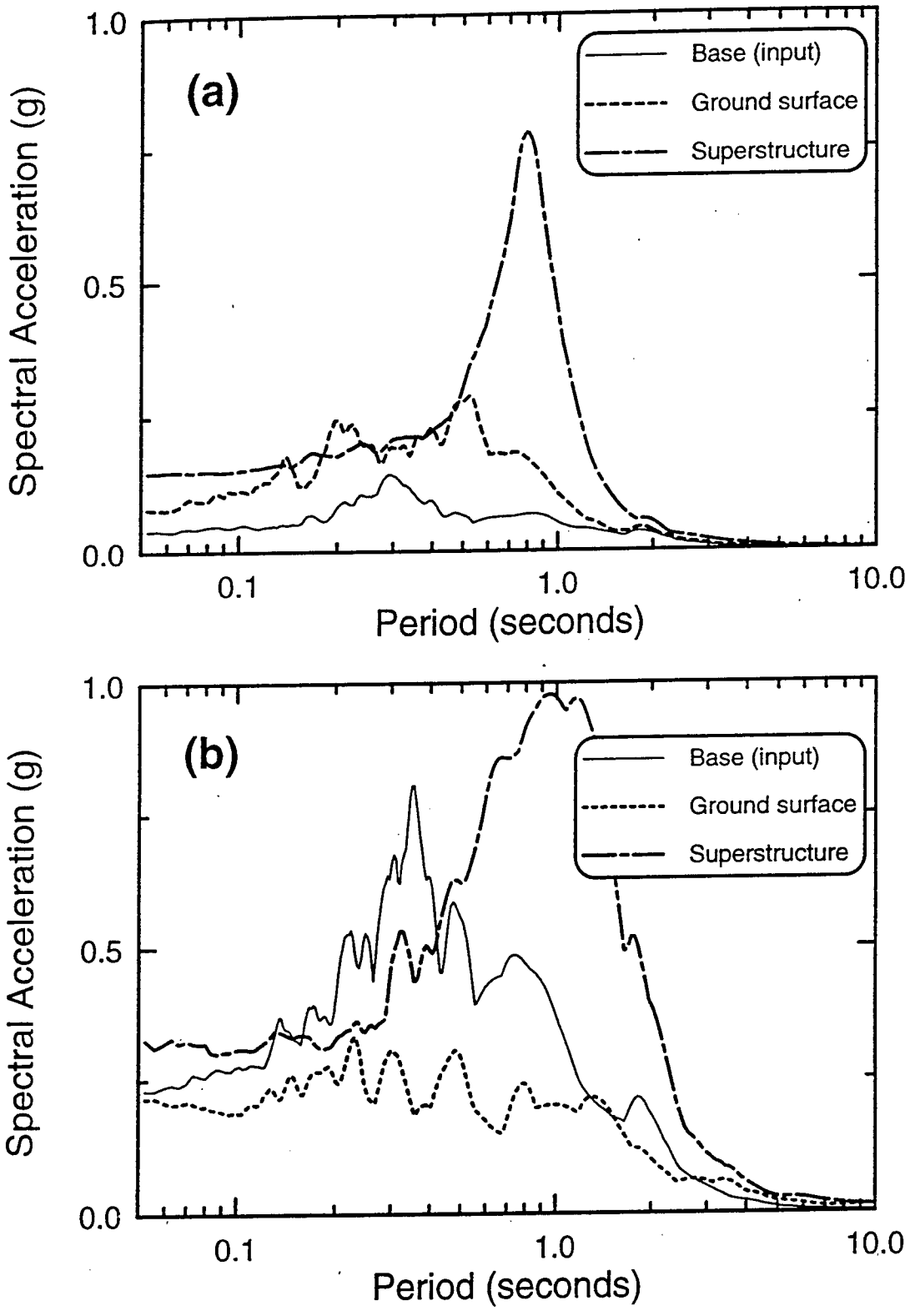

Fig. 6-6: Acceleration Response Spectra of Input, Ground Surface, and Single Pile Superstructure in Container 2: (a) Event D; (b) Event F.

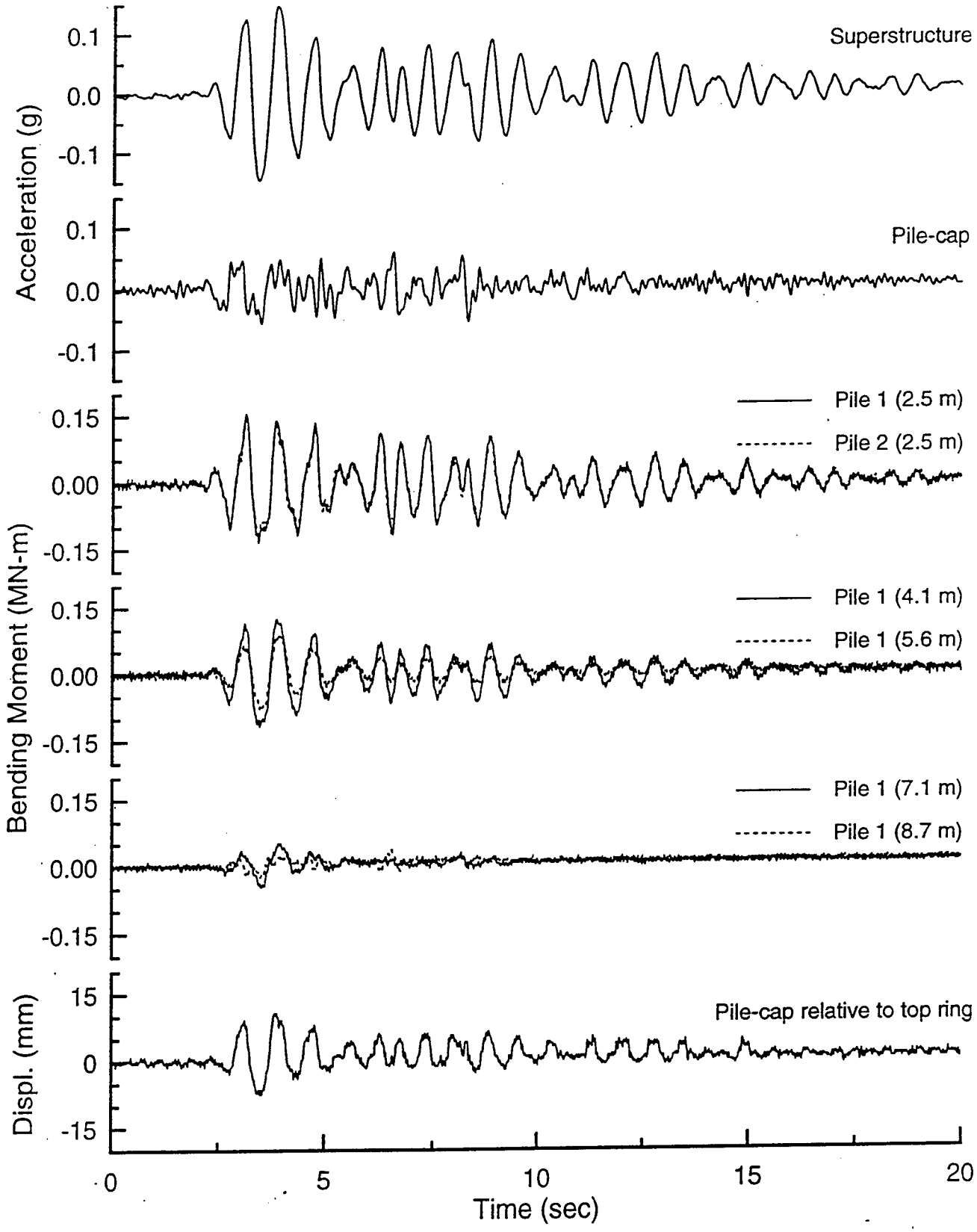

Fig. 6-7: Response of Pile Group PG22 - Event D

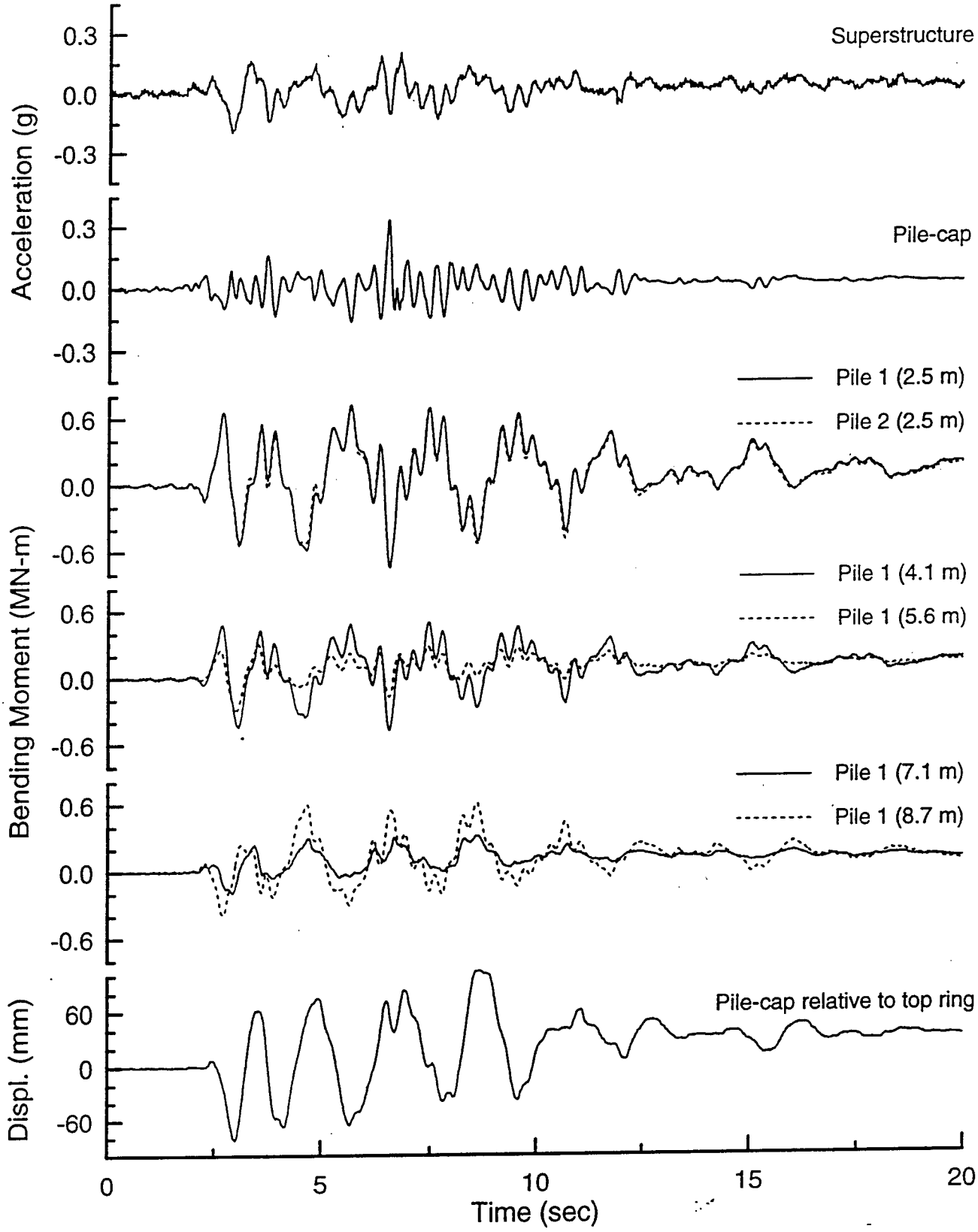

Fig. 6-8: Response of Pile Group PG22 - Event F

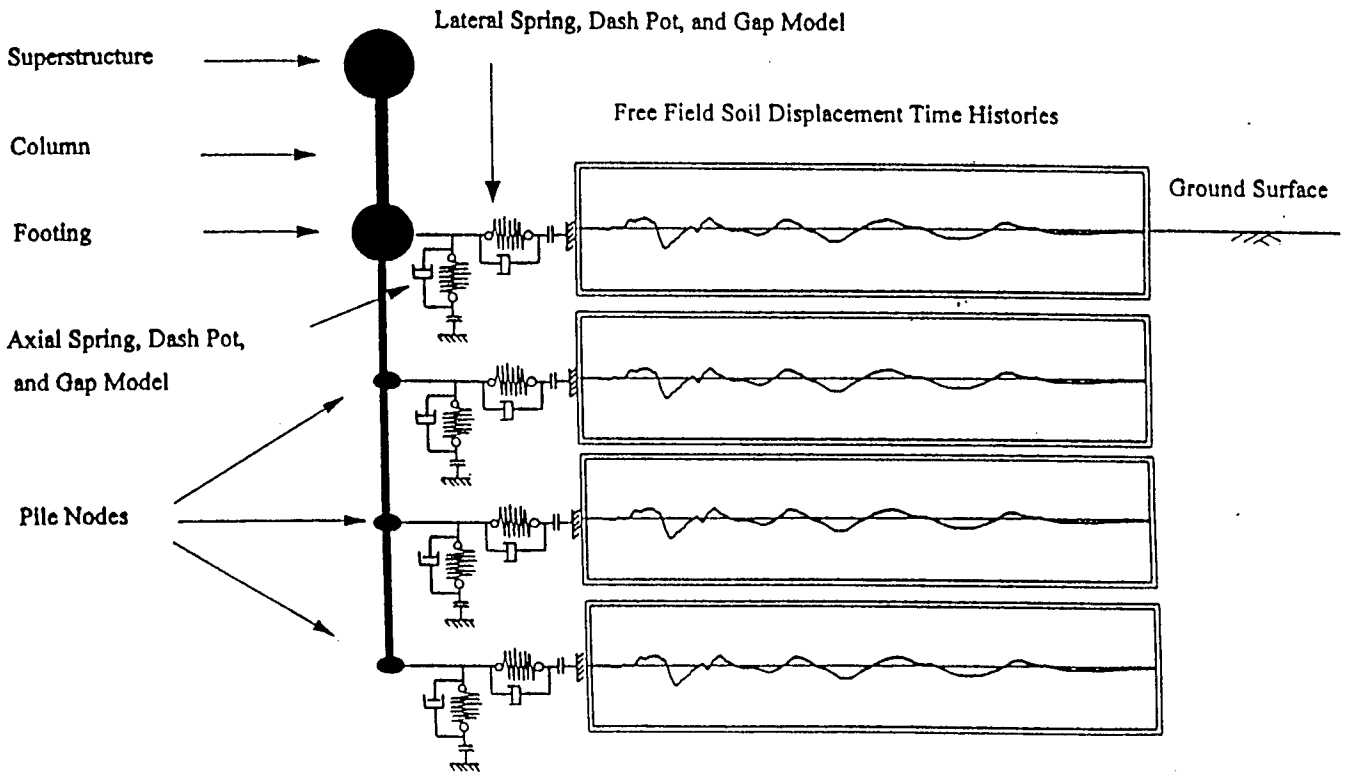

Fig. 6-9: Schematic of Dynamic Beam on a Nonlinear Winkler Foundation (BNWF) Analysis Model (Abghari and Chai 1995)

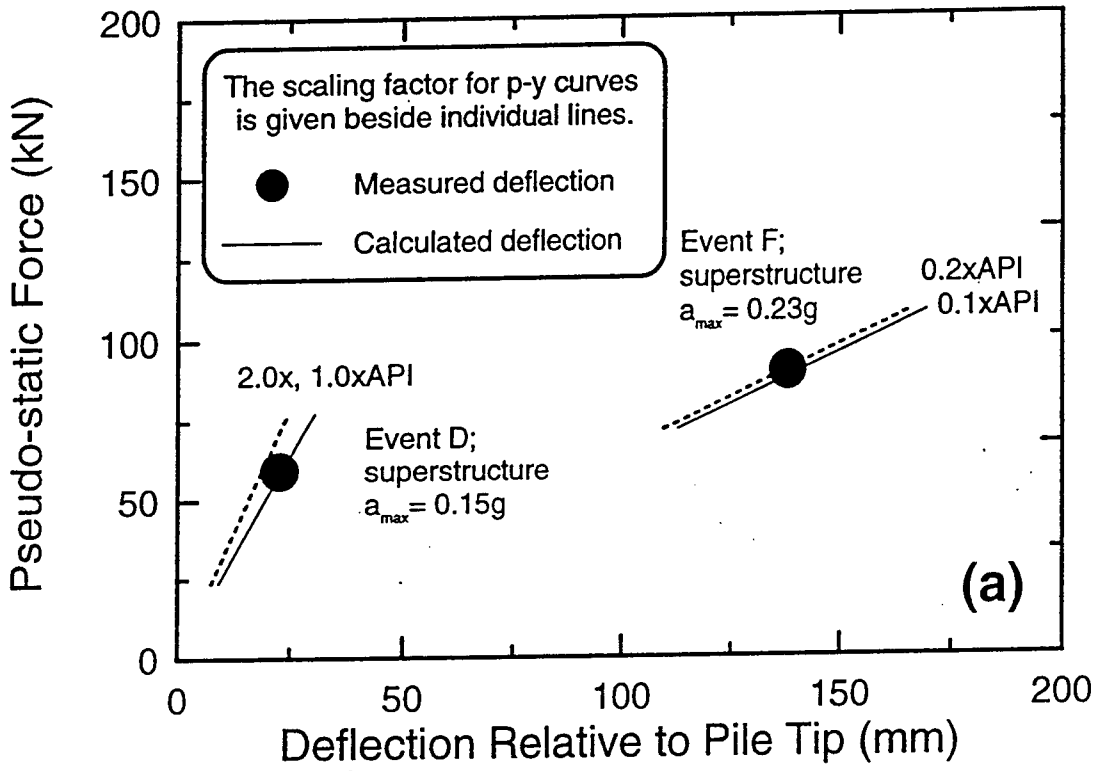

Fig. 6-10 Inertial Force Versus Superstructure Deflection of Single Pile in Container 2 - Events D and F

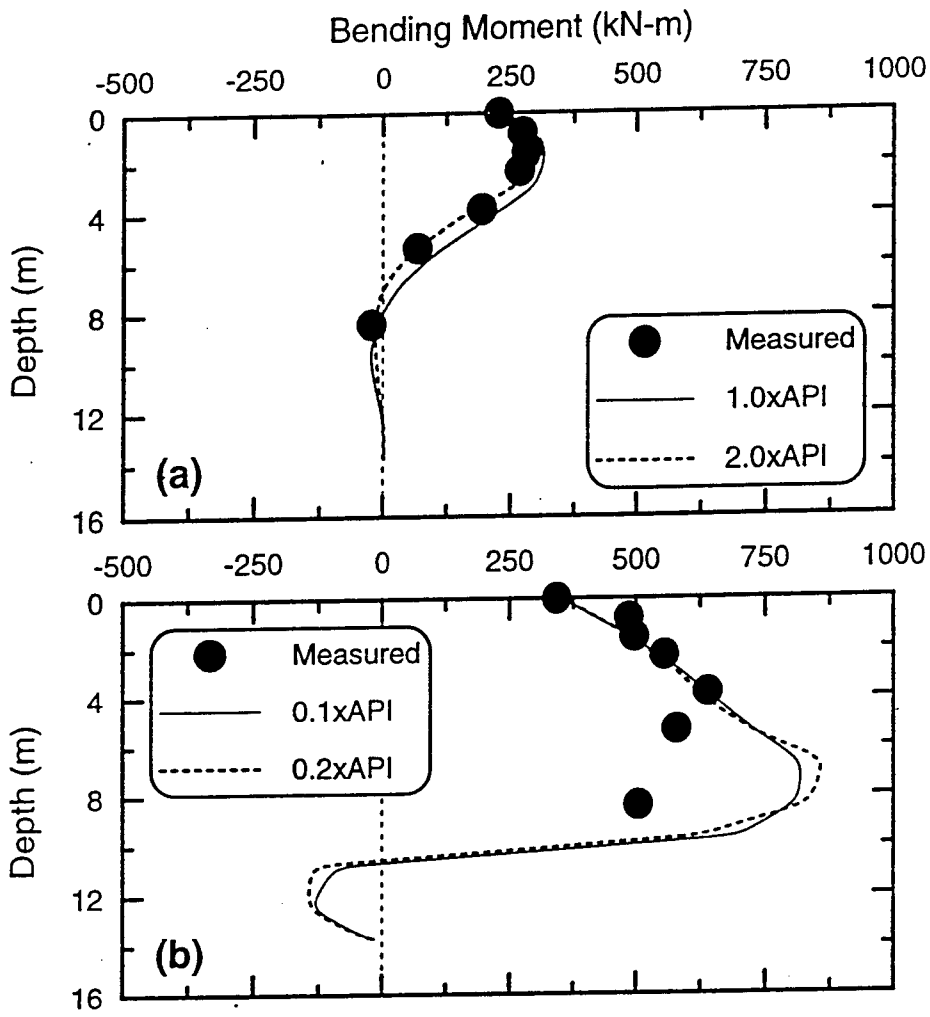

Fig. 6-11 Bending Moment Versus Depth For Single Pile in Container 2 - Events D and F:
(a) Time=4.0 sec in Event D Without Liquefaction;
(b) Time=4.1 sec in Event F With Liquefaction.

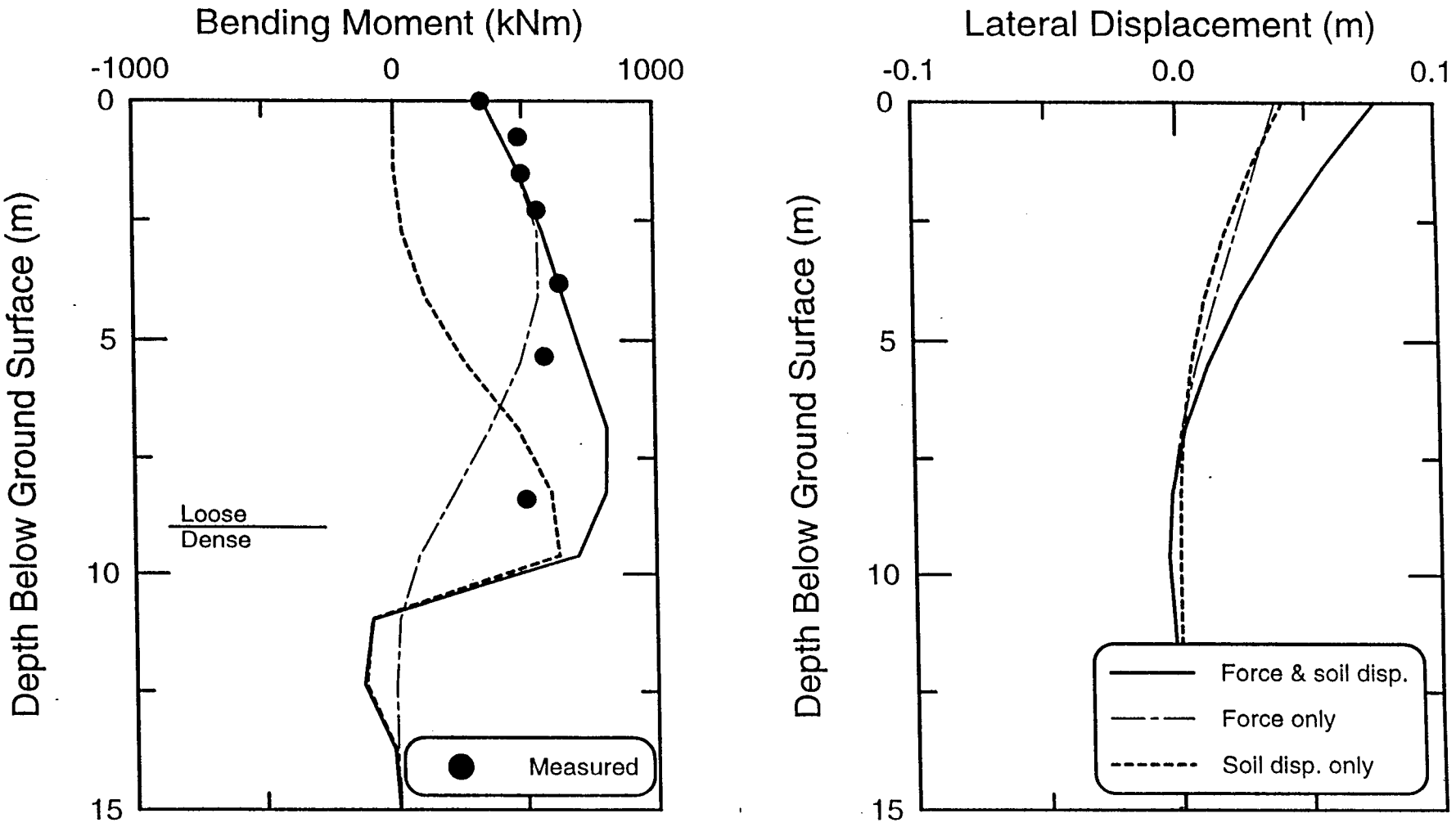

Fig. 6-12: Contributions of Inertial Force and Soil Displacements in Pseudo-Static Analysis of Single Pile in Container 2 - Event F, with C=0.1

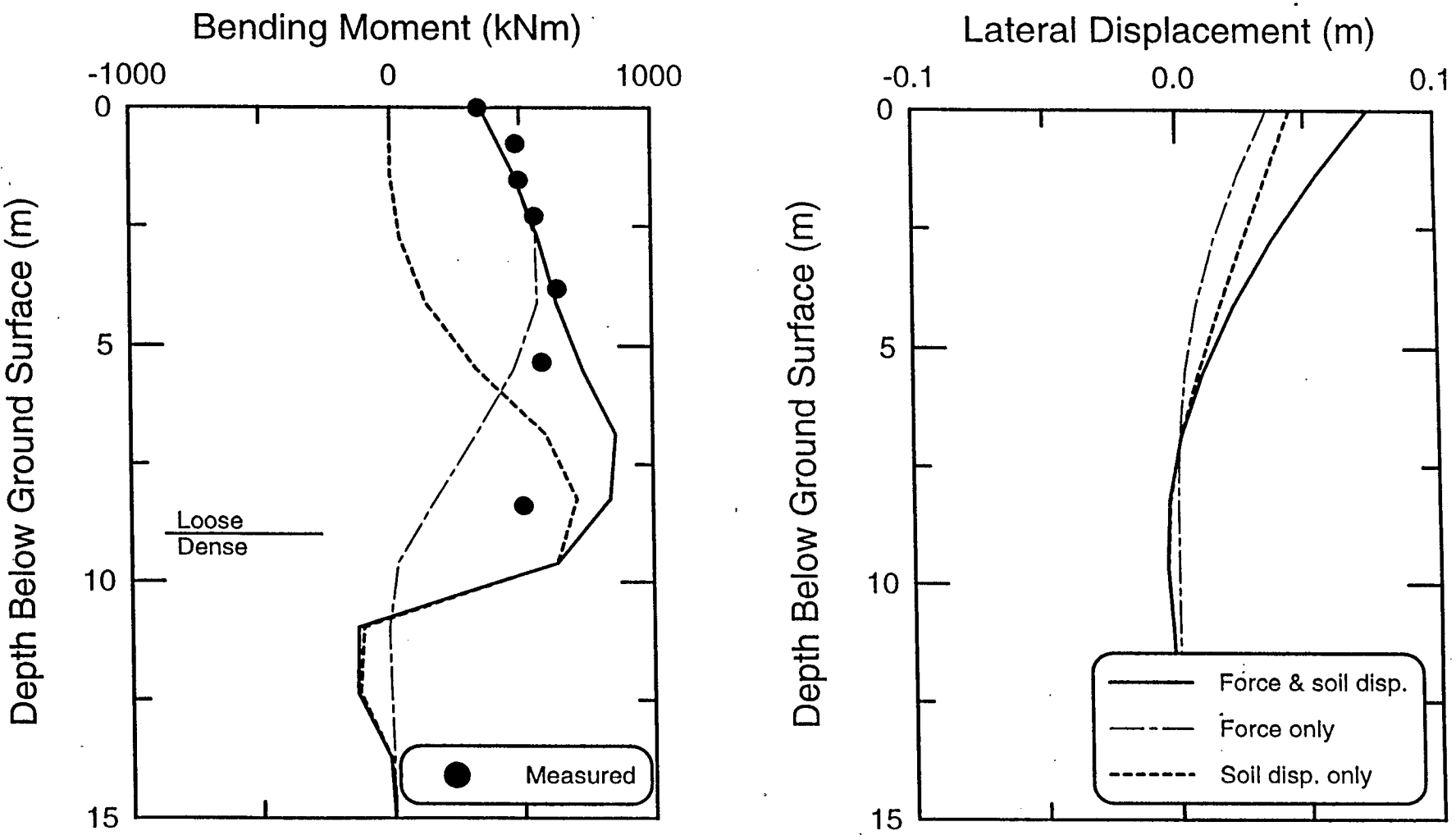

Fig. 6-13: Contributions of Inertial Force and Soil Displacements in Pseudo-Static Analysis of Single Pile in Container 2 - Event F, with C=0.2

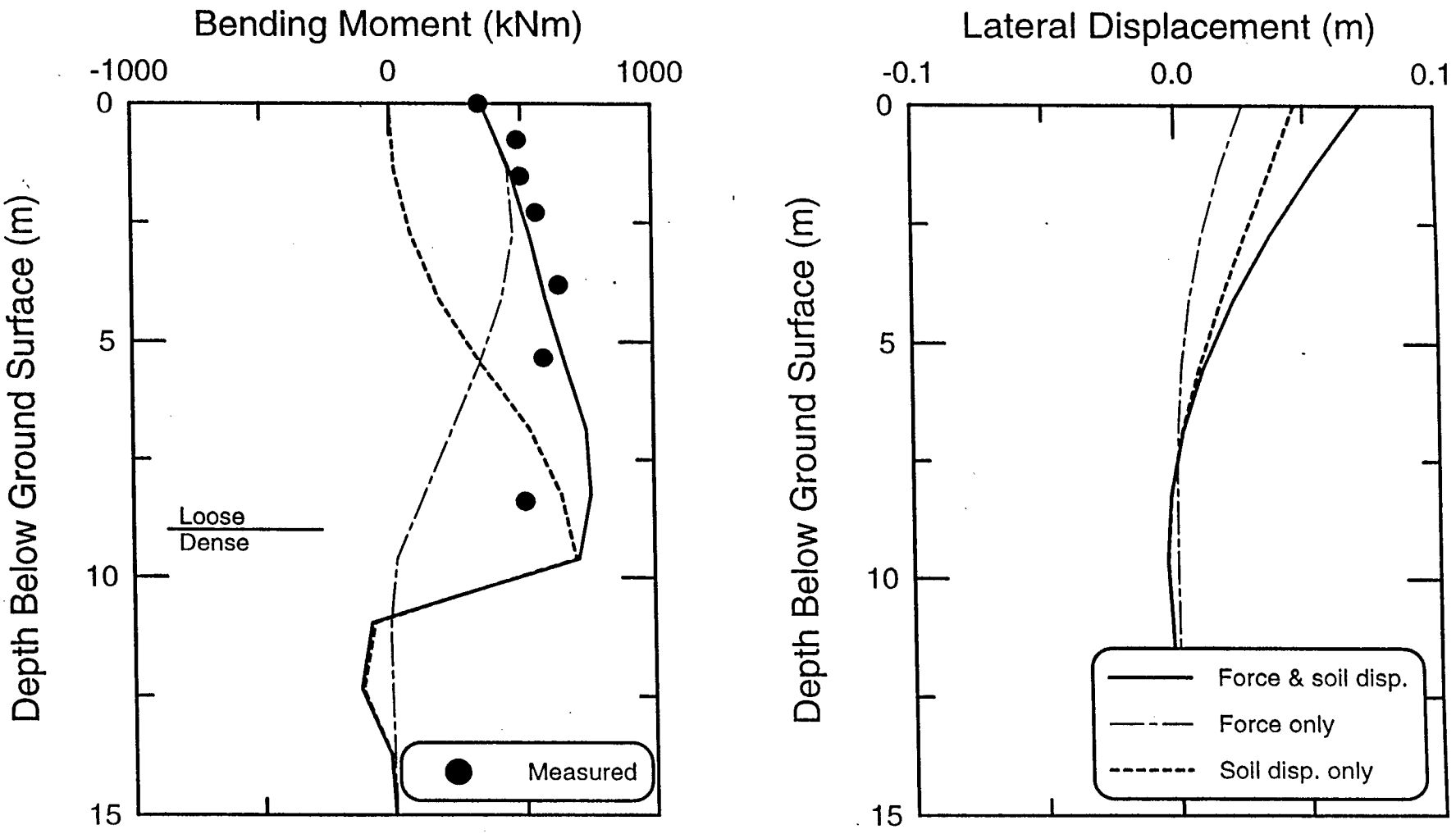

Fig. 6-14: Contributions of Inertial Force and Soil Displacements in Pseudo-Static Analysis of Single Pile in Container 2 - Event F, with S_r = 25 kPa.

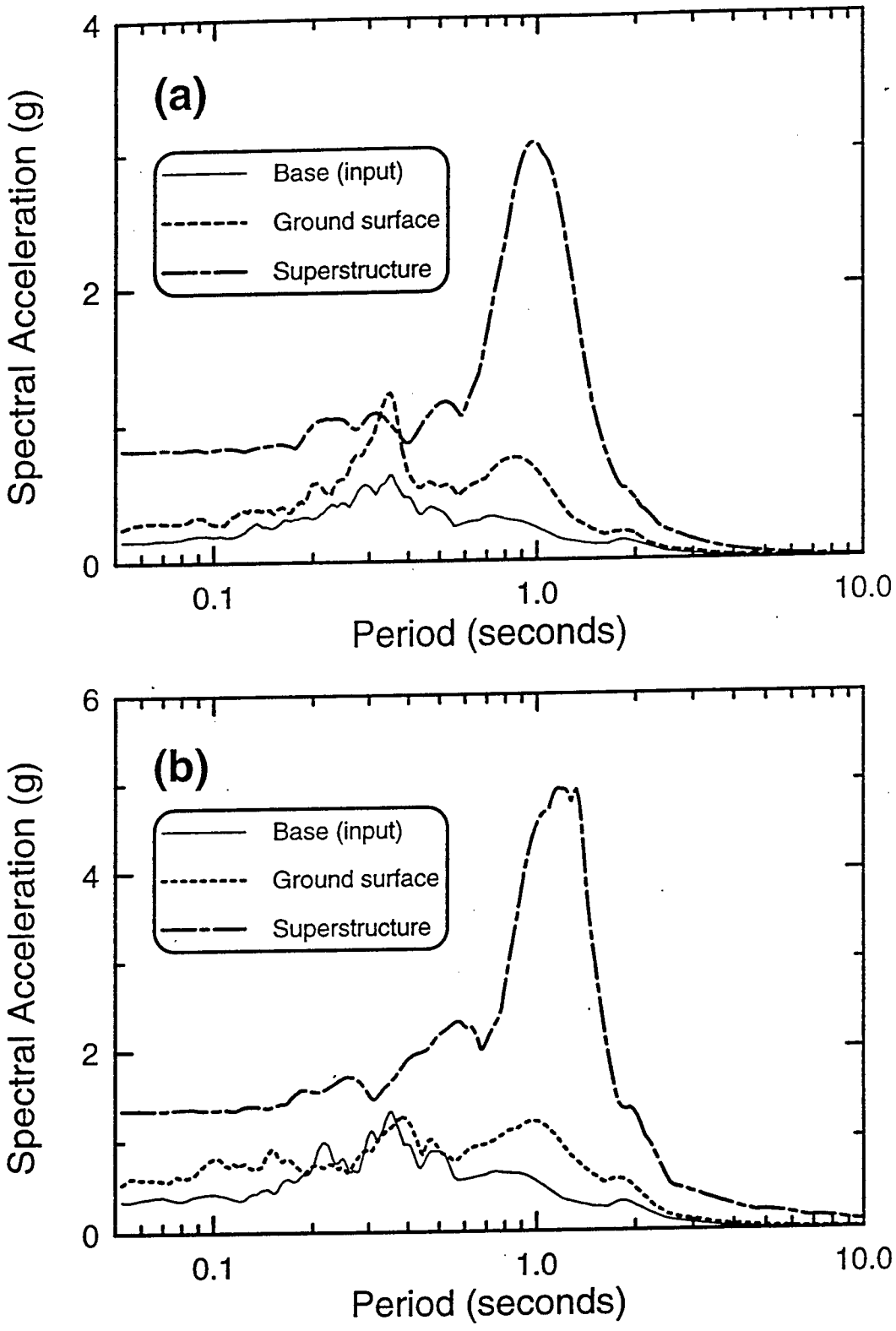

Fig. 6-15: Acceleration Response Spectra of Input, Ground Surface, and Single Pile Superstructure in Container 1: (a) Event F; (b) Event H.

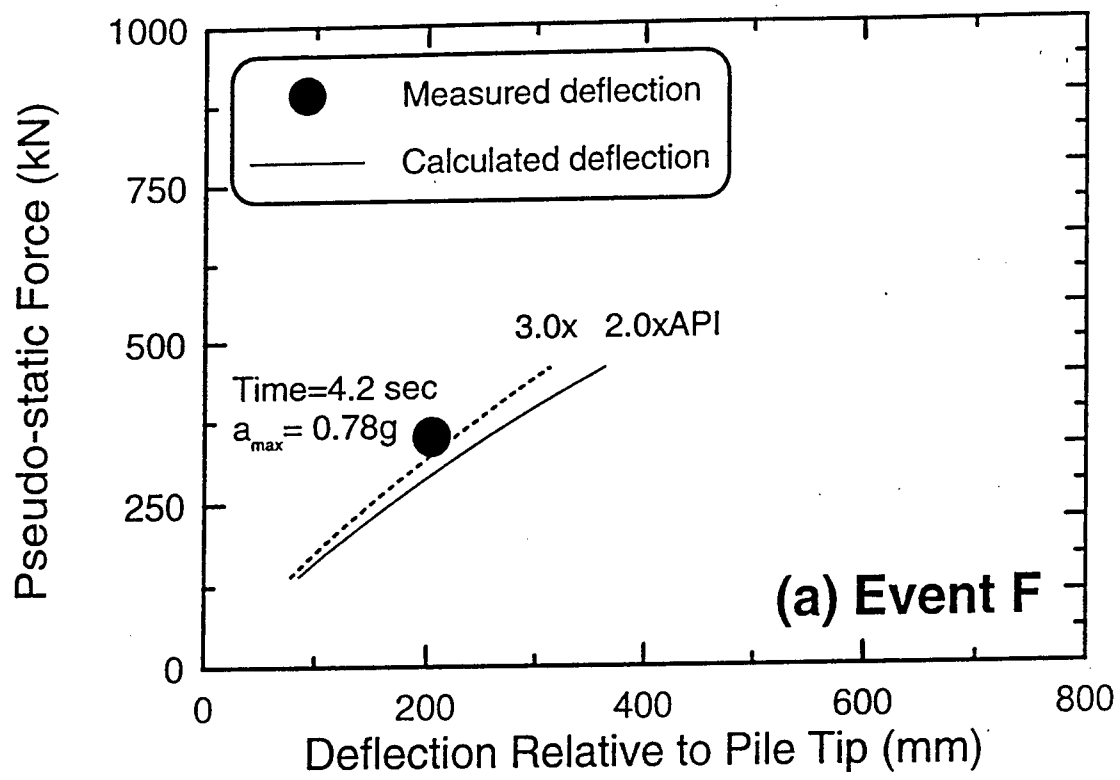

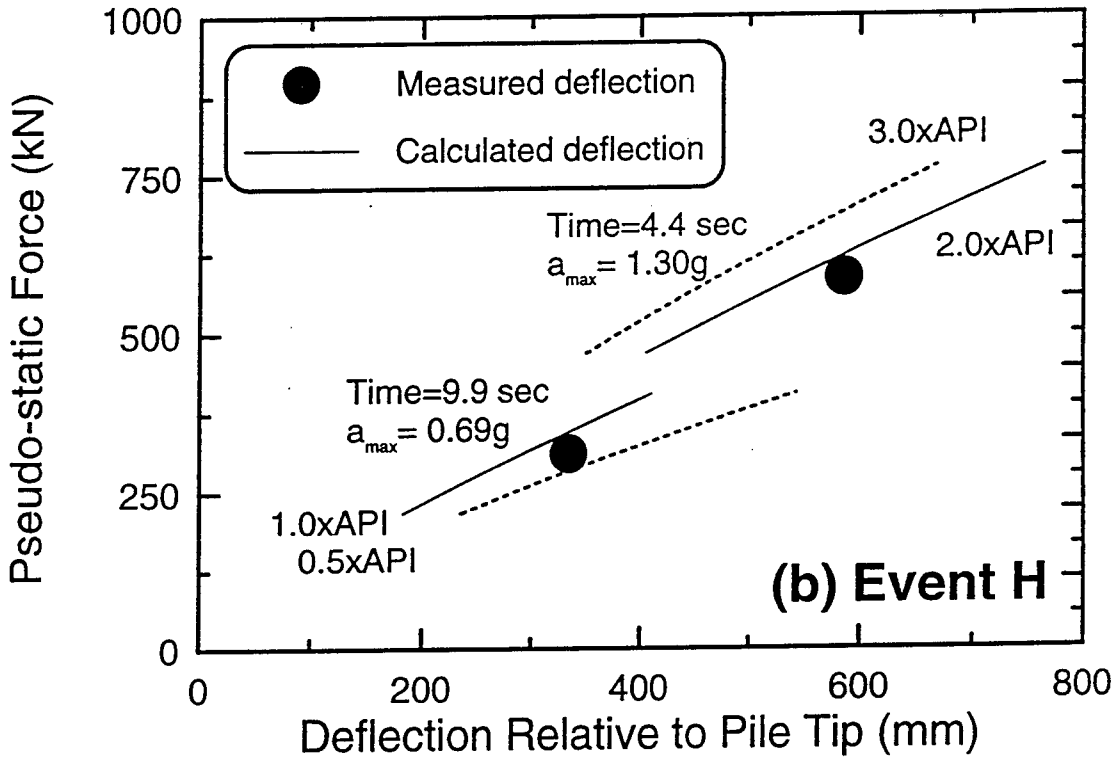

Fig. 6-16: Inertial Force Versus Superstructure Deflection of Single Pile in Container 1: (a) Event F; and (b) Event H.

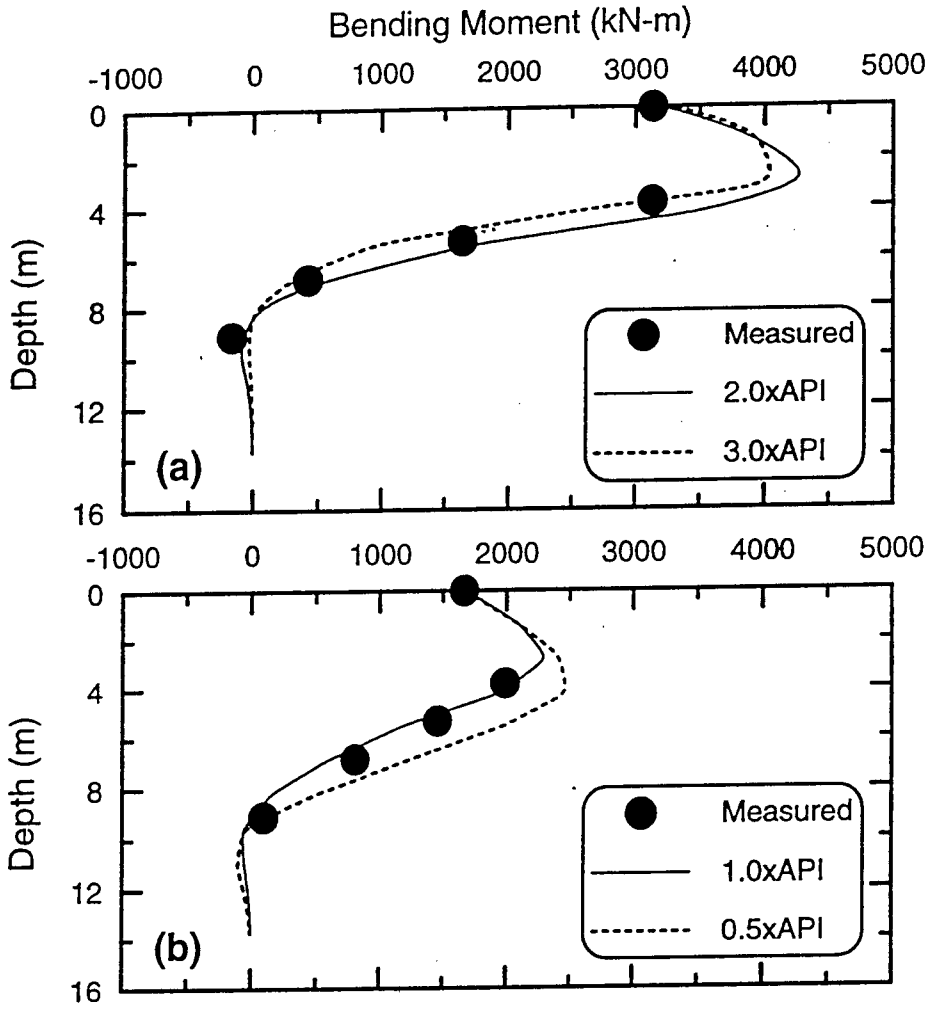

Fig. 6-17: Bending Moment Versus Depth for Single Pile in Container 1 - Two Different Times in Event H:
(a) Time=4.4 sec, when r_u =0-40%;
(b) Time=9.9 sec, when r_u =70-90%.

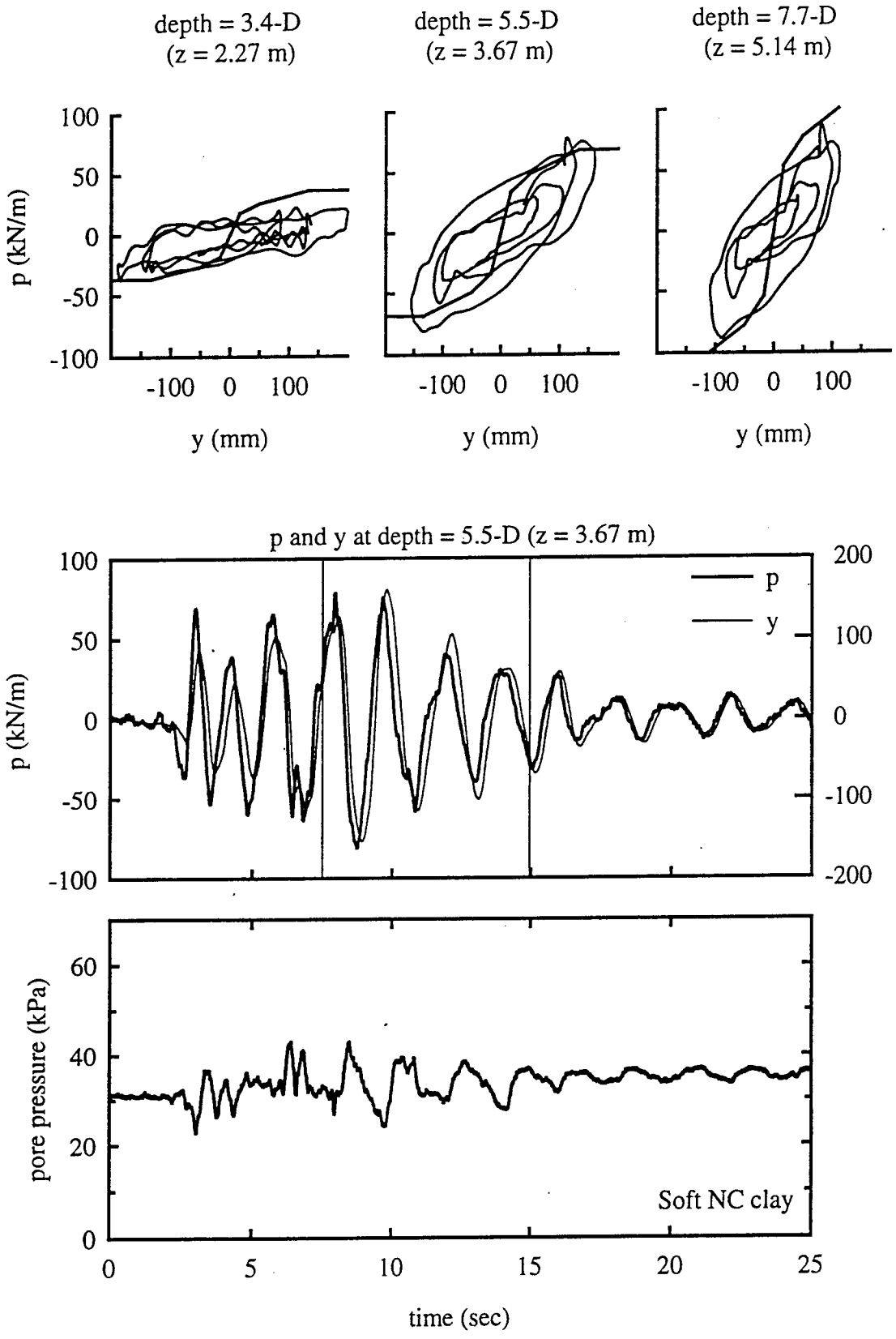

Fig. 6-18: p-y behavior in test Csp4 event E
Kobe motion with $a_{max,base}$=0.58 g

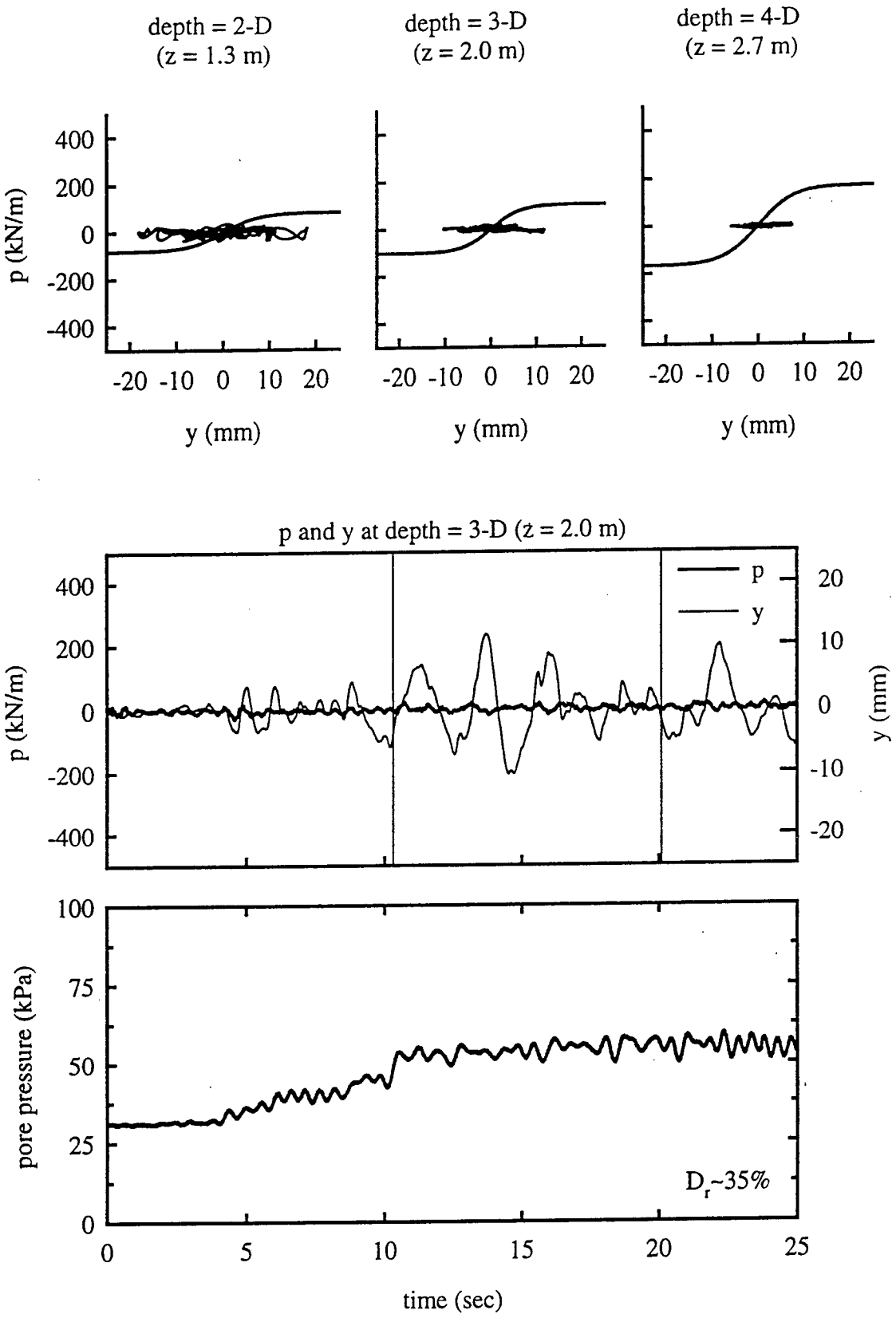

Fig. 6-19: p-y behavior in test Csp2 event K modified Santa Cruz motion with $a_{max,base}$=0.12 g

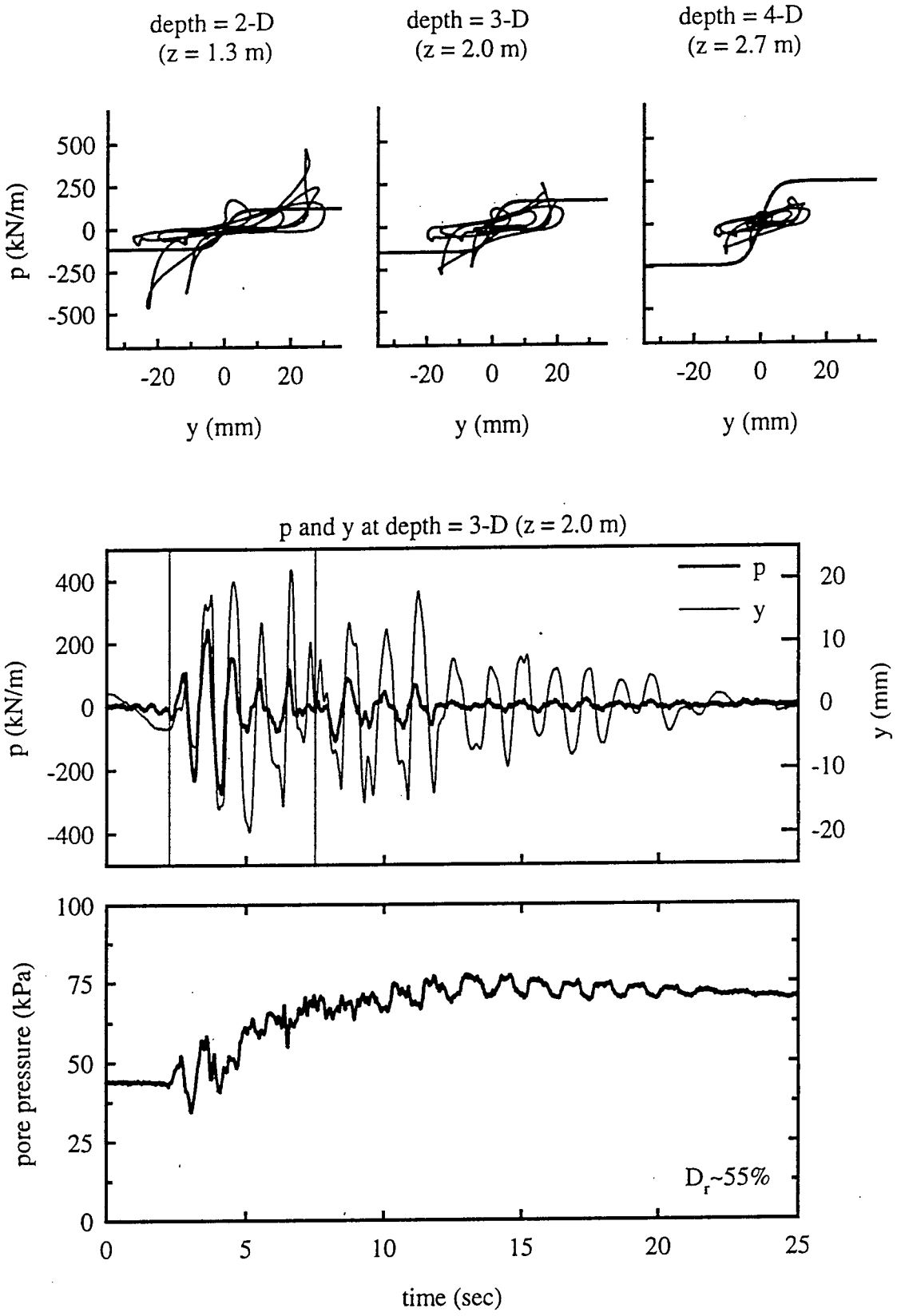

Fig. 6-20: p-y behavior in test Csp3 event J
Kobe motion with $a_{max,base}$=0.22 g

7 SUMMARY AND CONCLUSIONS

7.1 CENTRIFUGE MODELING

Results from the dynamic centrifuge tests of pile-supported structures were used to critically evaluate several aspects of the modeling system that could potentially affect subsequent interpretations and analyses. Detailed examination of the centrifuge modeling system was necessary because of the newness of the shaking table, and since recent reviews have highlighted important limitations that can exist in dynamic centrifuge systems (Scott 1994, Arulanandan et al. 1994).

Procedures were developed for signal processing, including the appropriate filtering and integration techniques required for calculating velocities and displacements from the accelerometer measurements. Filtering and integration of accelerometer measurements were shown to provide reliable estimates of transient displacement time histories, but cannot capture permanent displacements (as expected). These filtering and integration procedures will benefit other current and future projects utilizing the large centrifuge facilities.

Performance of the shaking table on the large centrifuge at UC Davis was shown to be satisfactory. Full frequency spectra of desired input motions (including real earthquake records) were recreated, with the motions being scaleable and repeatable. Dynamic vertical displacements at the ends of the container base were limited to about 10% of the dynamic horizontal displacements, indicating that rocking of the container base was reasonably small over the full operating range of the shaker.

The FSB1 container produced satisfactorily uniform and coherent horizontal motions, with relatively little rocking of the soil column, in tests on nonliquefied sand or even liquefied D_r~55% Nevada sand. Incoherent horizontal motions and differential vertical displacements developed at shallow depths in upper layers of liquefied D_r~35% Nevada sand or strongly-shaken soft clay, indicating that the soil column had become effectively "softer" than the FSB1 container in these tests.

Changing pore fluid viscosity by a factor of ten between two containers had negligible effect on the soil-pile interaction, with or without liquefaction of the upper soil layer. Furthermore, the nearly identical dynamic pore pressures and bending moment distributions obtained in these two tests showed that reasonably repeatable test results could be obtained nearly a year apart.

The density, uniformity and repeatability of sand layers were evaluated by penetration tests with a miniature conical probe. The results of these tests proved valuable in adjusting the pluviation process to improve specimen uniformity, and then later for quantifying the effect of pile installation method on sand density near the piles.

7.2 ANALYSIS METHODS

Different computer programs used in this study for analyzing piles as a beam on a nonlinear Winkler foundation (BNWF) problem all produced consistent results when analyzing the same hypothetical idealization (similar formulation of springs and dashpots, same soil properties, same input motions) (Chacko 1995, Wang et al. 1997). PAR offered the advantage of

a relatively easy to use interface with graphics, but had the disadvantage that we did not have access to the source code to implement new p-y elements for liquefying soils. GeoFEAP was selected for further development because it was the most general code, has graphics, allowed new elements to be implemented, and should be well maintained in the future.

The analysis of the free-field site response continues to be a difficult challenge when dealing with soft clays under strong levels of shaking or with liquefying sands. In such cases, the use of a nonlinear program like SUMDES is necessary. In cases where the soil nonlinearity is not as pronounced, the program SHAKE may be adequate. It is emphasized that a reliable estimation of the free-field site response is one of the most important steps in analyzing soil-structure interaction by the BNWF method.

The representation of radiation damping by inclusion of viscous damping on p-y springs was found to have a potentially significant effect on analysis results under certain conditions. Radiation damping has often been represented by placing linear viscous dashpots in parallel with the hysteretic p-y elements ("parallel damping"). This arrangement can result in unrealistically large dashpot forces if the p-y element is loaded into the highly nonlinear range. This problem can be avoided by placing the linear viscous dashpots in series with the nonlinear (hysteretic) component of the p-y element ("series damping"). The importance of these damping details depends on the soil-structure system, and may range from a negligible effect (e.g., as observed in some cases involving pile groups in firm soils) to a large effect (e.g., as observed for the single-pile-column systems studied herein). While it may not always have a significant effect, a series radiation damping formulation is always recommended for BNWF analyses because it is more rational and it does not add any complexity to the analyses. In any case, it is important to evaluate the importance of the radiation damping used when conducting nonlinear dynamic analyses. For example, one could perform at least one analysis with the radiation damping omitted on any p-y elements loaded past their elastic range to determine if it is having a large effect on the response of the system.

Two new p-y elements based on bounding surface concepts were developed and coded for GeoFEAP by Wang (1998). These new elements provide a means of representing the p-y resistance of soft clays, with or without the effects of gapping. A third element for representing the effects of liquefaction has been formulated (Wang 1997), but still requires coding for use in GeoFEAP. The software routines developed to represent the cyclic p-y behavior of soft clays are listed in Wang (1998), and were submitted to Caltrans on diskette. These software subroutines were written to interface with the program GeoFEAP (Bray et al. 1997), as developed and maintained at U.C. Berkeley and being used on other Caltrans projects. Analyses using GeoFEAP with the new p-y elements gave results in good agreement with those obtained using DRAIN-2D for the same model conditions.

The inclusion of gap formation in GeoFEAP was shown to improve the agreement between the calculated and measured dynamic response for the centrifuge model tests evaluated in this study. The main effects of gap formation were: (1) the system's fundamental period was slightly lengthened; and (2) less hysteretic energy was dissipated by the p-y springs.

Reasonable agreement was obtained between the BNWF calculations and the centrifuge model results for piles in soft clay, provided that the radiation damping was reasonably represented and effects of gap formation were included. This finding suggests that the BNWF analysis method has promise as a design tool for seismic soil-pile-structure interaction problems. Additional physical model data for other soil-pile-structure configurations, and systematic analyses of such data are needed to fully evaluate the reliability of the BNWF analysis method.

7.3 General Recommendations for Piles in Liquefied Soil

The p-y resistance of liquefied sand was shown in this study to be strongly dependent upon the relative density of the sand and displacement level. In addition, recent experimental results published by other investigators show that the p-y resistance of liquefied sand is also dependent upon group effects, loading rate (and hence permeability), pile installation method, pile displacement level, and excess pore pressure ratio (if less than 100%).

A rational form for the p-y resistance of liquefied sand is not yet available, and thus recourse has been made to representing it as either: (1) a scaled version of the static p-y resistance, or (2) a version based on the liquefied soil having an undrained residual shear strength. If the p-y resistance of liquefied sand is represented as a scaled version of its static p-y resistance, then the scaling factor should be selected based upon the relative density of the sand deposit. Our experimental results suggest this scaling factor may be about 0.1 to 0.2 for relative densities of 35-40%, and about 0.25-0.35 for relative densities of 55-60% (Boulanger et al. 1997). The work of Liu and Dobry (1995) suggested a scaling factor of about 0.10 for liquefied sand (100% excess pore pressure ratio) at a relative density of about 60%, based on post-shaking quasi-static cyclic displacement loading of a model pile in a centrifuge test. These scaling factors are reasonably consistent with recommendations made by the Japanese Road Association and Architectural Institute of Japan. However, it should be noted that the JRA and AIJ recommendations were based on minimal physical data, and are currently being revised in accordance with ongoing studies of pile damage in the 1995 Kobe earthquake.

The back-calculated p-y curves for liquefied sand (Wilson 1998) clearly demonstrate that the use of an apparent p-y scaling factor for liquefied sand is a simplistic approximation to a complex phenomenon. The back-calculated p-y curves for liquefied sand show characteristics that are consistent with the expected stress-strain response of liquefied sand. The p-y resistance of $D_r \approx 35$-40% sand is much smaller and softer than for $D_r \approx 55$-60% sand layer; this observation is consistent with the expected effects of D_r on the undrained shear resistance (or cyclic mobility) of saturated sand. The p-y curves for the $D_r \approx 55$-60% sand show: (1) a stiffening effect as relative displacement (y) increases beyond a certain limit, and (2) maximum lateral resistances that are significantly greater than expected for drained conditions at depths less than about 3 diameters. This behavior for the $D_r \approx 55$-60% sand is consistent with the expectation that a medium dense sand, under the range of confining stresses involved, would be dilatant at large enough shear strains (i.e., large enough to move the sand through a phase transformation). The p-y curves show a memory of past maximum relative displacements (y), and are softest (smallest p-y slope) for relative displacements less than the maximum past values. The shape and magnitude of the p-y curves for these liquefied sands were not well represented by any scalar multiple of the common static p-y curves used in practice, indicating that more research is needed to evaluate whether such simple concepts can be reliably applied in design. Therefore, caution must be exercised when design calculations are sensitive to reasonable variations in the assumed p-y resistance.

The deformations and bending moments experienced by a pile embedded in liquefied soil are due to both the inertial loads from the superstructure and the kinematic loads imposed by the soil profile deformations. Inertial loads have the greatest influence at shallow depths, although it should be noted that the depth of fixity for liquefied soil is much greater than for nonliquefied soil. Estimation of inertial loads requires a dynamic response analysis that accounts for the effects of liquefaction on the free-field response and on the soil-pile interaction.

Kinematic loads from the soil profile are very dependent on the soil stratigraphy and the

degree of lateral spreading. In our centrifuge experiments, the soil surface was level (no lateral spreading) and the liquefiable sand layer extended to the ground surface. Even in this situation, the kinematic loading from the soil profile had a strong effect on the bending moments in the pile near the bottom of the liquefied sand layer (near the contact with the underlying dense sand layer that the piles were embedded in). The kinematic loading also had a strong effect on the pile head's lateral displacements (with respect to the pile tip) since even modest lateral pressures from the liquefied sand layer (being 13.4 pile diameters thick) could cause significant lateral deflections at the pile head.

The presence of a nonliquefied crust over a laterally spreading liquefied layer can dominate the kinematic loads imposed on a pile foundation. In such cases, the loads imposed on the piles may be limited by either the passive resistance of the nonliquefiable crust or by the magnitude of the lateral spreading deformations.

It is worth noting that there are certain cases in which the analysis of pile foundations in liquefied soil is not overly sensitive to the assumed p-y properties of the liquefied soils. One such case is where the kinematic loads imposed by a laterally spreading nonliquefied crust overlying a liquefied soil layer govern the pile design. In such a situation, the maximum bending moments in the piles may be relatively insensitive to a reasonable range of assumed p-y characteristics for the liquefied layer. This observation has been made by Abdoun et al. (1997), Moriwaki (1997, U.S. Japan Workshop, unpublished), and Fujii et al. (1997). In essence, it is sometimes sufficient for the p-y resistance of the liquefied layer to be "soft" relative to the nonliquefied layers above and below it, with the degree of softness being less important.

7.4 Continuing Efforts

We are continuing research on the seismic response of pile-supported structures in liquefiable or soft soils using the data from the centrifuge tests performed under this contract. In particular, Mr. Daniel Wilson is continuing his analyses of the centrifuge model results, which will form the basis of his doctoral thesis. He has completed an evaluation of back-calculation procedures for evaluating the p-y resistance of the liquefied or soft soil layers, and will present his findings in his Ph.D. dissertation. Ms. Christina Curras is evaluating the ability of the nonlinear site response program SUMDES to capture the effects of liquefaction. Analyses with this program under this contract showed reasonable promise, but had identified the need for a very systematic evaluation against numerous shaking events to assess the reliability of the approach. Through these efforts, the centrifuge data obtained under the current contract will contribute to ongoing research aimed at addressing the needs of Caltrans and the State of California.

Data reports continue to be made available to other interested researchers without restriction. It is expected that use of these data by other researchers will generate additional benefits to Caltrans in the long-term.

7.5 Recommendations for Future Research

The performance of pile foundations in soft or liquefied ground under earthquake loading is a complex problem involving consideration of design motions, free-field site response, lateral spreading deformations, superstructure response, and soil-pile-superstructure interaction. Analysis and design procedures for pile foundations in soft clay and liquefied sands have been developed, but their reliability and accuracy can only be evaluated through systematic

evaluations against a range of physical data (case histories and centrifuge data). In addition, the fundamental mechanisms of soil-pile interaction in liquefied soils are poorly understood, and only crudely approximated in current practice. Thus, the following items are considered the most pressing research needs.

Detailed case histories ranging from good to poor performance of pile foundations in soft clay or liquefied ground under earthquake loading are needed. Note that the BTL Committee in Japan is currently addressing this need by its efforts in Kobe.

Research is needed on the phenomena of soil-pile interaction in liquefied soils using physical model studies, laboratory studies, and numerical analyses. The goals of these studies should be to understand the fundamental nature of the soil-pile interaction so that rational methods for its representation can be developed.

Physical modeling experiments are also needed for evaluating the physical behavior of pile foundations over a wide range of soil, foundation, and earthquake characteristics. Issues that need to be addressed include the lateral loads imposed on foundations by laterally spreading ground, the influence of nonliquefied crusts overlying liquefied soils, and the influence of pile caps.

Systematic evaluations of analysis and design procedures against a number of case histories or physical models are needed to evaluate their reliability. Analyses of single case histories or single experiments can be misleading with regard to the robustness of the analysis over a range of influencing factors. Systematic evaluations against several sets of data are valuable in identifying the limitations of any analysis method.

Improvements in the analysis and design methods will undoubtedly be made as our understanding of soil-pile interaction in soft clay or liquefied soil improves. The continuing efforts of researchers and practitioners, in the U.S. and Japan, on these problems are expected to lead to significant improvements in design and construction practices for pile foundations. Such improvements are expected to improve the effectiveness of earthquake hazard remediation programs throughout California and the U.S.

REFERENCES

Abdoun, T., Dobry, R., and O'Rourke, T. D. (1997). "Centrifuge and numerical modeling of soil-pile interaction during earthquake induced soil liquefaction and lateral spreading." Observation and Modeling in Numerical Analysis and Model Tests in Dynamic Soil-Structure Interaction Problems, T. Nogami, Ed., Geotechnical Special Publication No. 64, ASCE, New York, N.Y., pp. 76-90.

Abghari A. and Chai, J. (1995). "Modeling of soil-pile-superstructure interaction in the design of bridge foundations," Geotechnical Special Pub. No. 51, Performance of Deep Foundations under Seismic Loading, ASCE, John Turner (ed.) pp. 45-59.

AIJ (1988). Recommendations for design of building foundations. Architectural Institute of Japan. (in Japanese).

Akiyama, T., and Morimoto, H. (1997). "The damage and reinforcement of piles for oil storage tanks in a thermal power station." Distributed at the workshop. Details of publication unknown.

American Petroleum Institute. (1987). Recommended Practice for Planning, Designing and Constructing Fixed Offshore Platforms. API Recommended Practice 2A (RP 2A), Seventeenth Edition, April 1.

Angelides, D. C. and Roesset, J. M. (1980). "Nonlinear dynamic stiffness of piles," Research Report R80-13, Dept. of Civil Engineering, MIT, Cambridge, Massachusetts.Arulanandan, K., Dobry, R., Elgamal, A.-W., Ko, H. Y., Kutter, B. L., Prevost, J., Riemer, M. F., Schofield, A. N., Scott, R. F., R. B. Seed, Whitman, R. V., and Zeng, X. (1994). "Interlaboratory studies to evaluate the repeatability of dynamic centrifuge model tests." *Dynamic Geotechnical Testing II, ASTM STP 1213*, R. J. Ebelhar, V. P. Drnevich, and B. L. Kutter, Eds., American Society for Testing and Materials, Philadelphia, pp. 400-422.

Badoni, D. and Makris, N. (1996). "Nonlinear response of single piles under lateral inertial and seismic loads," Soil Dynamics and Earthquake Engineering, Vol. 15, pp. 29-43.

Berger, E., Mahin, S. A., and Pyke, R., (1977). "Simplified method for evaluating soil-pile structure interaction effects", Proceedings of the 9th Offshore Technology Conference, OTC Paper 2954, Houston, Texas, pp. 589-598.

Boulanger, R. W., Wilson, D. W., Kutter, B. L., and Abghari, A. (1997). "Soil-pile-superstructure interaction in liquefiable sand." Transportation Research Record No. 1569, TRB, National Research Council, National Academy Press, Washington, D.C. pp. 55-64.

Chacko, M. J. (1994). "Analysis of dynamic soil-pile-structure interaction," Master's Thesis, University of California, Davis.

Chang, G. S. (1990). "Centrifuge and numerical modeling of soil-pile-structure interaction during earthquake loading," Ph.D. Thesis, University of California, Davis.

Dafalias, Y.F. (1986) "Bounding surface plasticity. I: Mathematical foundation and hypoplasticity," Journal of Engineering Mechanics, Vol. 112, No. 9 September, pp. 966-987.

Dickenson, S. E. (1994). "Dynamic response of soft and deep cohesive soils during the Loma Prieta earthquake of Oct 17, 1989," Ph.D. Thesis, University of California, Berkeley.

Divis, C. J., Kutter, B. L., Idriss, I. M., Goto, Y., and Matsuda, T. (1996). "Uniformity of specimen and response of liquefiable sand model in a large centrifuge shaker." *Proc., Sixth Japan-U.S. Workshop on Earthquake Resistant Design of Lifeline Facilities and Countermeasures Against Soil Liquefaction*, Hamada and O'Rourke, Eds., NCEER-96-0012,

SUNY, Buffalo, pp. 259-273.
Dobry, R., Taboada, V., and Liu, L, (1995). "Centrifuge modeling of liquefaction effects during earthquakes." Proc. First International Conference on Earthquake Geotechnical Engineering, Tokyo, Japan.
Bray, J. D., Espinoza, R. D., Soga, K., and Taylor, R. L. (1995). GeoFEAP: Geotechnical Finite Element Analysis Program. Version 1.2, Report No. UCBGT/95-05, Department of Civil and Environmental Engineering, University of California, Berkeley.
Faruque, M. O. and Desai, C. S. (1982). "3-D material and geometric nonlinear analysis of piles," Proceedings of the Second International Conference on Numerical Methods in Offshore Pilling, University of Texas at Austin, Texas, pp. 553-575.
Fiegel, G. L. (1995). "Centrifugal and analytical modeling of soft soil subjected to strong seismic shaking," Ph.D. Thesis, Department of Civil and Environmental Engineering., University of California, Davis.
Fiegel, G. L., Hudson, M., Idriss, I. M., Kutter, B. L., and Zeng, X. (1994). "Effect of model containers on dynamic soil response." *Proc. Centrifuge 94*, C. F. Leung, F. H. Lee and T. S. Tan Eds., Balkema, Rotterdam, pp. 145-150.
Finn, W.D. Liam and Gohl, W.B. (1992) "Response of model pile groups to strong shaking", Geotechnical Special Publication No. 34 , pp. 27-55.
Fujii, S., Tokimatsu, K., Cubrinovski, M., and Hayashi, T. (1997). "Analysis of pile foundations on liquefied soil during the 1995 Hyogoken Nanbu earthquake." Abstract submitted for the 1998 Specialty Conference on Geotechnical Earthquake Engineering and Soil Dynamics, Seattle, WA.
Gazetas, G. and Dobry, R. (1984a). "Simple radiation damping model for piles and footings," Journal of Engineering Mechanics, Vol. 110, No. 6, pp. 937-956.
Gazetas, G. and Dobry, R. (1984b). "Horizontal response of piles in layered soils," Journal of Geotechnical Engineering, Vol. 110, No. 1, pp. 20-40.
Gazetas, G, Fan, K., Tazoh, T., Shimizu, K., Kavvadas, M. And Makris, N. (1992) "Seismic pile-group-structure interaction," Geotechnical Special Publication No. 34, pp. 56-93.
Horikoshi, K., Ohtsu, H., Tanaka, M., and Sueoka, T. (1997). "Centrifuge modeling of a pile subjected to lateral spreading of liquefied soil." Proceedings of the Third Kansai International Geotechnical Forum on Comparative Geotechnical Engineering, Kansai Branch of the Japanese Geotechnical Society, Japan, pp. 199-208.
JRA (1980). Specifications for highway bridges. Japan Road Association. (in Japanese).
Kagawa, T. (1980a). "Soil-pile-structure interaction of offshore structures during an earthquake," 12 Annual OTC in Houston, Texas, OTC 3820.
Kagawa, T. (1980b). "SRANG: users manual," McClelland Engineers Inc., Houston, Texas.
Kagawa, T. (1983). "NONSPS: users manual," McClelland Engineers Inc., Houston, Texas.
Kagawa, T. (1992) "Effect of liquefaction on lateral pile responses", Geotechnical Special Publication No. 34, 1992, pp. 207-223.
Karube, D., and Kimura, M. (1996). "Damage to foundations of railway structures." Soils and Foundations, Special Issue on Geotechnical Aspects of the January 17 1995 Hyogoken-Nambu Earthquake, Japanese Geotechnical Society, January.
Kuhlemeyer, R. L. (1979). "Vertical vibration of piles," Journal of Geotechnical Engineering 105(GT2), pp. 273-288.
Kutter, B. L., X. S. Li, W. Sluis, and J. A. Cheney. (1991). "Performance and Instrumentation of the Large Centrifuge at Davis." Proc. Centrifuge 91, Ko and McLean (eds), Balkema,

Rotterdam, pp. 19-26.
Kutter, B. L., Idriss, I. M., Kohnke, T., Lakeland, J., Li, X. S., Sluis, W., Zeng, X., Tauscher, R., Goto, Y., and Kubodera, I. (1994). "Design of a large earthquake simulator at UC Davis." *Proc. Centrifuge 94*, Leung, Lee & Tan, Eds., Balkema, Rotterdam, pp. 169-175.
Kutter, B. L. (1995). "Dynamic centrifuge modeling of geotechnical structures." *Transportation Research Record 1336*, TRB, National Research Council, Washington, D.C., pp. 24-30.
Li, X. S. (1990). Ph.D. Dissertation, University of California, Davis.
Liu, L. and Dobry, R. (1995). "Effect of Liquefaction on Lateral Response of Piles by Centrifuge Model Tests." National Center for Earthquake Engineering Research (NCEER) Bulletin, Vol. 9, No. 1, January, pp. 7-11.
Matlock, H. (1970). "Correlations for design of laterally loaded piles in soft clay," Proceedings, 2nd Annual Offshore Technology Conference, Houston, Texas, OTC 1204.
Matlock, H., Foo, S. H., and Bryant, L. L. (1978). "Simulation of lateral pile behavior." Proc. Earthquake Engineering and Soil Dynamics, ASCE July, pp. 600-619.
Matsui, T. (1996). "Foundation damage of structures." Special Issue of Soils and Foundations, Japanese Society of Soil Mechanics and Foundation Engineering.
Matsuo, O., Tamura, K., Hamada, T., Azuma, T., Shimazu, T., and Murata, K. (1996). "Revised liquefaction potential evaluation procedure and seismic design treatment of liquefaction for bridge foundations." Proc., 12th U.S.-Japan Bridge Engineering Workshop, FHWA, pp. 137-159.
Nogami, T., and Konagai, K. (1986). "Time-domain axial response of dynamically loaded single piles," Journal of Engineering Mechanics, ASCE, 113(3), pp. 417-430.
Nogami, T., Otani, J., Konagai, K. and Chen, H.-L., (1992). " Nonlinear soil-pile interaction model for dynamic lateral motion," Journal of Geotechnical Engineering, Vol. 118, No. 1, pp. 89-106.
Novak, M., Nogami, T., and Aboul-Ella, F. (1978). "Dynamic soil reactions for plane strain case," Journal of the Engineering Mechanics Division, ASCE, Vol. 104, No. EM4, Proc. Paper 13914, pp. 953-959.
Novak, M., and Sheta, M. (1980). "Approximate approach to contact problems of piles," Proc. ASCE, Nat. Convention, Dynamic Response of Pile Foundations: Analytical Aspects," ASCE, New York, N.Y., pp. 55-79.
Oh-Oka, H., Onishi, K., Nanba, S., Mori, T., Ishikawa, K, Koyama, S., and Shimazu, S. (1997). "Liquefaction-induced failure of piles in 1995 Kobe earthquake." Proceedings of the Third Kansai International Geotechnical Forum on Comparative Geotechnical Engineering, Kansai Branch of the Japanese Geotechnical Society, Japan, pp. 265-274.
PMB Engineering Inc. (1988). PAR (Pile Analysis Routine) Manual, 500 Sansome Street, San Francisco, CA 94111.
Prakash, V., Powell, G. H., and Campbell, S., (1993). "DRAIN-2DX base program description and user guide," Version 1.10, Report No., UCB/SEMM-93/17, University of California, Berkeley.
Randolph, M. F. (1981). "Response of flexible piles to lateral loading," Geotechnique, Vol. 31, No. 2, pp. 247-259.
Reese, L. C., Cox, W. R. and Koop, F. D., (1974). "Analysis of laterally loaded piles in sands," Sixth Annual Offshore Technology Conference, Houston, Texas, OTC 2080.
Sanchez, S. I. (1982). "Static and dynamic stiffnesses of single piles," Research Report GR82-31, Dept. of Civil Engineering, The University of Texas at Austin, Austin, Texas.

Sasaki, Y., Koseki, J., Shioji, K., Konishi, M., Kondo, Y., Terada, T. (1997). "Damage to Higashinada sewage treatment plant by the 1995 Hyogoken-Nanbu earthquake." Seismic Behavior of Ground and Geotechnical Structures, Special Volume of TC4, Proceedings of special discussion session on earthquake geotechnical engineering, Hamburg, 6-12 September 1997, Seco e Pinto, P. S. (ed.), A. A. Balkema.

Schnabel, P. B., Lysmer J. and Seed, H. B. (1972). "SHAKE: a computer program for earthquake response analysis of horizontally layered sites," Report No. UCB/EERC-72/12, Earthquake Engineering Research Center, University of California, Berkeley, Dec., 102p.

Scott, R. F. (1994). "Review of progress in dynamic geotechnical centrifuge research." *Dynamic Geotechnical Testing II, ASTM STP 1213*, R. J. Ebelhar, V. P. Drnevich, and B. L. Kutter, Eds., American Society for Testing and Materials, Philadelphia, pp. 305-329.

Seed, H. B. and Idriss, I. M. (1970). "Soil moduli and damping factors for dynamic response analysis," Report No. UCB/EERC-70/10, Earthquake Engineering Research Center, University of California, Berkeley.

Sen, R., Davis, T. G. and Barnerjee, P. K. (1985). "Dynamic analysis of piles and pile groups embedded in homogeneous soils," Int. J. Earthquake Eng. Struc. Dyn., 13, pp. 53-65.

Stewart, D. P., Kutter, B. L., Higuchi, S., Robins, P. N., Narayanan, K. R., and Thompson, D. J. (1997). "Centrifuge modeling of the seismic response of LNG production facility structures: Phase I." Report No. UCD/CGM-97/02, Center for Geotechnical Modeling, Department of Civil and Environmental Engineering, University of California, Davis, March.

Sun, J. I., Golesorkhi, R. and Seed, H. B., (1988). "Dynamic moduli and damping ratios for cohesive soils," Report No. UCB/EERC-88/15, Earthquake Engineering Research Center, University of California, Berkeley.

Tokida, K.-I., Matsumoto, H., and Iwasaki, H. (1992). "Experimental study of drag acting of piles in ground flowing by liquefaction." Proceedings of the Fourth Japan-U.S. Workshop on Earthquake Resistant Design of Lifeline Facilities and Countermeasures for Soil Liquefaction, Volume 1, Report NCEER 92-0019, National Center for Earthquake Engineering Research, SUNY, Buffalo, N.Y., pp. 511-523.

Tokimatsu, K., Mizuno, H., and Kakurai, M. (1996). "Building damage associated with geotechnical problems." Special Issue of Soils and Foundations, Japanese Society of Soil Mechanics and Foundation Engineering.

Tokimatsu, K., Oh-Oka, H., Shamoto, Y., Nakazawa, A., and Asaka, Y. (1997). "Failure and deformation modes of piles caused by liquefaction-induced lateral spreading in 1995 Hyogoken-Nambu earthquake." Proceedings of the Third Kansai International Geotechnical Forum on Comparative Geotechnical Engineering, Kansai Branch of the Japanese Geotechnical Society, Japan, pp. 239-248.

Trochanis, A. M., Bielak, J., and Christiano, P. (1991). "Simplified model for analysis of one or two piles," Journal of Geotechnical Engineering, Vol. 117, No. 3, pp. 448-466.

Van Laak, P. A., Taboada, V. M., Dobry, R., and Elgamal, A.-W. (1994). "Earthquake centrifuge modeling using a laminar box." *Dynamic Geotechnical Testing II, ASTM STP 1213*, R. J. Ebelhar, V. P. Drnevich, and B. L. Kutter, Eds., American Society for Testing and Materials, Philadelphia, pp. 370-384.

Vesic, A. S. (1961). "Bending of beams resting on isotropic elastic solids," Journal of the Engineering Mechanics, ASCE, Vol. 87, No. EM2, pp. 35-53.

Wang, S. (1997). "Nonlinear seismic soil-pile-structure interaction." M.S. thesis, University of California, Davis, CA.

Wen, Y.-K. (1976). "Method for random vibration of hysteretic systems," Journal of the Engineering Mechanics Division, ASCE, Vol. 102, No. EM2, pp. 249-263.

Whitman, R. V., and Lambe, P. C. (1986). "Effect of boundary conditions upon centrifuge experiments using ground motion simulation." *Geotechnical Testing Journal*, ASTM GTJODJ, Vol. 9, No. 2, pp. 61-71.

Wilson, D. W. (1998). "Soil-pile-superstructure interaction in soft clay and liquefiable sand," Ph.D. thesis, University of California, Davis, CA (in preparation).

Wilson, D. W., Boulanger, R. W., Kutter, B. L., and Abghari, A. (1995). "Dynamic centrifuge tests of pile-supported structures in liquefiable sand." *Proc., National Seismic Conference on Bridges and Highways*, Sponsored by Federal Highways Administration and Caltrans, San Diego, CA, December 10-13.

Wilson, D. W., Boulanger, R. W., Kutter, B. L., and Abghari, A. [1997 (a)]. "Aspects of dynamic centrifuge testing of soil-pile-superstructure interaction." Observation and Modeling in Numerical Analysis and Model Tests in Dynamic Soil-Structure Interaction Problems, T. Nogami, Ed., Geotechnical Special Publication No. 64, ASCE, New York, N.Y., pp. 47-63.

Wilson, D. W., Boulanger, R. W., and Kutter, B. L., [1997 (b)]. "Soil-pile-superstructure interaction at soft or liquefiable soil sites - Centrifuge data report for Csp1." Report No. UCD/CGMDR-97/02, Center for Geotechnical Modeling, Department of Civil and Environmental Engineering, University of California, Davis, February.

Wilson, D. W., Boulanger, R. W., and Kutter, B. L., [1997 (c)]. "Soil-pile-superstructure interaction at soft or liquefiable soil sites - Centrifuge data report for Csp2." Report No. UCD/CGMDR-97/03, Center for Geotechnical Modeling, Department of Civil and Environmental Engineering, University of California, Davis, February.

Wilson, D. W., Boulanger, R. W., and Kutter, B. L., [1997 (d)]. "Soil-pile-superstructure interaction at soft or liquefiable soil sites - Centrifuge data report for Csp3." Report No. UCD/CGMDR-97/04, Center for Geotechnical Modeling, Department of Civil and Environmental Engineering, University of California, Davis, February.

Wilson, D. W., Boulanger, R. W., and Kutter, B. L., [1997 (e)]. "Soil-pile-superstructure interaction at soft or liquefiable soil sites - Centrifuge data report for Csp4." Report No. UCD/CGMDR-97/05, Center for Geotechnical Modeling, Department of Civil and Environmental Engineering, University of California, Davis, February.

Wilson, D. W., Boulanger, R. W., and Kutter, B. L., [1997 (f)]. "Soil-pile-superstructure interaction at soft or liquefiable soil sites - Centrifuge data report for Csp5." Report No. UCD/CGMDR-97/06, Center for Geotechnical Modeling, Department of Civil and Environmental Engineering, University of California, Davis, February.

Wolf, J. P. (1985). "Dynamic soil-structure interaction," Englewood Cliffs, NJ: Prentice-Hall.

Youd, T. L., and Bartlett, S. F. (1989). "Case histories of lateral spreads from the 1964 Alaskan earthquake." Proc., Third Japan-U.S. Workshop on Earthquake Resistant Design of Lifeline Facilities and Countermeasures for Soil Liquefaction, NCEER-91-0001, Feb. 1.

APPENDIX A: PUBLICATIONS UNDER CONTRACT 65V495

Boulanger, R. W., Wilson, D. W., Kutter, B. L., and Abghari, A. (1997). "Soil-pile-superstructure interaction in liquefiable sand." Accepted February 1997 for publication in Transportation Research Record, TRB, National Research Council, National Academy Press, Washington, D.C.

Chacko, M. J. (1995). "Analysis of dynamic soil-pile-structure interaction." M.S. thesis, University of California, Davis, CA.

Wang, S. (1997). "Nonlinear seismic soil-pile-structure interaction." M.S. thesis, University of California, Davis, CA.

Wang, S., Kutter, B. L., Chacko, J., Wilson, D. W., Boulanger, R. W., and Abghari, A. (1997). "Nonlinear seismic soil-pile-structure interaction." Accepted February 1997 for publication in Earthquake Spectra, Earthquake Engineering Research Institute.

Wilson, D. W., Boulanger, R. W., Kutter, B. L., and Abghari, A. (1995). "Dynamic centrifuge tests of pile-supported structures in liquefiable sand." *Proc., National Seismic Conference on Bridges and Highways*, Sponsored by Federal Highways Administration and Caltrans, San Diego, CA, December 10-13.

Wilson, D. W., Boulanger, R. W., Kutter, B. L., and Abghari, A. (1996). "Soil-pile-superstructure interaction experiments with liquefiable sand in the centrifuge." The Fourth Caltrans Seismic Research Workshop, Radisson Hotel, Sacramento, California, July 9-11.

Wilson, D. W., Boulanger, R. W., and Kutter, B. L., [1997 (a)]. "Soil-pile-superstructure interaction at soft or liquefiable soil sites - Centrifuge data report for Csp1." Report No. UCD/CGMDR-97/02, Center for Geotechnical Modeling, Department of Civil and Environmental Engineering, University of California, Davis, February.

Wilson, D. W., Boulanger, R. W., and Kutter, B. L., [1997 (b)]. "Soil-pile-superstructure interaction at soft or liquefiable soil sites - Centrifuge data report for Csp2." Report No. UCD/CGMDR-97/03, Center for Geotechnical Modeling, Department of Civil and Environmental Engineering, University of California, Davis, February.

Wilson, D. W., Boulanger, R. W., and Kutter, B. L., [1997 (c)]. "Soil-pile-superstructure interaction at soft or liquefiable soil sites - Centrifuge data report for Csp3." Report No. UCD/CGMDR-97/04, Center for Geotechnical Modeling, Department of Civil and Environmental Engineering, University of California, Davis, February.

Wilson, D. W., Boulanger, R. W., and Kutter, B. L., [1997 (d)]. "Soil-pile-superstructure interaction at soft or liquefiable soil sites - Centrifuge data report for Csp4." Report No. UCD/CGMDR-97/05, Center for Geotechnical Modeling, Department of Civil and Environmental Engineering, University of California, Davis, February.

Wilson, D. W., Boulanger, R. W., and Kutter, B. L., [1997 (e)]. "Soil-pile-superstructure interaction at soft or liquefiable soil sites - Centrifuge data report for Csp5." Report No. UCD/CGMDR-97/06, Center for Geotechnical Modeling, Department of Civil and Environmental Engineering, University of California, Davis, February.

Wilson, D. W., Boulanger, R. W., Kutter, B. L., and Abghari, A. [1997 (f)]. "Aspects of dynamic centrifuge testing of soil-pile-superstructure interaction." Proceedings, Numerical and Physical Modeling for Dynamic Soil-Structure Interaction Phenomena, T. Nogami, Ed., ASCE, New York, N.Y. (in press).